RESEARCH MEMORANDUM

for the

Bureau of Aeronautics, Navy Department

THE EFFECT OF AN OPERATING PROPELLER ON THE AERODYNAMIC CHARACTERISTICS OF A 1/10-SCALE MODEL OF THE LOCKHEED XFV-1 AIRPLANE AT HIGH SUBSONIC SPEEDS

(TED NO. NACA DE-377)

By Fred B. Sutton and Donald A. Buell

Ames Aeronautical Laboratory
Moffett Field, Calif.

NATIONAL ADVISORY COMMITTEE
FOR AERONAUTICS

WASHINGTON

May 6, 1952

NATIONAL ADVISORY COMMITTEE FOR AERONAUTICS

RESEARCH MEMORANDUM

for the

Bureau of Aeronautics, Navy Department

THE EFFECT OF AN OPERATING PROPELLER ON THE AERODYNAMIC CHARACTERISTICS OF A 1/10-SCALE MODEL OF THE LOCKHEED XFV-1 AIRPLANE AT HIGH SUBSONIC SPEEDS

(TED NO. NACA DE-377)

By Fred B. Sutton and Donald A. Buell

SUMMARY

An investigation was conducted in the Ames 12-foot pressure wind tunnel to determine the effect of an operating propeller on the aerodynamic characteristics of a 1/10-scale model of the Lockheed XFV-1 airplane. Several full-scale power conditions were simulated at Mach numbers from 0.50 to 0.92; the Reynolds number was constant at 1.7 million.

Lift, longitudinal force, pitch, roll, and yaw characteristics, determined with and without power, are presented for the complete model and for various combinations of model components. Results of an investigation to determine the characteristics of the dual-rotating propeller used on the model are given also.

INTRODUCTION

The investigation discussed herein was made on a model of the Lockheed XFV-1 convoy-fighter airplane at the request of the Bureau of Aeronautics, Department of the Navy. The XFV-1 is powered with an Allison T-40 gas-turbine engine in combination with a dual-rotating Curtiss propeller of advanced design. The configuration of the airplane is aerodynamically conventional with the exception of an interdigitated tail on which all the movable control surfaces are located. Longitudinal, lateral, and directional control is achieved by appropriate combinations

of movements of the control surfaces. The airplane is to be capable of vertical take-off, and of high subsonic speeds after translation into horizontal flight. Data presented in this report pertain only to airplane characteristics in the normal flight attitudes and at comparatively high speeds. Geometric characteristics of the airplane are presented in table I.

NOTATION

The results of the investigation are presented in the form of standard NACA coefficients of forces and moments and are referred to the conventional stability axes. The coefficients and symbols used are defined as follows:

C_L lift coefficient $\left(\frac{\text{lift}}{qS}\right)$

C_l rolling-moment coefficient measured about the center of gravity $\left(\frac{\text{rolling moment}}{qbS}\right)$

C_m pitching-moment coefficient measured about the center of gravity $\left(\frac{\text{pitching moment}}{q\bar{c}S}\right)$

C_n yawing-moment coefficient measured about the center of gravity $\left(\frac{\text{yawing moment}}{qbS}\right)$

C_P power coefficient $\left(\frac{P}{\rho n^3 D^5}\right)$

C_T thrust coefficient $\left(\frac{T}{\rho n^2 D^4}\right)$

C_X longitudinal-force coefficient $\left(\frac{X}{qS}\right)$

c_{l_d} propeller-blade-section design lift coefficient

b wing span, feet

b' propeller-blade width, feet

c	wing chord, feet
$\bar{c}$	mean aerodynamic wing chord $\left(\frac{\int_0^{b/2} c^2 dy}{\int_0^{b/2} c\, dy}\right)$, feet
C.G.	center-of-gravity location (See fig. 1.)
D	propeller diameter, feet
h	maximum thickness of propeller-blade section, feet
J	propeller advance-diameter ratio $\left(\frac{V}{nD}\right)$
M	free-stream Mach number
n	propeller rotational speed, revolutions per second
P	model-motor shaft power, foot-pounds per second
R	propeller-tip radius, feet
r	propeller-blade-section radius, feet
q	free-stream dynamic pressure $\left(\frac{1}{2}\rho V^2\right)$, pounds per square foot
S	wing area, square feet
T	propeller thrust, pounds
V	free-stream velocity, feet per second
X	longitudinal force, parallel to stream and positive in a thrust direction, pounds
y	lateral distance from plane of symmetry, feet
α	angle of attack, degrees
β	propeller-blade angle, degrees
δ	control-surface deflection with respect to a section of the fixed surface taken perpendicular to the hinge line of the movable surface, degrees

δ_a aileron deflection, positive when lift is decreased on the right tail surface and increased on the left tail surface (The control surfaces were deflected differentially to the same angular magnitude.)

δ_e elevator deflection, positive to increase lift on tail

η propeller efficiency $\left(\frac{C_T J}{C_P}\right)$

ρ free-stream mass density of air, slugs per cubic foot

ψ angle of yaw, degrees

MODEL AND APPARATUS

The investigation was conducted in the Ames 12-foot pressure wind tunnel using a 1/10-scale model of the Lockheed XFV-1 convoy-fighter airplane supplied by the Lockheed Aircraft Corporation. The prototype-airplane contours were slightly modified at the base of the model fuselage to accommodate a sting-type model support. Figure 1 presents dimensions and details of the model and figure 2 shows the model mounted in the tunnel test section.

The dual-rotating propeller employed on the model was designed by the Curtiss-Wright Corporation specifically for convoy-fighter aircraft. Figure 3 presents propeller plan-form and blade-form curves.

The model, including the propeller, was constructed of aluminum alloy with the exception of the fuselage duct contours which were faired with a lead alloy. Model control-surface deflections were simulated with replaceable control surfaces machined to predetermined angles. The model-propeller blades could be adjusted manually to any desired angle. The surfaces of the wing, body, and tail were filled, painted, and polished smooth.

Model power was supplied by two water-cooled induction motors mounted in tandem in the model fuselage. Each motor developed a maximum of 36 horsepower at 12,000 revolutions per minute. A continuous speed control for the two motors was obtained by the use of a variable-frequency power supply common to both motors. Each component of the dual-rotating propeller was directly driven by one of the model motors. Propeller speed was measured by means of a tachometer on the front motor (rear propeller) used in conjunction with an electronic frequency-measuring device. It was assumed that both motors turned at the same speed.

A sting-type model-support system was used with a wire-resistance strain-gage balance of the flexure-pivot type enclosed in the model fuselage to measure lift, longitudinal force, side force, pitching moment, rolling moment, and yawing moment. Angle of attack was measured visually by means of a cathetometer.

TESTS AND PROCEDURES

Test Ranges

The characteristics of the model were investigated over a Mach number range of 0.50 to 0.92; Reynolds number was constant at 1.7 million. Several full-scale-airplane power conditions were simulated for various propeller-blade angles through an angle-of-attack range of -4° to $+8^\circ$ at each Mach number.

A summary of the power-on tests for several model configurations is presented in table II. Simulated full-scale powers could not be exactly duplicated for the different model configurations as the tunnel temperatures and model-motor efficiencies could not be accurately predetermined. The power-coefficient values presented in table II are the average of the values measured through an angle-of-attack range.

Propeller Calibration

Propeller calibrations were made by testing the propeller in combination with the model fuselage less the pilot's cab (fig. 4). Forces were measured through Mach number, angle of attack, model power, and propeller-blade angle ranges which included the test ranges of the power-on model investigation. The propeller thrust coefficient was determined from the following relation:

$$C_T = KC_{X_p}$$

where

$$K = J^2 \frac{S}{2D^2}$$

and

$$C_{X_p} = C_{X_{\text{propeller operating}}} - C_{X_{\text{propeller off}}}$$

The shaft power of the model motors was determined by measuring the input power to the motors and applying corrections for the motor losses. Interference effects between the body and the propeller were neglected and the efficiencies presented are the propulsive efficiencies of the propeller-body combination.

Yaw Tests

It was not possible to yaw the model with respect to the air stream due to limitations of the model support system. However, as the tail of the model was symmetrical about both the horizontal and vertical planes, yaw tests at zero lift were simulated by testing the model with the wings and pilot's cab removed. The normal angle-of-attack range of the model was assumed to be an angle-of-yaw range. Yaw data are presented for the model with the propeller removed, for the model with windmilling propeller, and for the power conditions listed in table II.

CORRECTIONS

Tunnel-Wall Interference

Corrections for the induced effects of the tunnel walls resulting from lift on the model were made according to the methods of reference 1. The corrections added to the angle of attack and longitudinal-force coefficient were as follows:

$$\Delta\alpha = 0.2078\ C_L$$

$$\Delta C_X = -0.00363\ C_L^2$$

No corrections were made to the pitching-moment coefficients as calculations by the method of reference 1 indicated the corrections to be negligible.

The effects of wind-tunnel-wall constraint on the model-propeller slipstream were evaluated by the method of references 2 and 3. These effects were indicated to be negligible.

The effects of constriction of the flow by the tunnel walls were evaluated by the method of reference 4. The following table shows the magnitude of the corrections:

Corrected Mach number	Uncorrected Mach number	$\frac{q_{corrected}}{q_{uncorrected}}$
0.500	0.500	1.0014
.700	.699	1.0021
.800	.798	1.0030
.850	.847	1.0042
.900	.894	1.0064
.920	.912	1.0083

Sting Interference

In order to partially correct the longitudinal-force data for sting interference, the pressure was measured at the base of the model fuselage and the drag data were adjusted to correspond to a base pressure equal to the static pressure of the free stream.

RESULTS

Figures 5 through 10 show the characteristics of the Curtiss 1058-1059-XC-4 dual-rotating propeller. Because of the small thrust available at Mach numbers of 0.90 and 0.92, only one power condition in addition to propeller windmilling was investigated at these Mach numbers. The fairing of propeller-performance curves for these conditions (indicated by broken lines) is based on propeller-performance data obtained at lower Mach numbers. Figures 11 through 16 show the effect of power on the aerodynamic characteristics of the model fuselage. The effects of power on the aerodynamic characteristics of the complete model are shown in figures 17 through 22, and power effects on the aerodynamic characteristics of the model with the tail removed are presented in figure 23. Figure 24 shows longitudinal control-effectiveness data for several elevator deflections and one combination of elevator and aileron deflections; the effects of power on the simulated yaw characteristics of the model are shown in figure 25. Roll characteristics of the model are presented in figure 26 for one aileron deflection and for a combination of aileron and elevator deflections. Figure 27 presents aerodynamic characteristics for several combinations of model components with the propeller removed, and figure 28 shows the aerodynamic characteristics for the body alone, the body and cab, and the body and tail.

Ames Aeronautical Laboratory
National Advisory Committee for Aeronautics
Moffett Field, California

REFERENCES

1. Silverstein, Abe, and White, James H.: Wind-Tunnel Interference with Particular Reference to Off-Center Positions of the Wing and to the Downwash at the Tail. NACA Rep. 547, 1935.

2. Glauert, H.: The Elements of Aerofoil and Airscrew Theory. American ed., The Macmillan Company, N.Y., 1943, pp. 222-226.

3. Young, A. D.: Note on the Application of the Linear Perturbation Theory to Determine the Effect of Compressibility on the Wind Tunnel Constraint on a Propeller. R.A.E. TN No. Aero. 1539, Nov. 1944.

4. Herriot, John G.: Blockage Corrections for Three-Dimensional-Flow Closed-Throat Wind Tunnels, with Consideration of the Effect of Compressibility. NACA Rep. 995, 1950. (Formerly NACA RM A7B28)

TABLE I.- GEOMETRIC CHARACTERISTICS OF THE LOCKHEED XFV-1 AIRPLANE

Wing	
Span, feet	27.500
Root chord, feet	13.500
Tip chord, feet	4.417
Mean aerodynamic chord, feet	9.708
Aspect ratio	3.07
Taper ratio	0.327
Area, square feet	246.0
Dihedral of wing reference plane through 40-percent chord, degrees	5.0
Incidence, root and tip, degrees	1.0
Length, wing-tip armament pods, feet	14.0
Diameter, wing-tip armament pods, feet	1.5
Airfoil section, root and tip	NACA 65A206
Tail	
Span, feet	12.255
Root chord, feet	7.083
Tip chord, feet	2.667
Mean aerodynamic chord, feet	5.208
Aspect ratio	3.55
Taper ratio	0.376
Total area, 4 surfaces, square feet	169.0
Total area, 4 fixed surfaces, square feet	136.2
Total area, 4 movable surfaces, square feet	32.8
Incidence (angle in vertical plane) between fuselage reference line and intersection of all chord planes, degrees	-4.0
Sweepback angle, quarter chord, degrees	30.0
Airfoil section, root and tip	NACA 65A007
Propeller	
Diameter, feet	16.00
Number of blades	6 (3 in each disc)
Propeller activity factor	140

TABLE II.- SUMMARY OF XFV-1 MODEL POWER-ON TESTS

Mach No.	Tunnel density altitude (ft)	Propeller-blade angle (deg)	Complete model configuration			Tail-off model configuration			Simulated yaw configuration		
			$C_{P_{av}}$	Equivalent full scale hp[1]	Fig. No.	$C_{P_{av}}$	Equivalent full scale hp[1]	Fig. No.	$C_{P_{av}}$	Equivalent full scale hp[1]	Fig. No.
0.50	22,100	50	0.84	2950	17(a)	- - -	- - -	- - -	- - -	- - -	- - -
.50	22,100	50	.56	1650	17(a)	- - -	- - -	- - -	- - -	- - -	- - -
.50	22,100	55	1.25	2700	17(b)	1.27	2700	23(a)	1.13	2300	25
.50	22,100	55	.94	1650	17(b)	1.02	1850	23(a)	- - -	- - -	- - -
.70	31,500	50	.64	4100	18(a)	- - -	- - -	- - -	- - -	- - -	- - -
.70	31,500	55	.86	3100	18(b)	.89	3150	23(b)	.81	2950	25
.70	31,500	55	.79	2750	18(b)	.88	3050	23(b)	- - -	- - -	- - -
.70	31,500	60	1.32	2750	18(c)	- - -	- - -	- - -	- - -	- - -	- - -
.70	31,500	60	1.13	2150	18(c)	- - -	- - -	- - -	- - -	- - -	- - -
.80	35,100	50	.42	3150	19(a)	- - -	- - -	- - -	- - -	- - -	- - -
.80	35,100	55	.76	3350	19(b)	.81	3650	23(c)	.69	3200	25
.80	35,100	55	.66	2800	19(b)	.73	3150	23(c)	- - -	- - -	- - -
.85	36,500	55	.78	3700	20(a)	.73	3650	23(d)	.65	3450	25
.85	36,500	60	1.09	3150	20(b)	- - -	- - -	- - -	- - -	- - -	- - -
.85	36,500	60	.97	2700	20(b)	- - -	- - -	- - -	- - -	- - -	- - -
.90	37,800	55	- - -	- - -	- - -	.74	4250	23(e)	.63	4050	25
.90	37,800	60	1.03	3300	21	- - -	- - -	- - -	- - -	- - -	- - -
.92	38,200	55	- - -	- - -	- - -	.69	4150	23(f)	.53	3500	25
.92	38,200	60	.98	3300	22	- - -	- - -	- - -	- - -	- - -	- - -

[1]Equivalent full-scale horsepower was calculated for airplane altitudes corresponding to the tunnel-density altitudes.

FIGURE LEGENDS

Figure 1.– Three-view drawing of the 1/10-scale model of the Lockheed XFV-1 airplane.

Figure 2.– The 1/10-scale model of the Lockheed XFV-1 airplane in the Ames 12-foot pressure wind tunnel.

Figure 3.– Plan-form and blade-form curves for the Curtiss 1058-1059-XC-4 dual-rotating propeller.

Figure 4.– The 1/10-scale model of the Curtiss 1058-1059-XC-4 propeller in the Ames 12-foot pressure wind tunnel.

Figure 5.– Characteristics of the Curtiss 1058-1059-XC-4 dual-rotating propeller. M, 0.50. (a) α, 0°.

Figure 5.– Continued. (b) α, 4°.

Figure 5.– Continued. (c) α, 8°.

Figure 5.– Continued. (d) α, 12°.

Figure 5.– Concluded. (e) α, 16°.

Figure 6.– Characteristics of the Curtiss 1058-1059-XC-4 dual-rotating propeller. M, 0.70. (a) α, 0°.

Figure 6.– Continued. (b) α, 4°.

Figure 6.– Continued. (c) α, 8°.

Figure 6.– Concluded. (d) α, 12°.

Figure 7.– Characteristics of the Curtiss 1058-1059-XC-4 dual-rotating propeller. M, 0.80. (a) α, 0°.

Figure 7.– Continued. (b) α, 4°.

Figure 7.– Concluded. (c) α, 8°.

Figure 8.– Characteristics of the Curtiss 1058-1059-XC-4 dual-rotating propeller. M, 0.85. (a) α, 0°.

Figure 8.– Continued. (b) α, 4°.

Figure 8.– Concluded. (c) α, 8°.

Figure 9.– Characteristics of the Curtiss 1058–1059–XC–4 dual–rotating propeller. M, 0.90. (a) α, 0°.

Figure 9.– Continued. (b) α, 4°.

Figure 9.– Concluded. (c) α, 8°.

Figure 10.– Characteristics of the Curtiss 1058–1059–XC–4 dual–rotating propeller. M, 0.92. (a) α, 0°.

Figure 10.– Continued. (b) α, 4°.

Figure 10.– Concluded. (c) α, 8°.

Figure 11.– The effect of power on the longitudinal characteristics of the Lockheed XFV–1 model fuselage. M, 0.50. (a) $\beta_{0.75R}$, 50°.

Figure 11.– Concluded. (b) $\beta_{0.75R}$, 55°.

Figure 12.– The effect of power on the longitudinal characteristics of the Lockheed XFV–1 model fuselage. M, 0.70. (a) $\beta_{0.75R}$, 50°.

Figure 12.– Continued. (b) $\beta_{0.75R}$, 55°.

Figure 12.– Concluded. (c) $\beta_{0.75R}$, 60°.

Figure 13.– The effect of power on the longitudinal characteristics of the Lockheed XFV–1 model fuselage. M, 0.80. (a) $\beta_{0.75R}$, 50°.

Figure 13.– Continued. (b) $\beta_{0.75R}$, 55°.

Figure 13.– Continued. (c) $\beta_{0.75R}$, 60°.

Figure 13.– Concluded. (d) $\beta_{0.75R}$, 65°.

Figure 14.– The effect of power on the longitudinal characteristics of the Lockheed XFV–1 model fuselage. M, 0.85. (a) $\beta_{0.75R}$, 55°.

Figure 14.– Continued. (b) $\beta_{0.75R}$, 60°.

Figure 14.– Concluded. (c) $\beta_{0.75R}$, 65°.

Figure 15.– The effect of power on the longitudinal characteristics of the Lockheed XFV–1 model fuselage. M, 0.90. (a) $\beta_{0.75R}$, 55°.

Figure 15.– Continued. (b) $\beta_{0.75R}$, 60°.

Figure 15.– Concluded. (c) $\beta_{0.75R}$, 65°.

Figure 16.– The effect of power on the longitudinal characteristics of the Lockheed XFV–1 model fuselage. M, 0.92. (a) $\beta_{0.75R}$, 55°.

Figure 16.– Continued. (b) $\beta_{0.75R}$, 60°.

Figure 16.– Concluded. (c) $\beta_{0.75R}$, 65°.

Figure 17.– The effect of power on the longitudinal characteristics of the 1/10–scale model of the Lockheed XFV–1 airplane. M, 0.50. (a) $\beta_{0.75R}$, 50°.

Figure 17.– Concluded. (b) $\beta_{0.75R}$, 55°.

Figure 18.– The effect of power on the longitudinal characteristics of the 1/10–scale model of the Lockheed XFV–1 airplane. M, 0.70. (a) $\beta_{0.75R}$, 50°.

Figure 18.– Continued. (b) $\beta_{0.75R}$, 55°.

Figure 18.– Concluded. (c) $\beta_{0.75R}$, 60°.

Figure 19.– The effect of power on the longitudinal characteristics of the 1/10–scale model of the Lockheed XFV–1 airplane. M, 0.80. (a) $\beta_{0.75R}$, 50°.

Figure 19.– Continued. (b) $\beta_{0.75R}$, 55°.

Figure 19.– Concluded. (c) $\beta_{0.75R}$, 60°.

Figure 20.– The effect of power on the longitudinal characteristics of the 1/10–scale model of the Lockheed XFV–1 airplane. M, 0.85. (a) $\beta_{0.75R}$, 55°.

Figure 20.– Concluded. (b) $\beta_{0.75R}$, 60°.

Figure 21.– The effect of power on the longitudinal characteristics of the 1/10–scale model of the Lockheed XFV–1 airplane. M, 0.90. $\beta_{0.75R}$, 60°.

Figure 22.– The effect of power on the longitudinal characteristics of the 1/10–scale model of the Lockheed XFV–1 airplane. M, 0.92. $\beta_{0.75R}$, 60°.

Figure 23.– The effect of power on the longitudinal characteristics of the 1/10–scale model of the Lockheed XFV–1 airplane, tail off. $\beta_{0.75R}$, 55°. (a) M, 0.50.

Figure 23.– Continued. (b) M, 0.70.

Figure 23.– Continued. (c) M, 0.80.

Figure 23.– Continued. (d) M, 0.85.

Figure 23.– Continued. (e) M, 0.90.

Figure 23.– Concluded. (f) M, 0.92.

Figure 24.– Longitudinal–control characteristics of the 1/10–scale model of the Lockheed XFV–1 airplane. (a) M, 0.50.

Figure 24.– Continued. (b) M, 0.70.

Figure 24.– Continued. (c) M, 0.80.

Figure 24.– Continued. (d) M, 0.85.

Figure 24.– Continued. (e) M, 0.90.

Figure 24.– Concluded. (f) M, 0.92.

Figure 25.– The effect of power on the simulated yaw characteristics of the 1/10–scale model of the Lockheed XFV–1 airplane. $\beta_{0.75R}$, 55°.

Figure 26.– Roll characteristics of the 1/10–scale model of the Lockheed XFV–1 airplane. ψ, 0°.

Figure 27.– The longitudinal characteristics of several combinations of model components. Propeller removed. (a) M, 0.50.

Figure 27.– Continued. (b) M, 0.70.

Figure 27.– Continued. (c) M, 0.80.

Figure 27.– Continued. (d) M, 0.85.

Figure 27.– Continued. (e) M, 0.90.

Figure 27.– Concluded. (f) M, 0.92.

Figure 28.– The longitudinal characteristics of the body alone, the body and tail, and the body and cab. Propeller removed. (a) M, 0.50.

Figure 28.– Continued. (b) M, 0.70.

Figure 28.– Continued. (c) M, 0.80.

Figure 28.– Continued. (d) M, 0.85.

Figure 28.– Continued. (e) M, 0.90.

Figure 28.– Concluded. (f) M, 0.92.

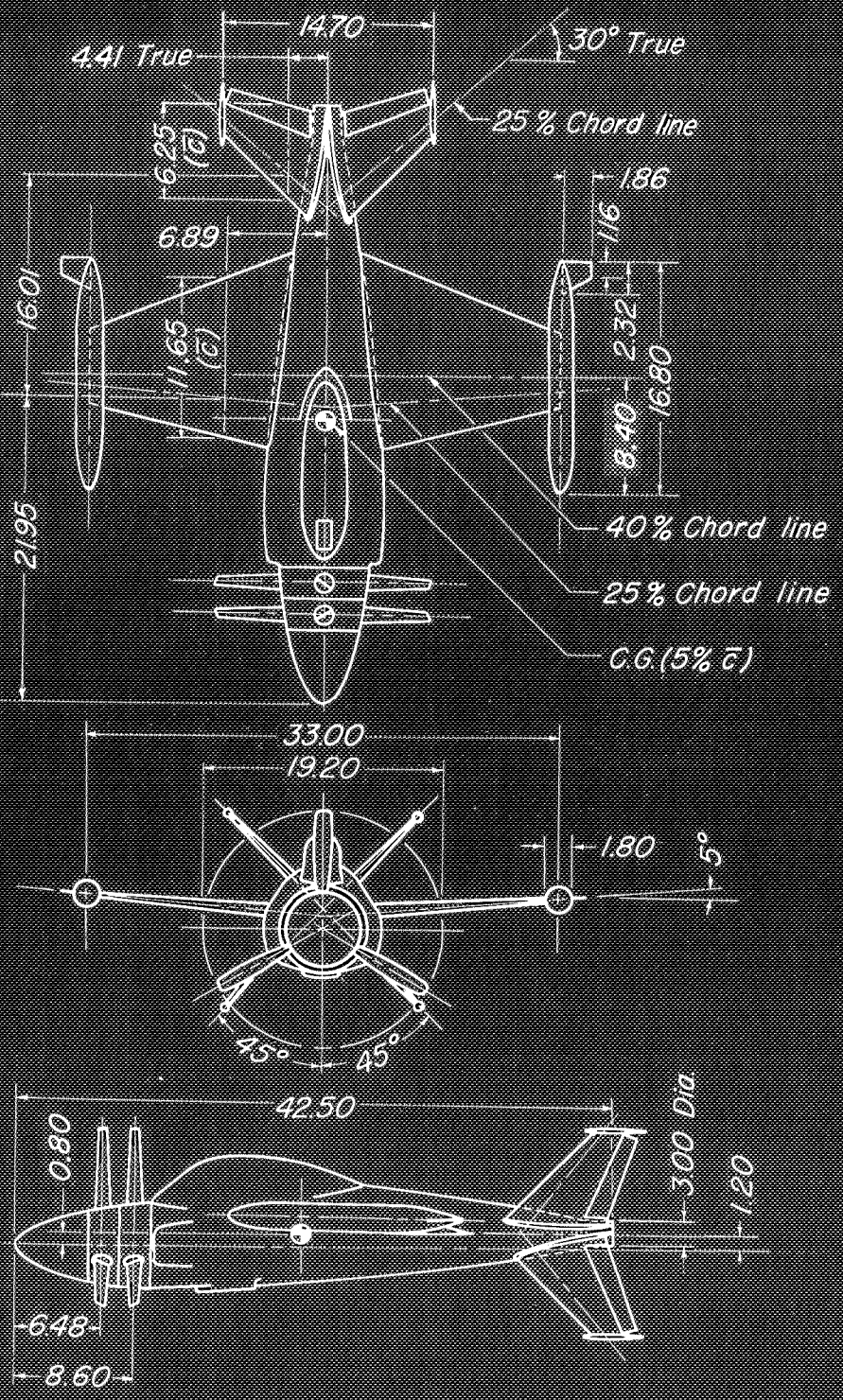

All dimensions in inches

Figure 1. — Three-view drawing of the 1/10-scale model of the Lockheed XFV-1 airplane.

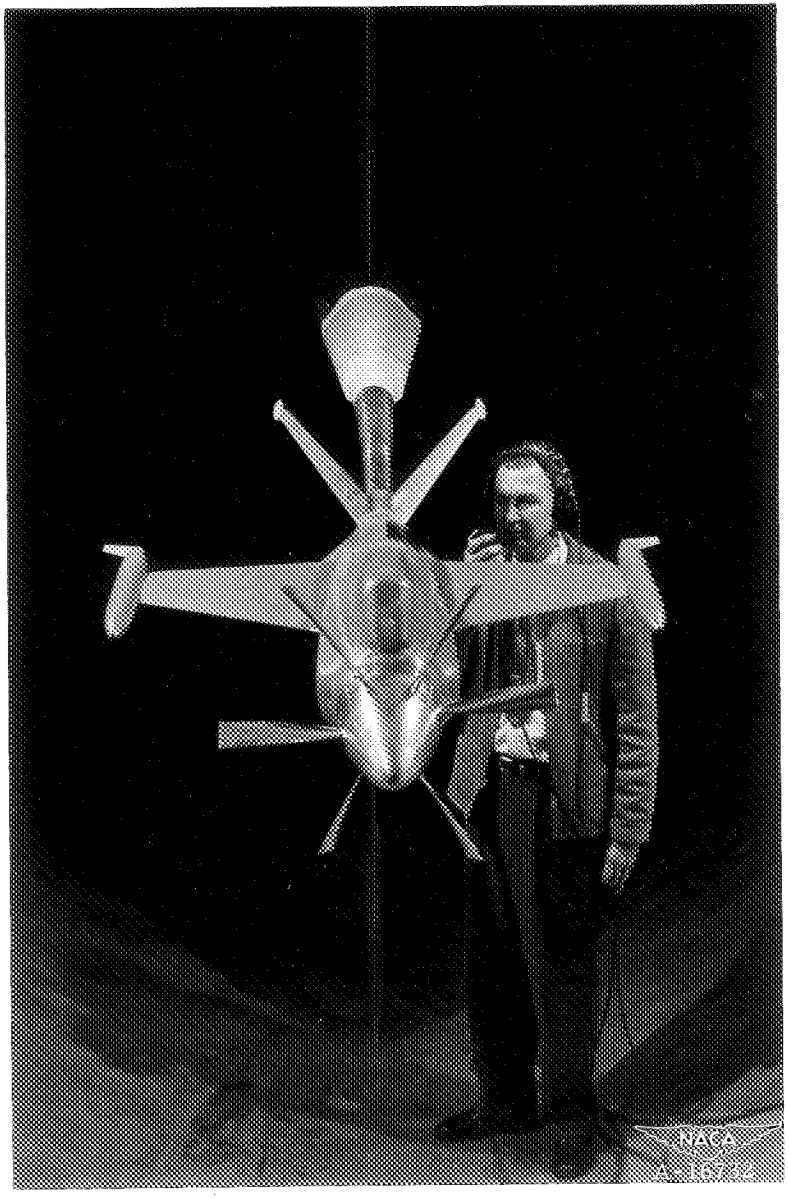

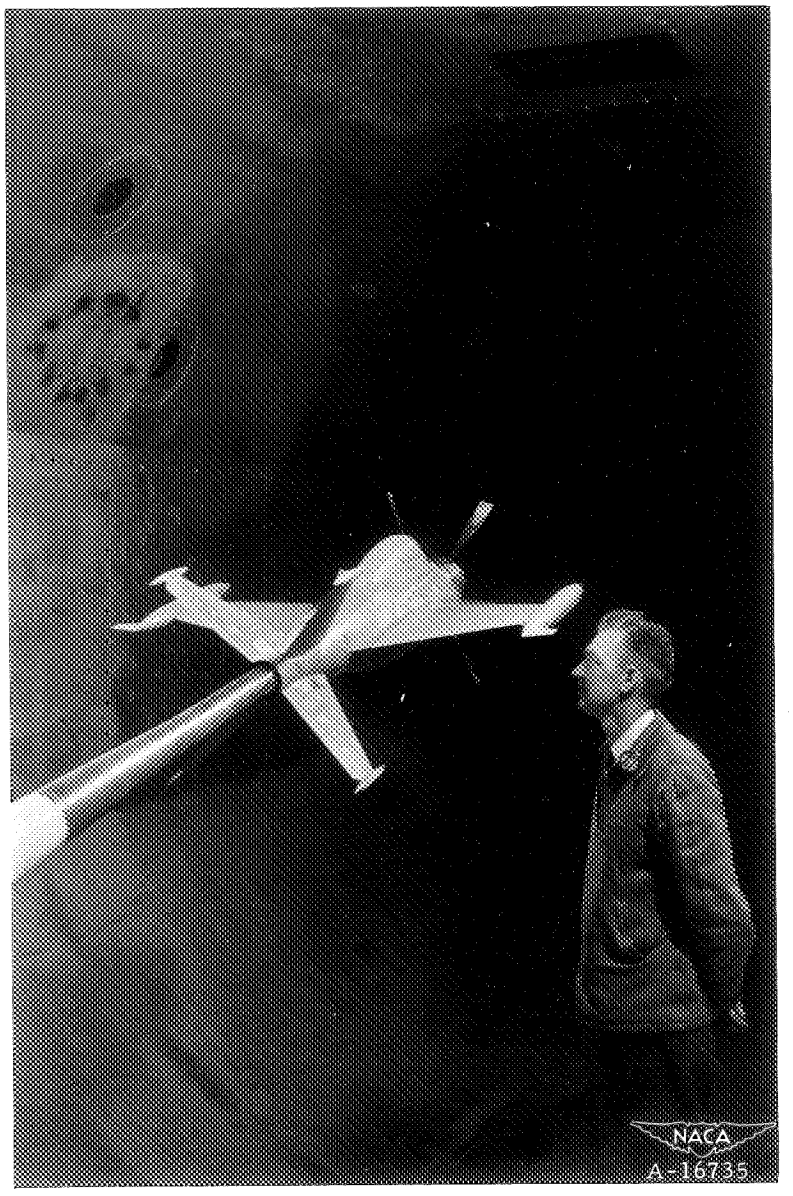

Figure 2.- The 1/10-scale model of the Lockheed XFV-1 airplane in the Ames 12-foot pressure wind tunnel.

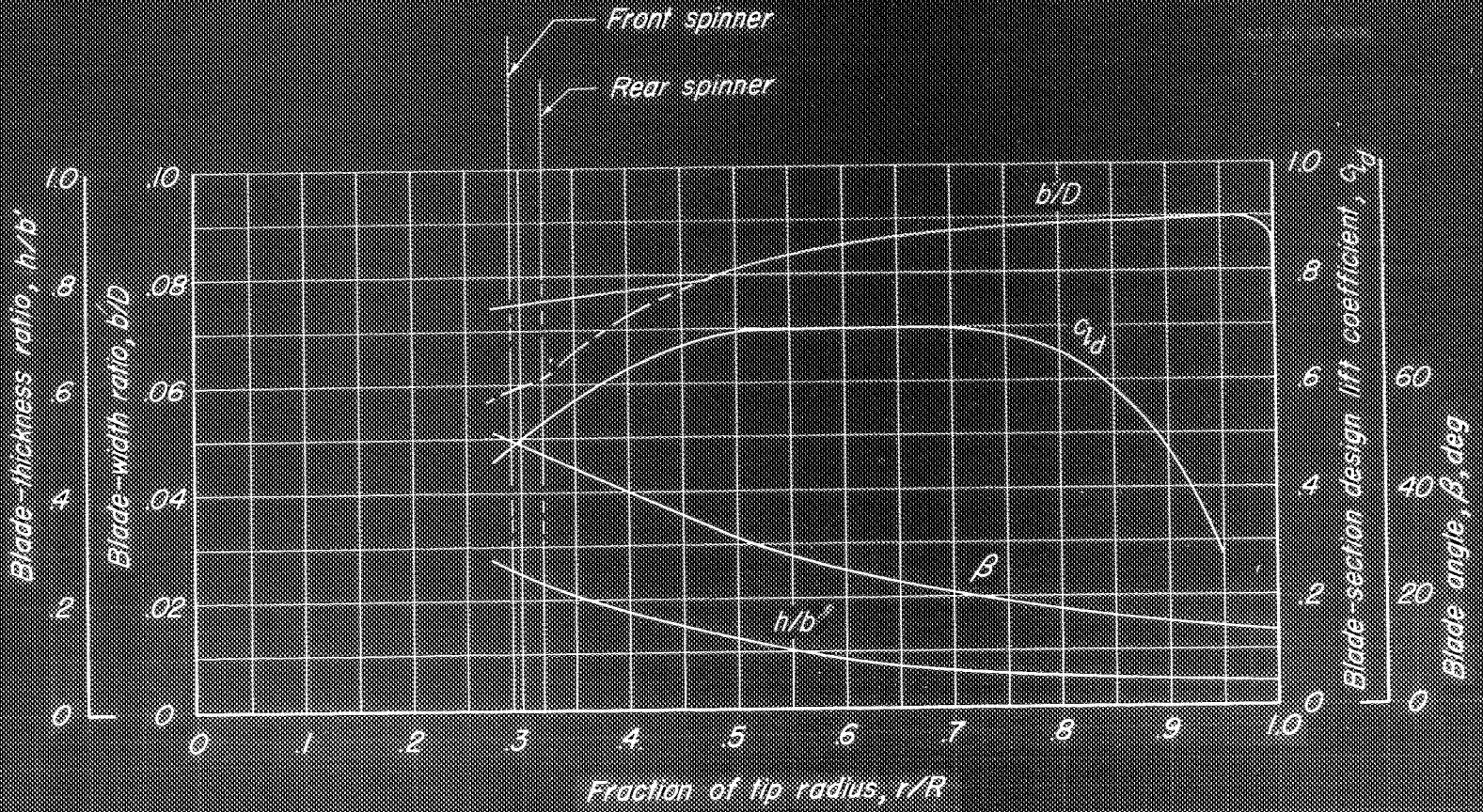

Figure 3.— Plan-form and blade-form curves for the Curtiss 1058-1059-XG-4 dual-rotating propeller.

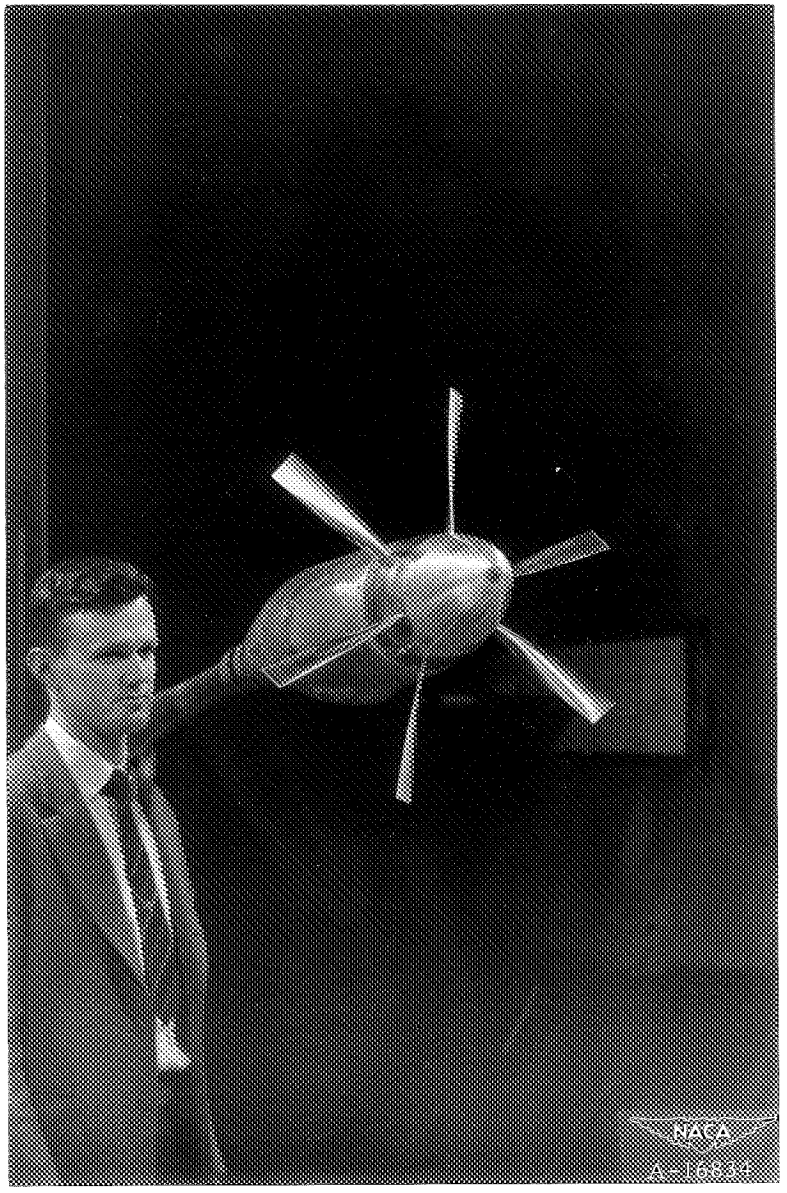

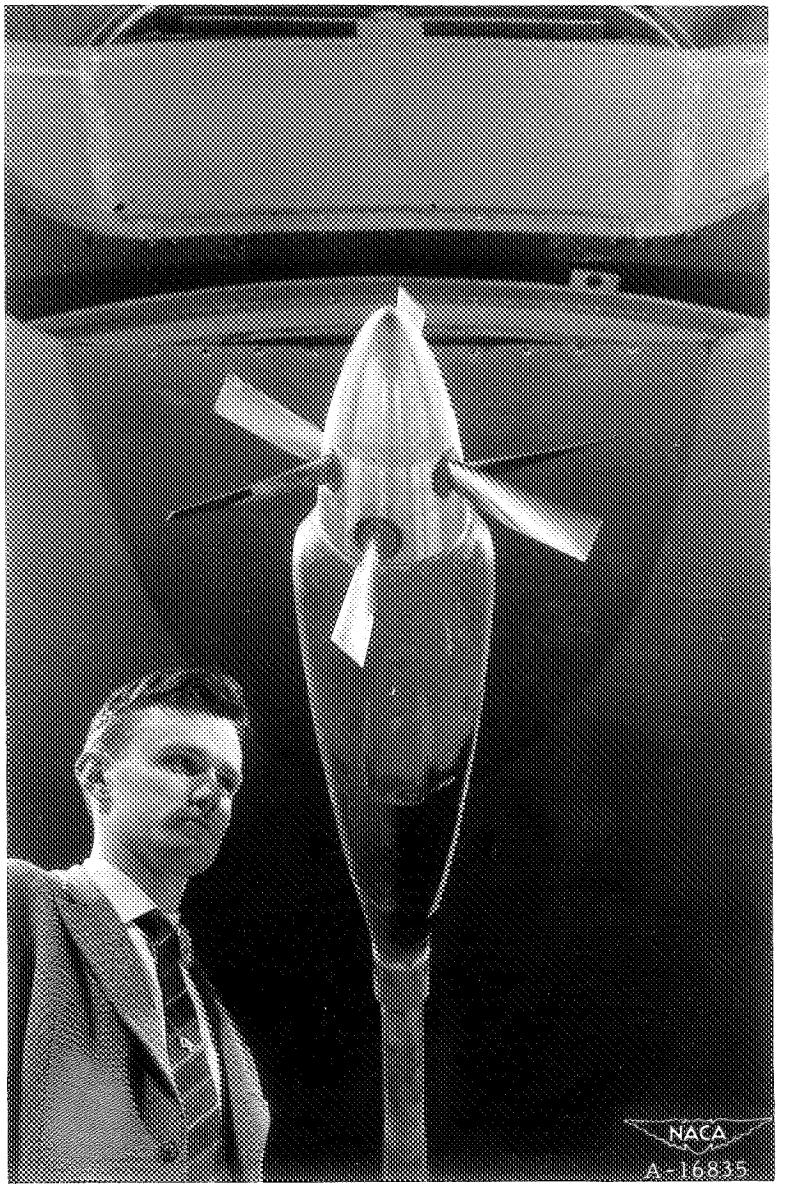

Figure 4.- The 1/10-scale model of the Curtiss 1058-1059-XC-4 propeller in the Ames 12-foot pressure wind tunnel.

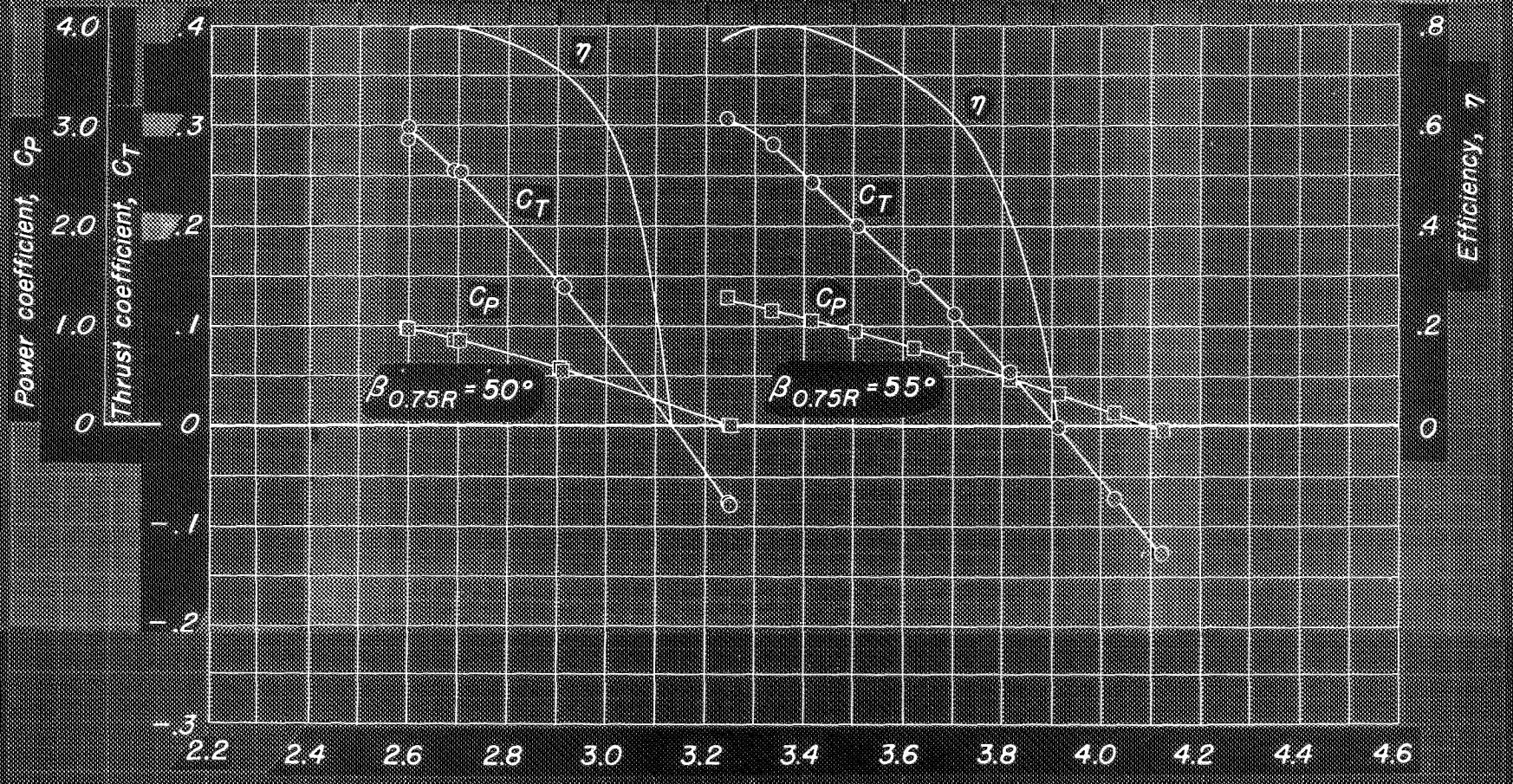

(a) α, 0°

CONFIDENTIAL

NATIONAL ADVISORY COMMITTEE FOR AERONAUTICS

Figure 5.— Characteristics of the Curtiss 1058-1059-XC-4 dual-rotating propeller. M, 0.50.

(b) α, 4°

Figure 5.- Continued.

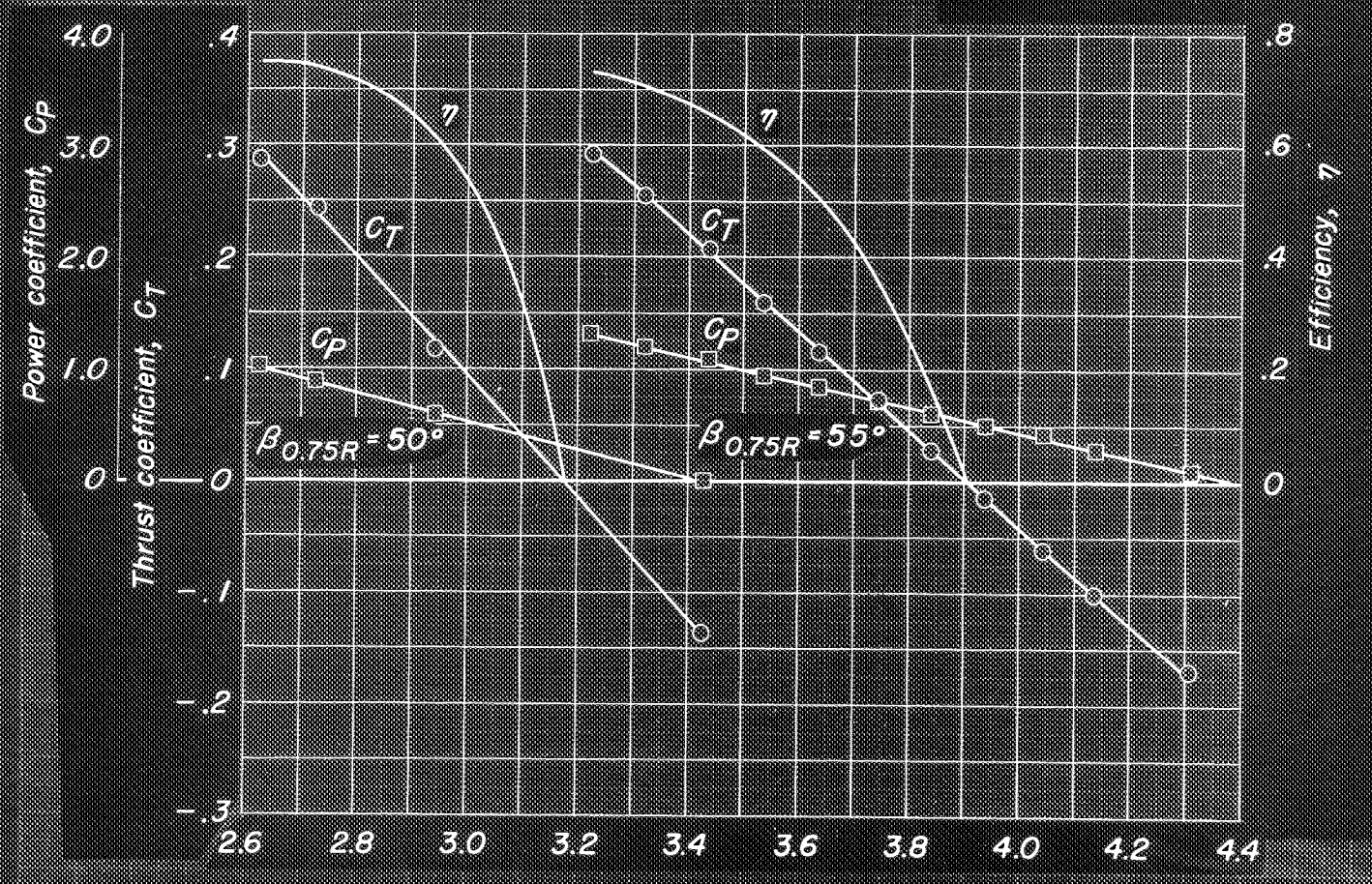

(c) α, 8°

Figure 5.- Continued.

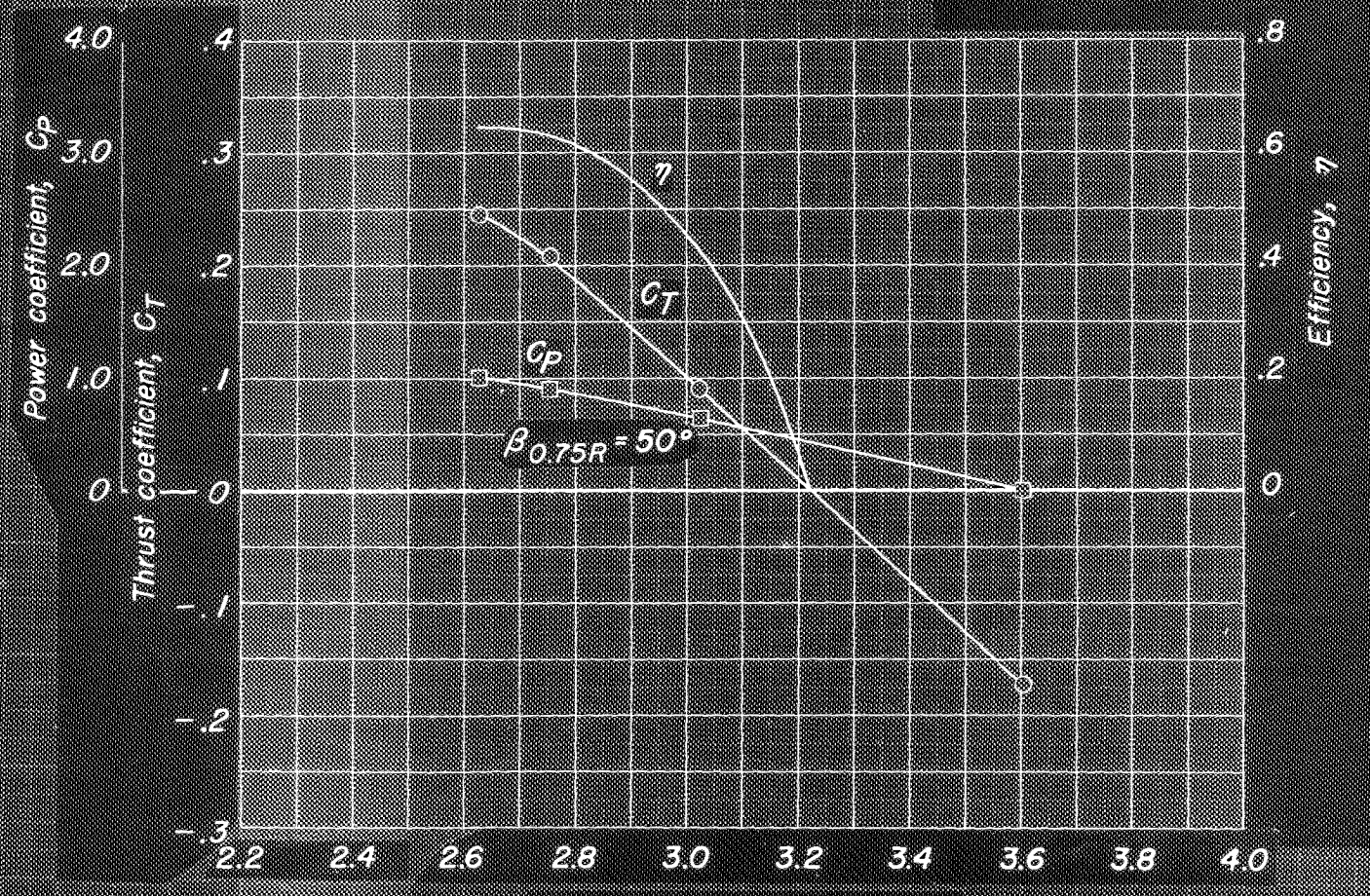

(d) α, 12°

Figure 5.- Continued.

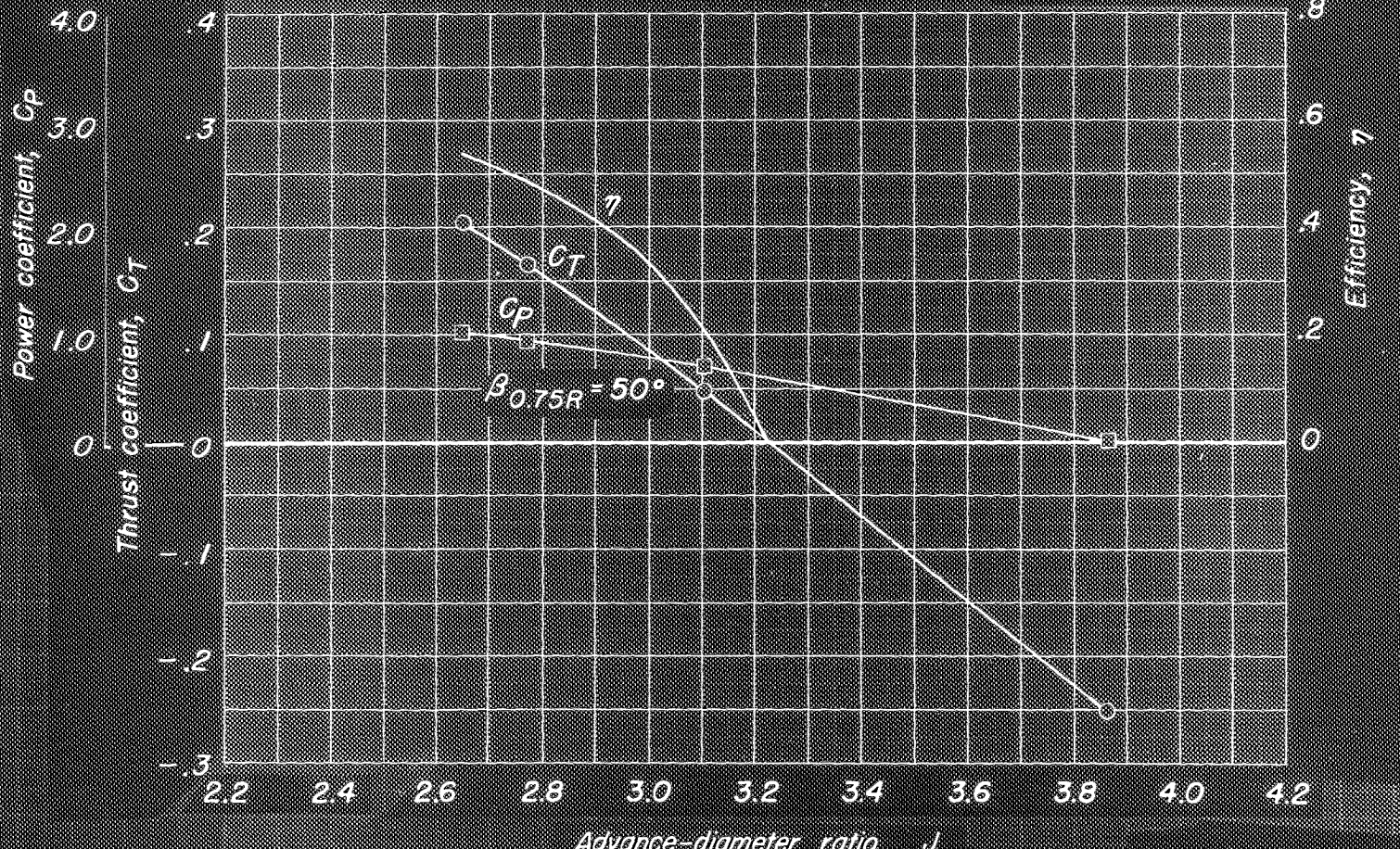

(e) α, 16°

Figure 5.- Concluded.

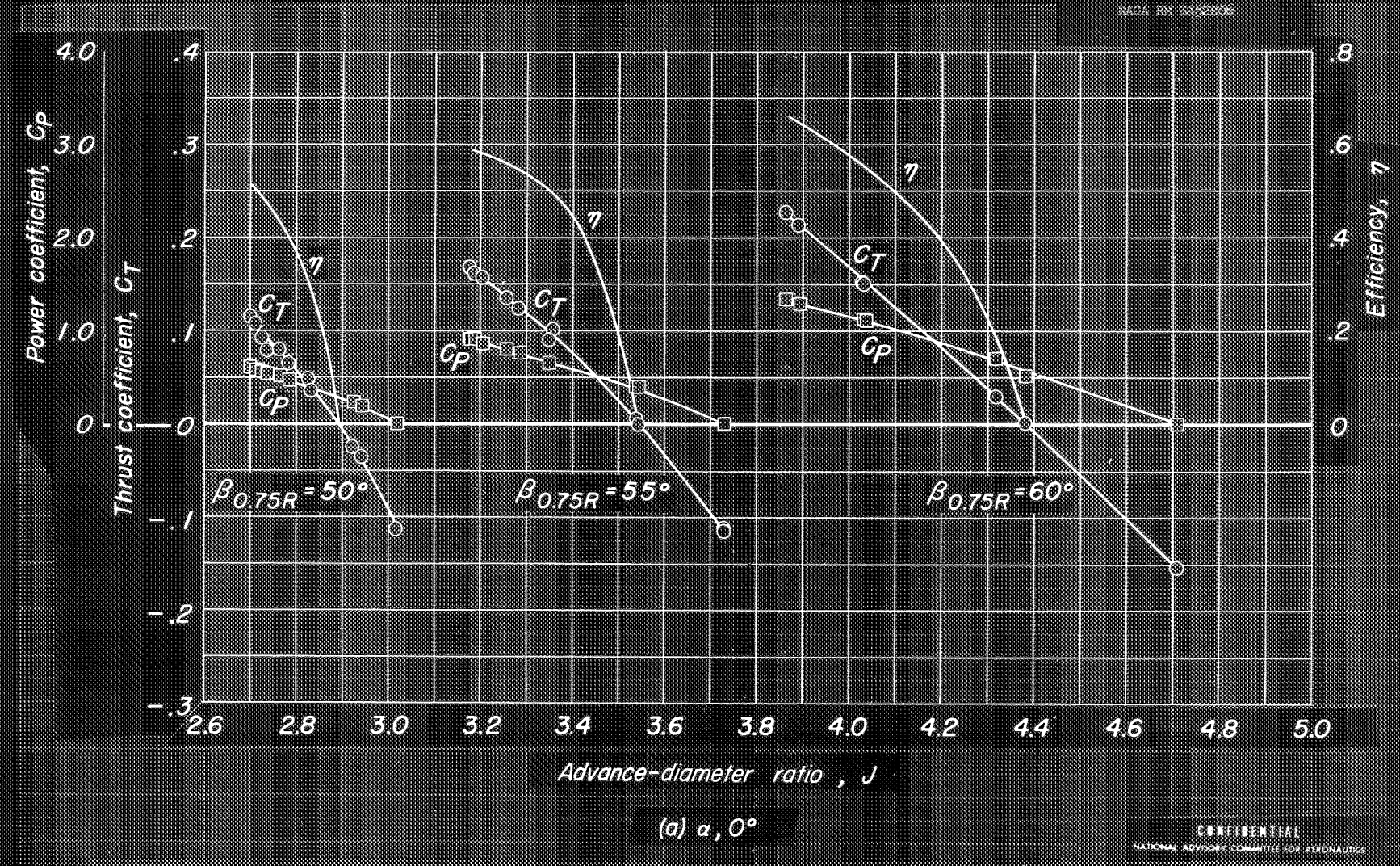

Figure 6.— Characteristics of the Curtiss 1058-1059-XC-4 dual-rotating propeller. M, 0.70.

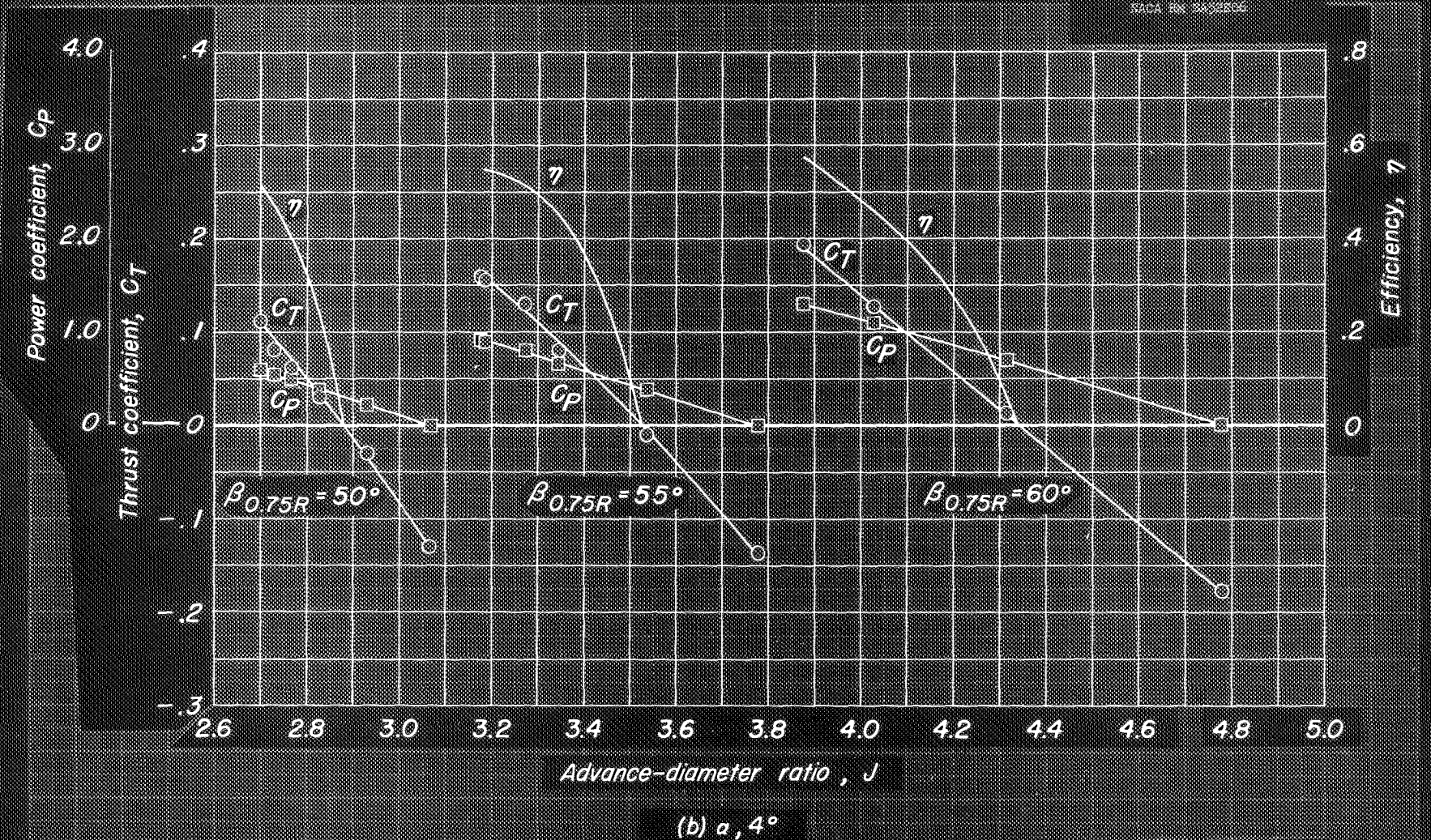

(b) α, 4°

Figure 6.- Continued.

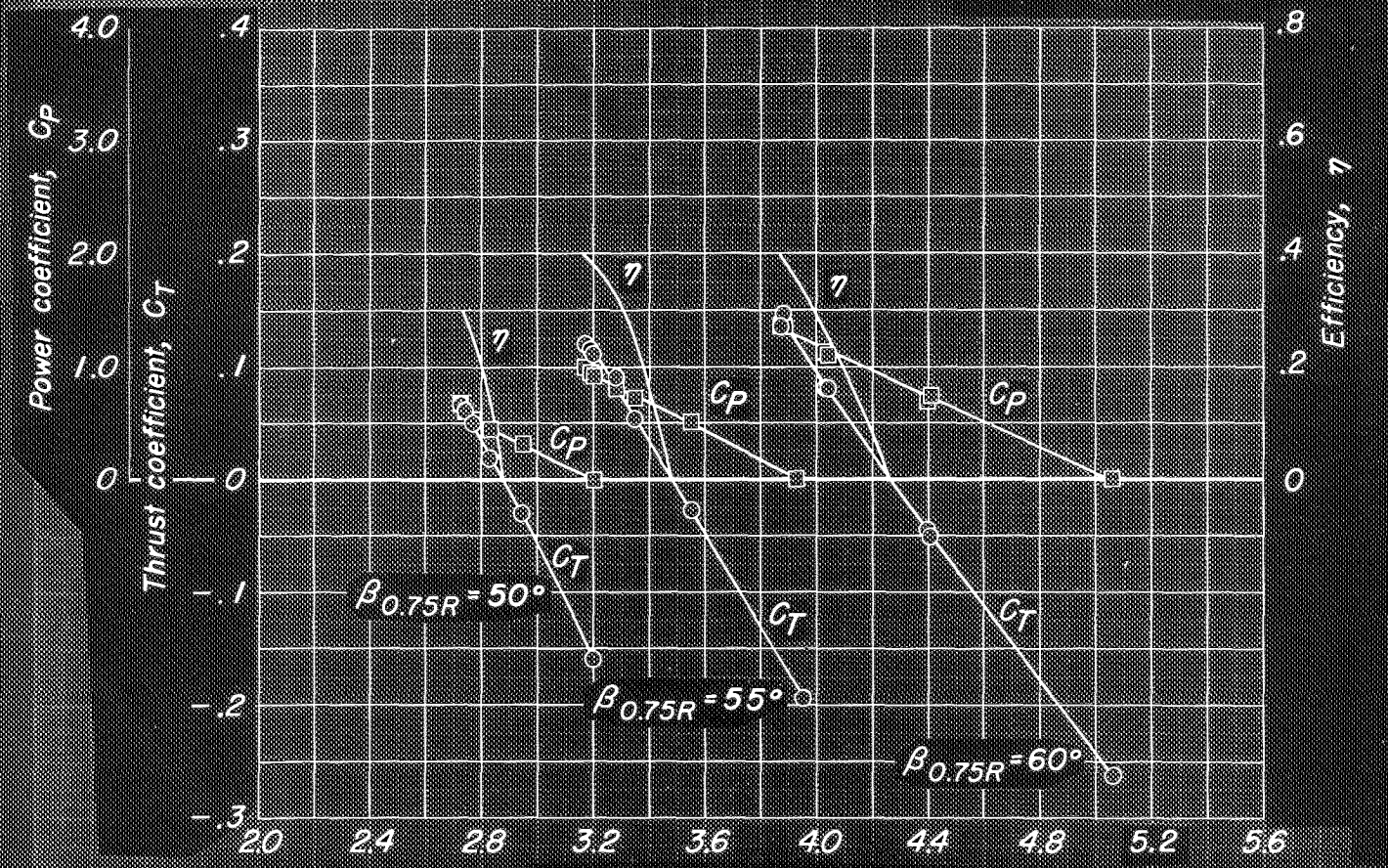

(c) α, 8°

Figure 6.- Continued.

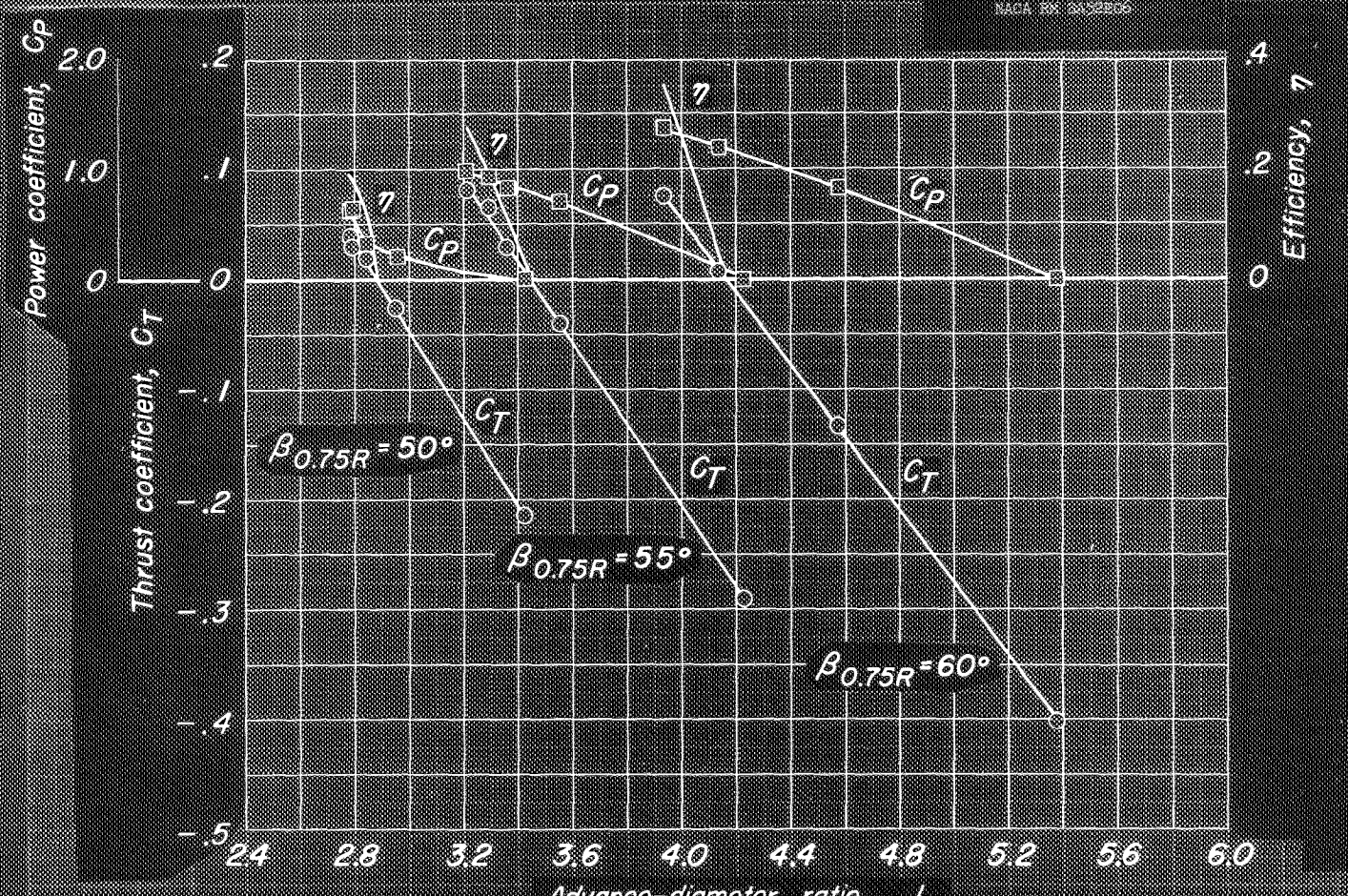

(d) α, 12°

Figure 6.- Concluded.

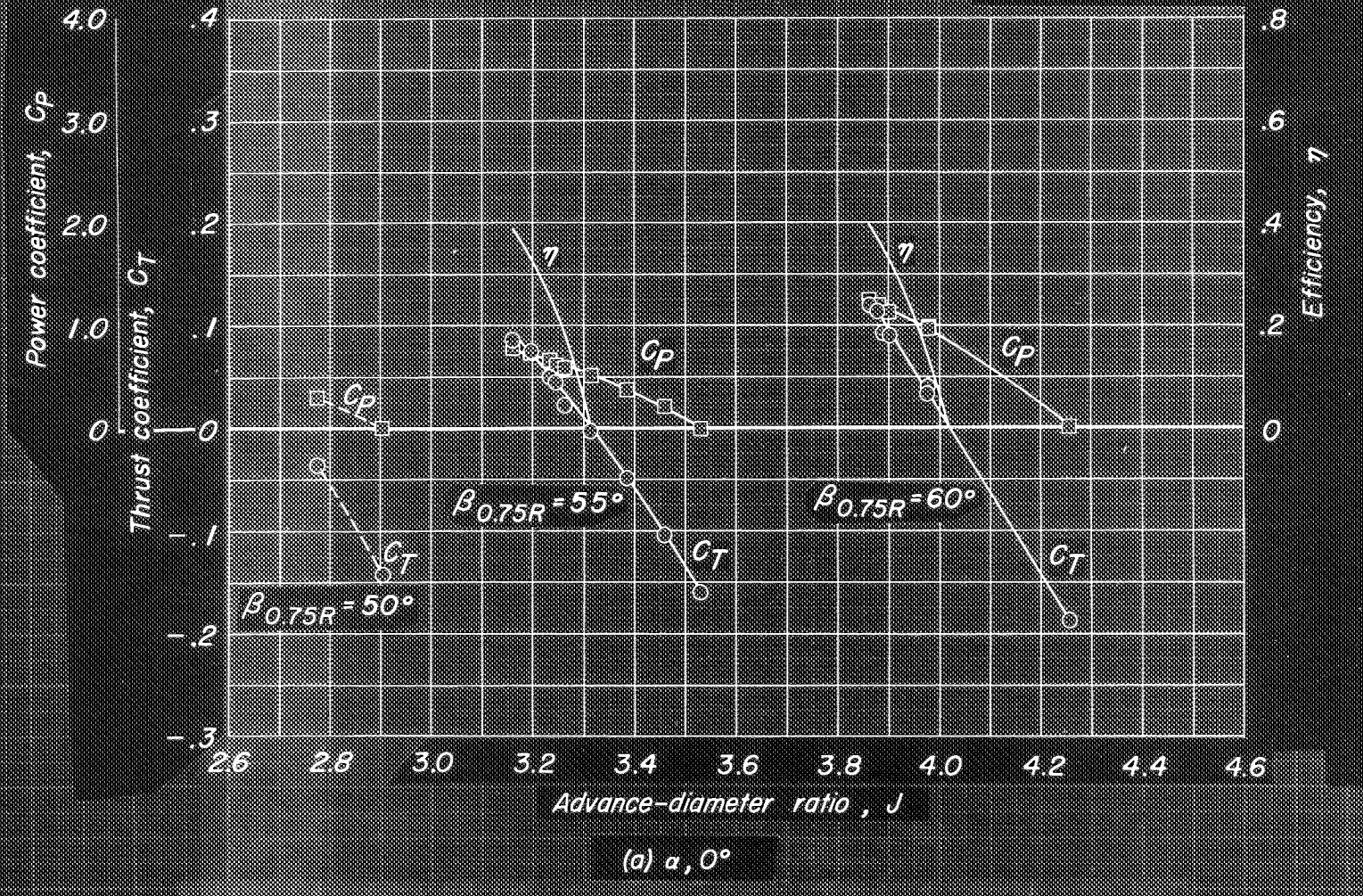

(a) α, 0°

Figure 7.—Characteristics of the Curtiss 1058-1059-XC-4 dual-rotating propeller. M, 0.80.

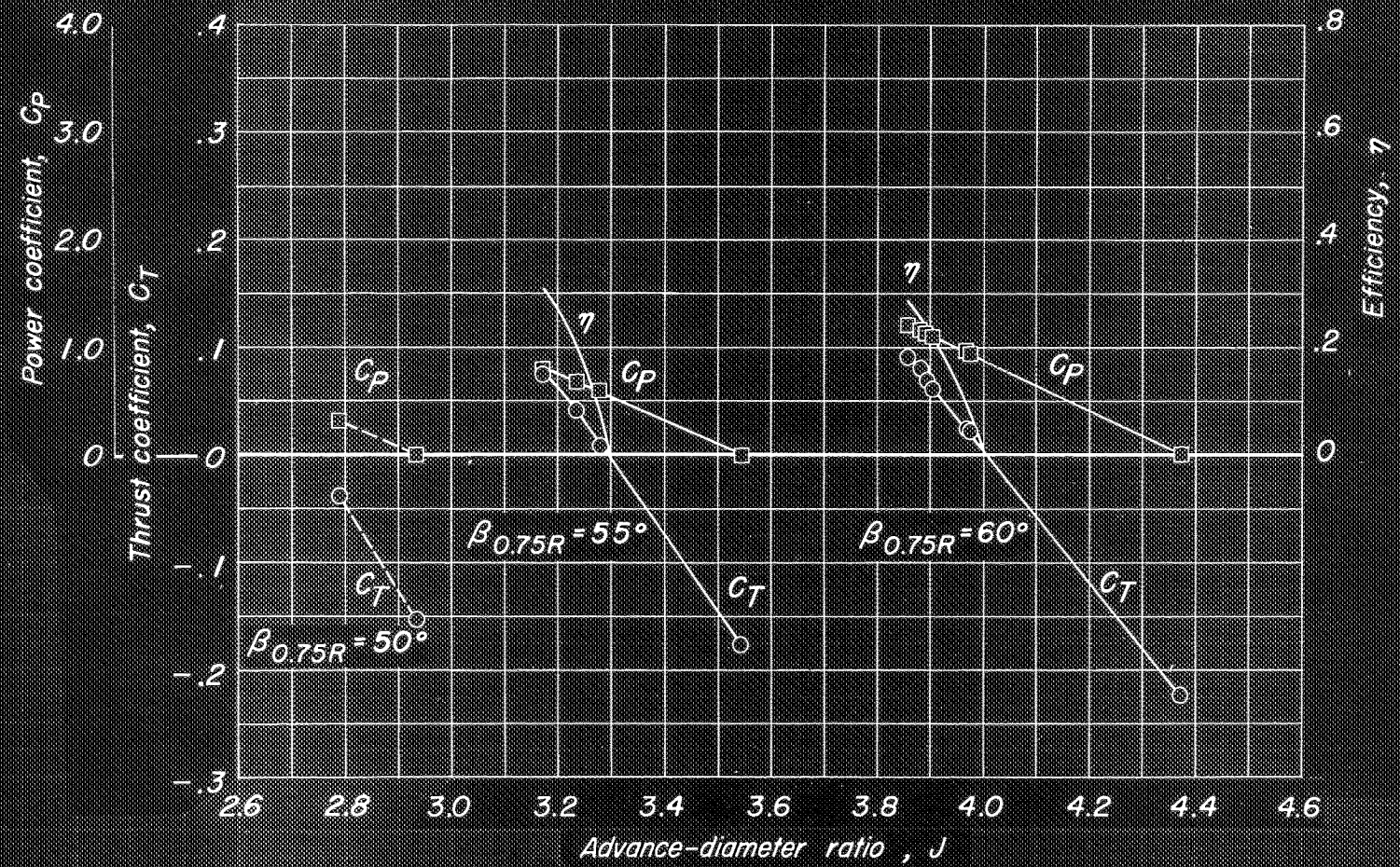

(b) α, 4°

CONFIDENTIAL
NATIONAL ADVISORY COMMITTEE FOR AERONAUTICS

Figure 7.- Continued.

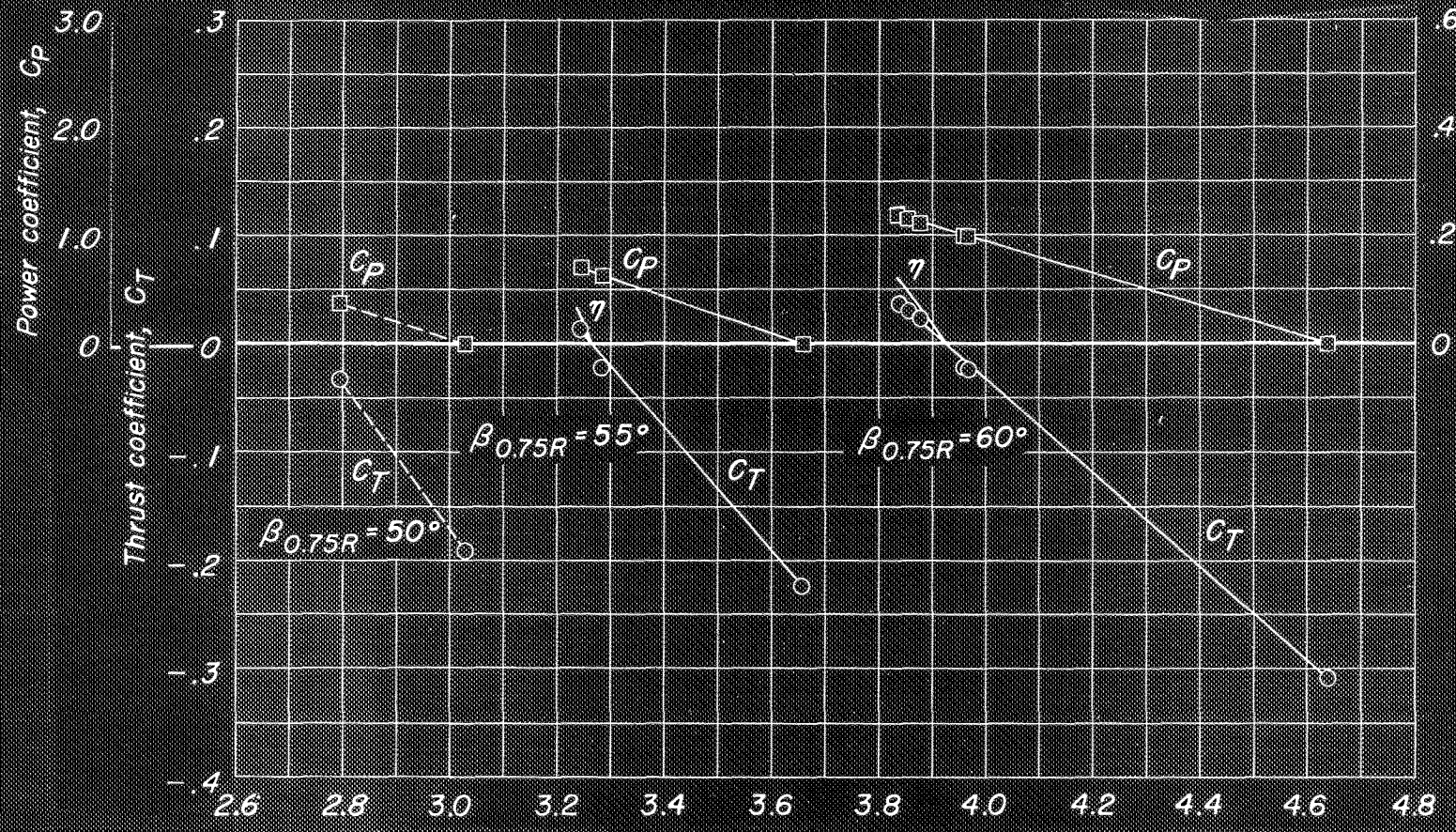

(c) α, 8°

Figure 7.- Concluded.

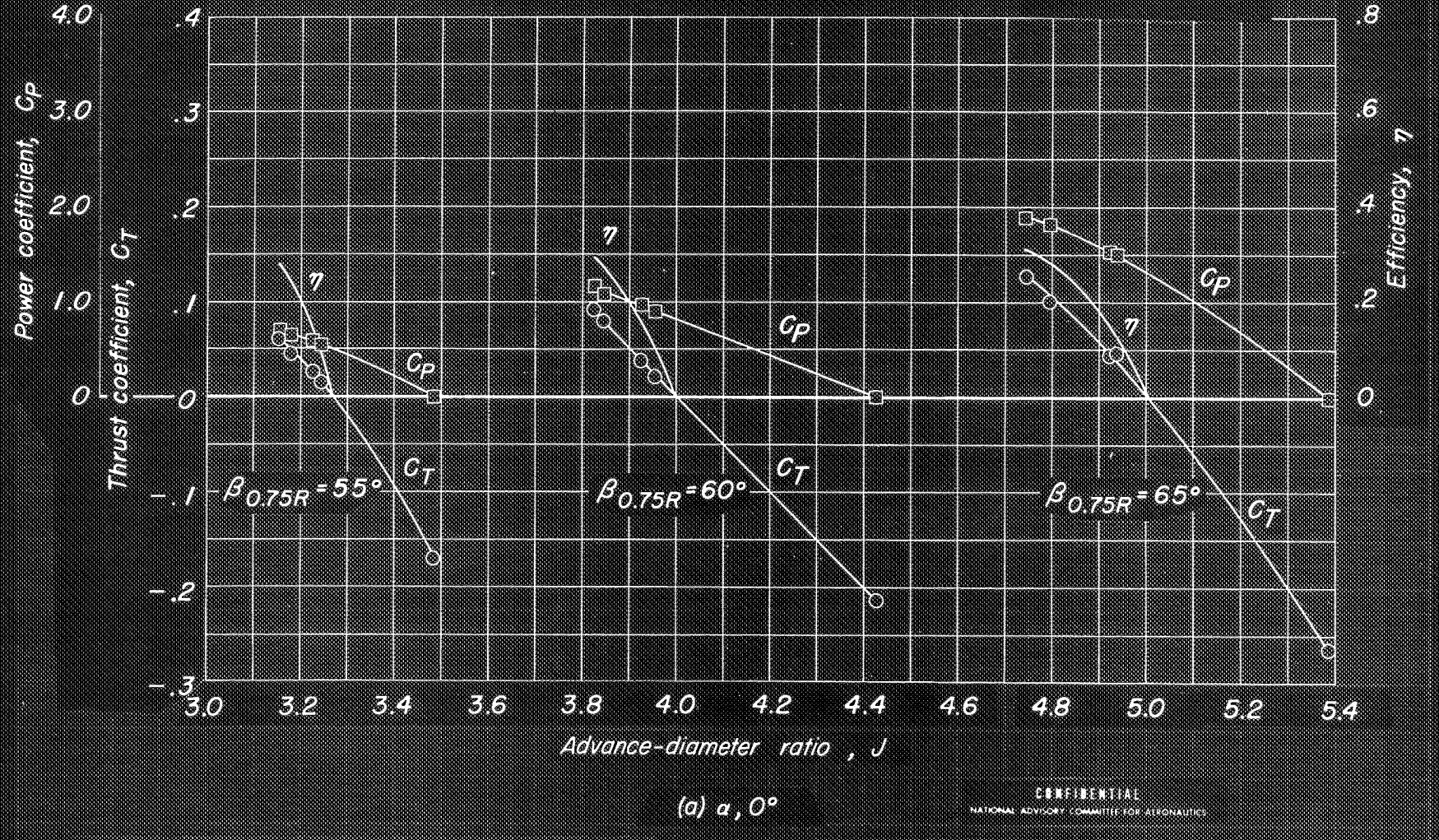

(a) α, 0°

CONFIDENTIAL
NATIONAL ADVISORY COMMITTEE FOR AERONAUTICS

Figure 8.— Characteristics of the Curtiss 1058-1059-XC-4 dual-rotating propeller. M, 0.85.

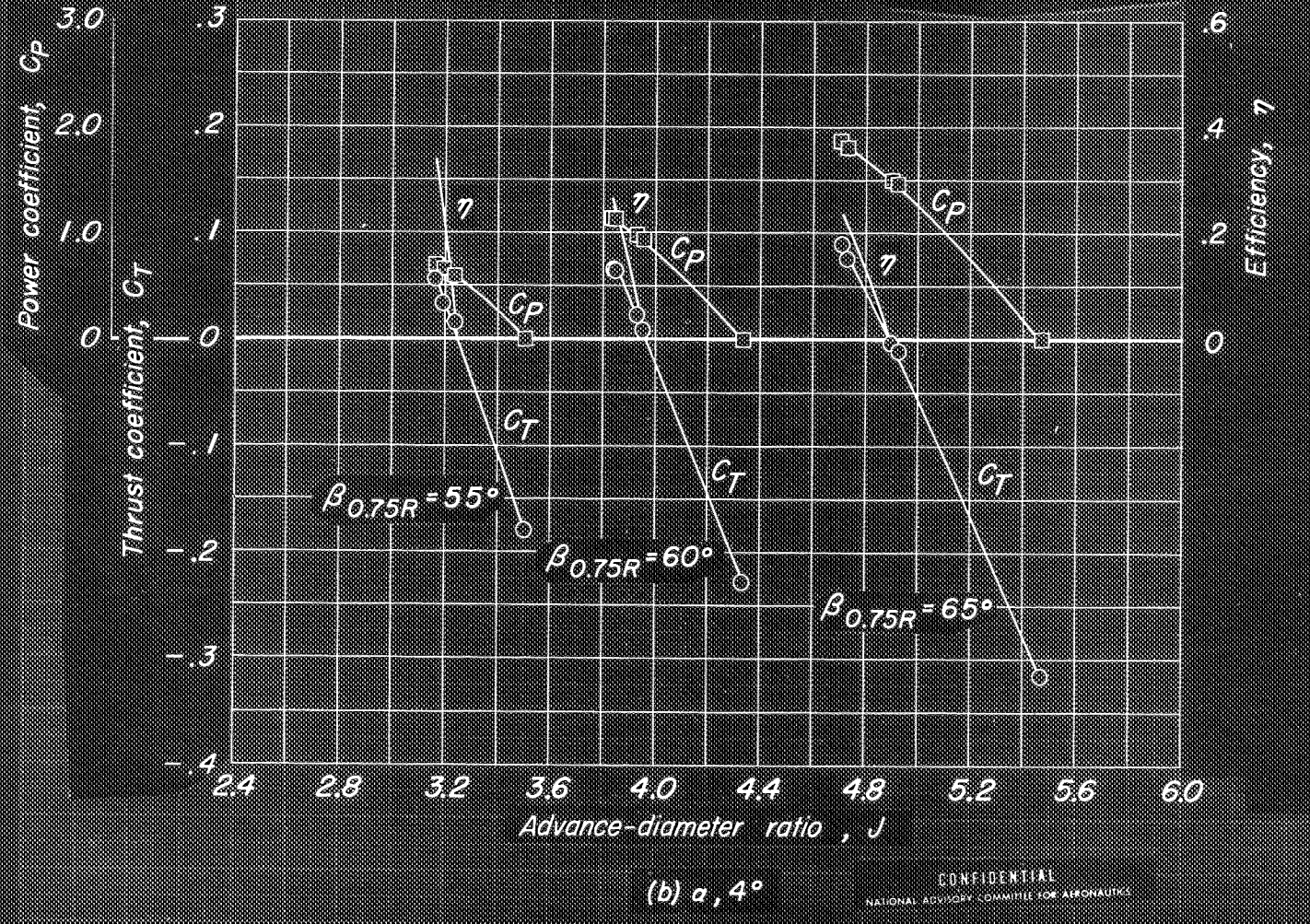

(b) α, 4°

Figure 8.- Continued.

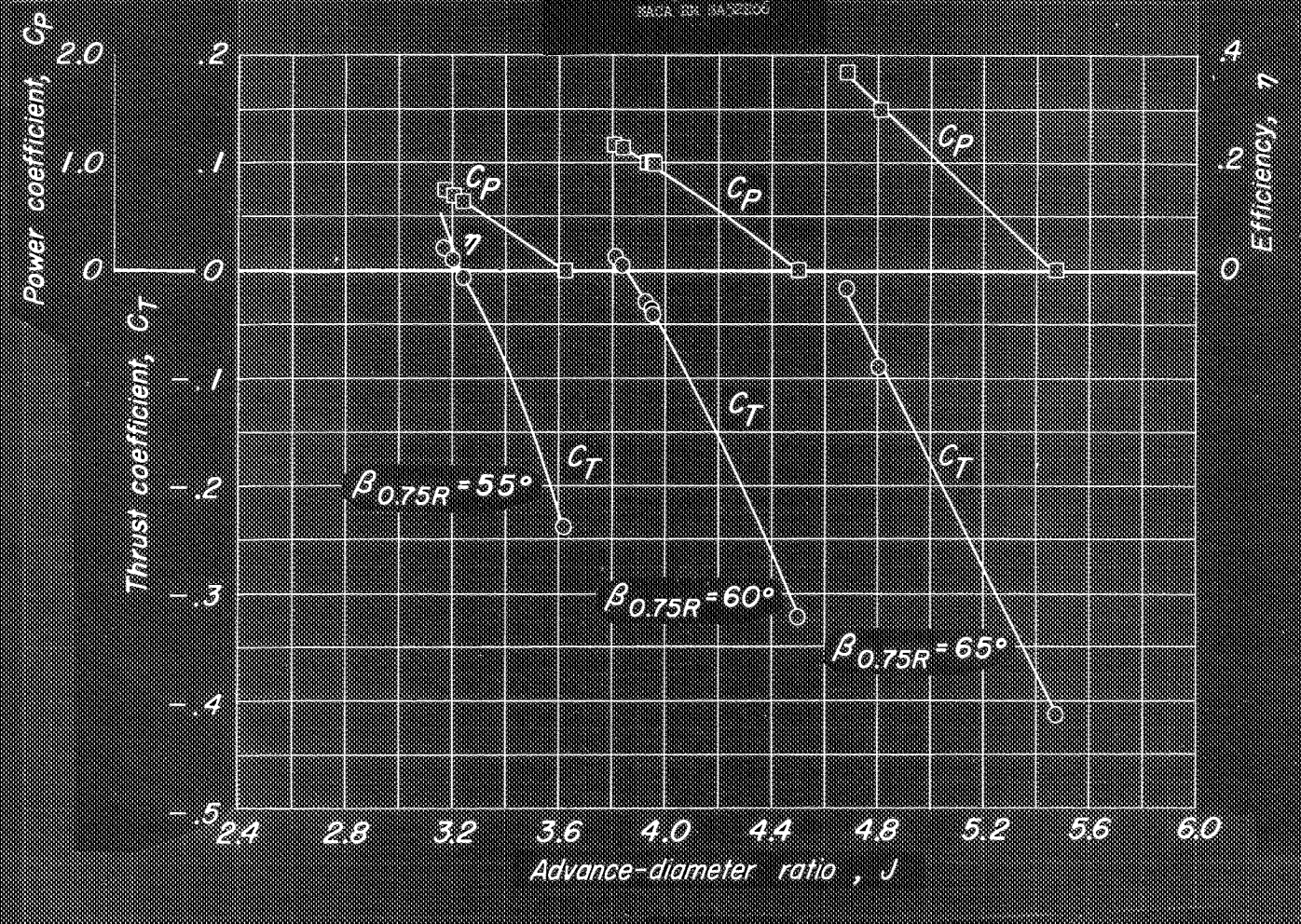

(c) α, 8°

Figure 8.- Concluded.

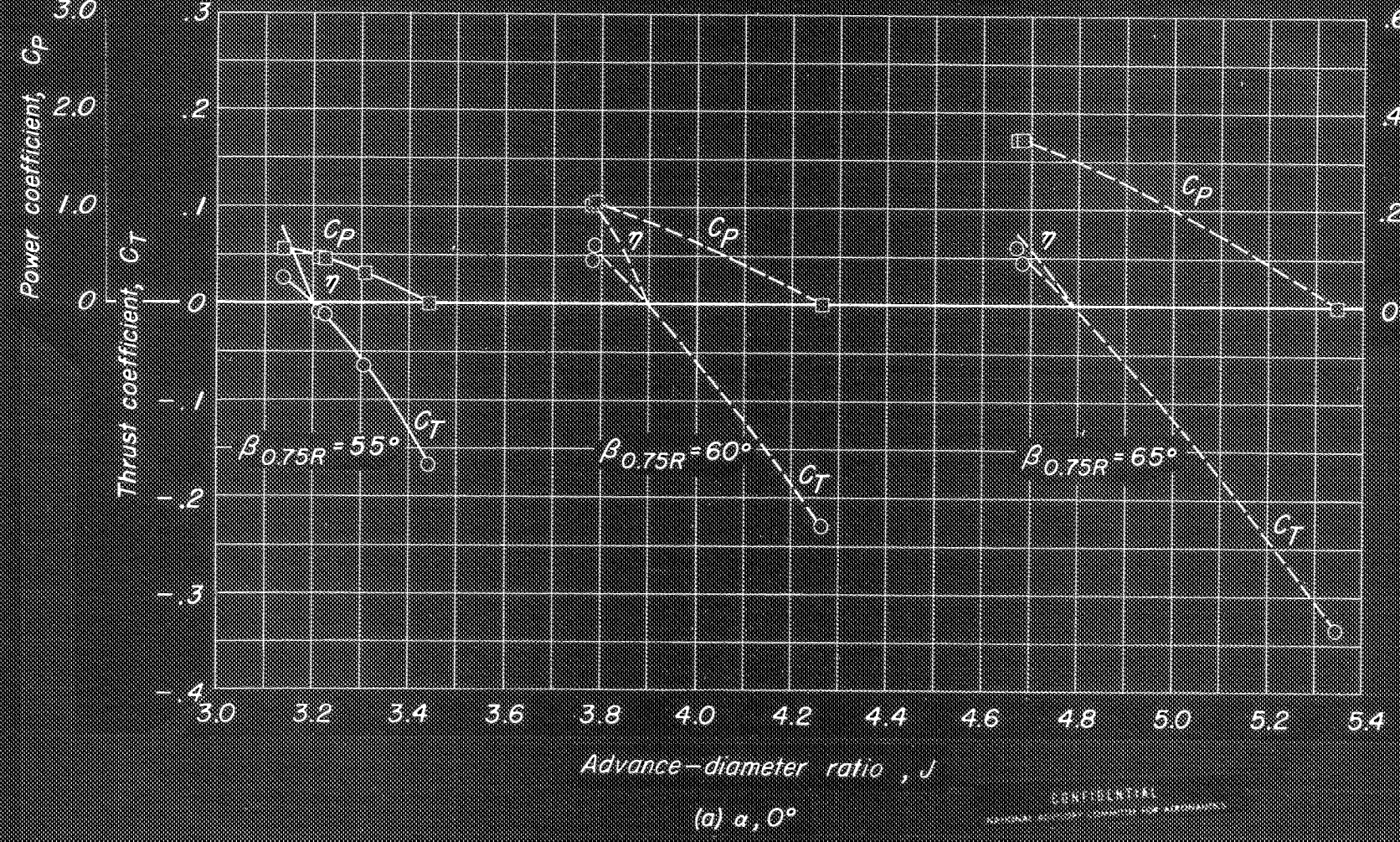

Figure 9. — Characteristics of the Curtiss 1058–1059–XC–4 dual-rotating propeller. M, 0.90.

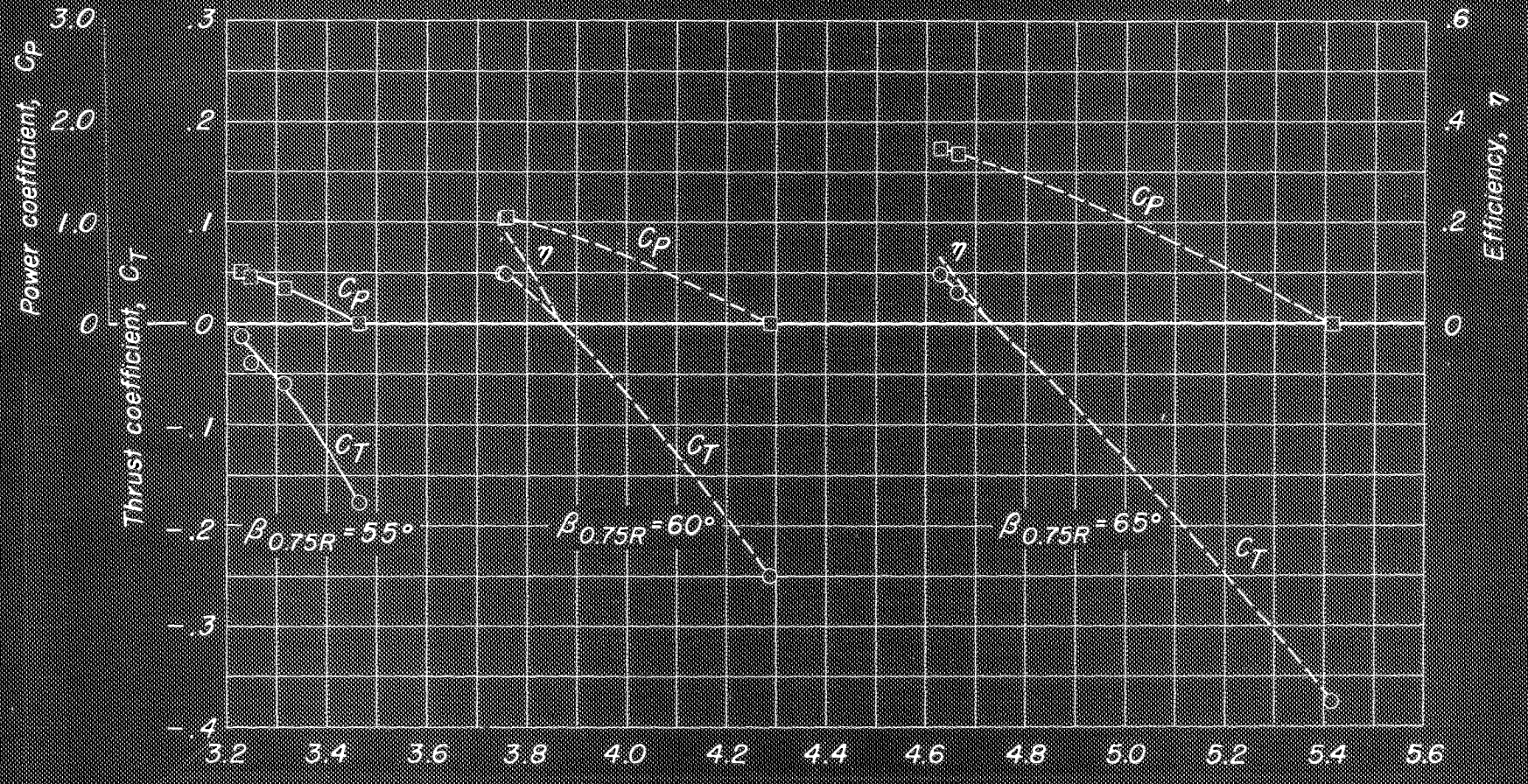

(b) α, 4°

Figure 9.- Continued.

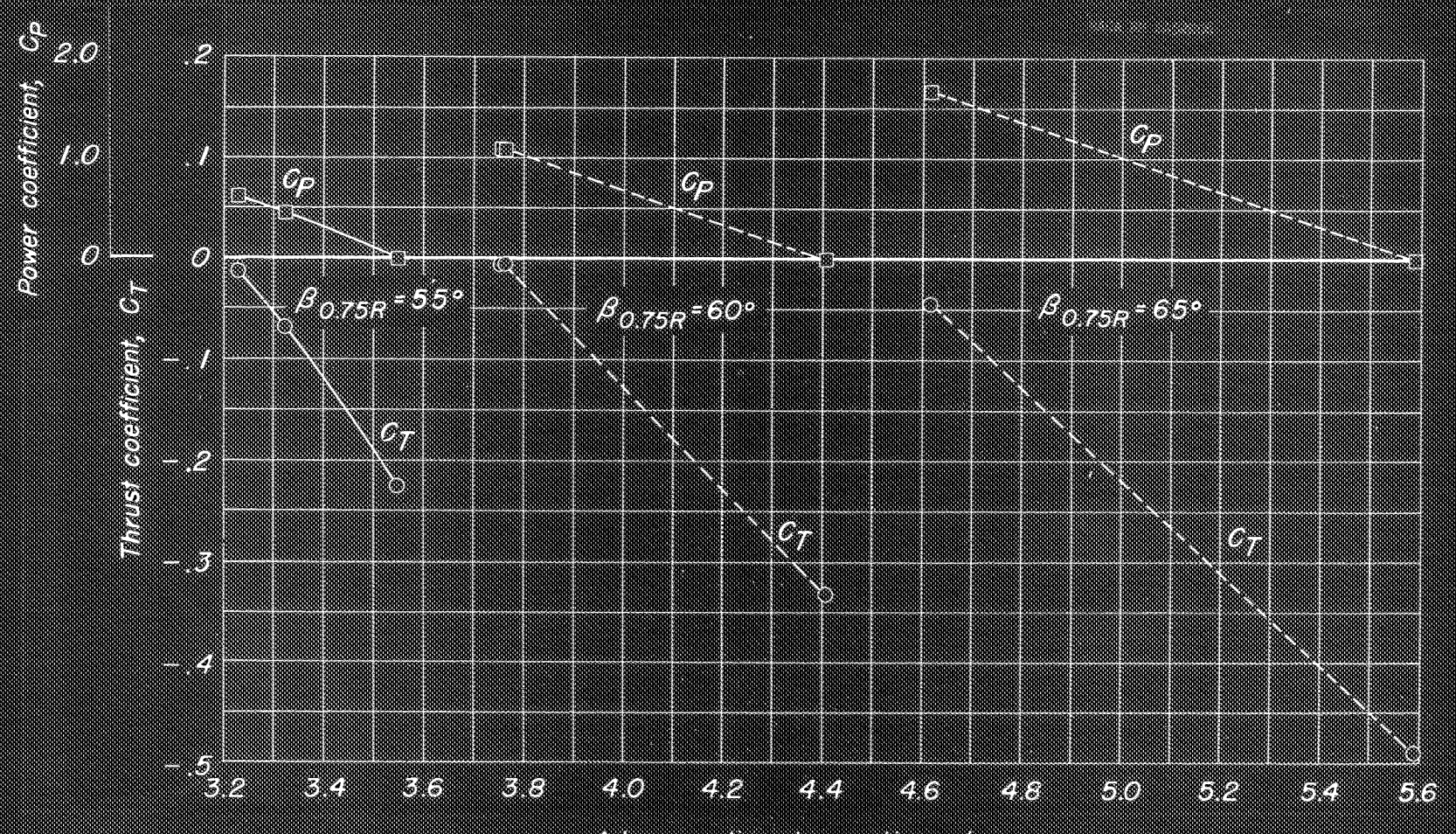

(c) α, 8°

Figure 9.- Concluded.

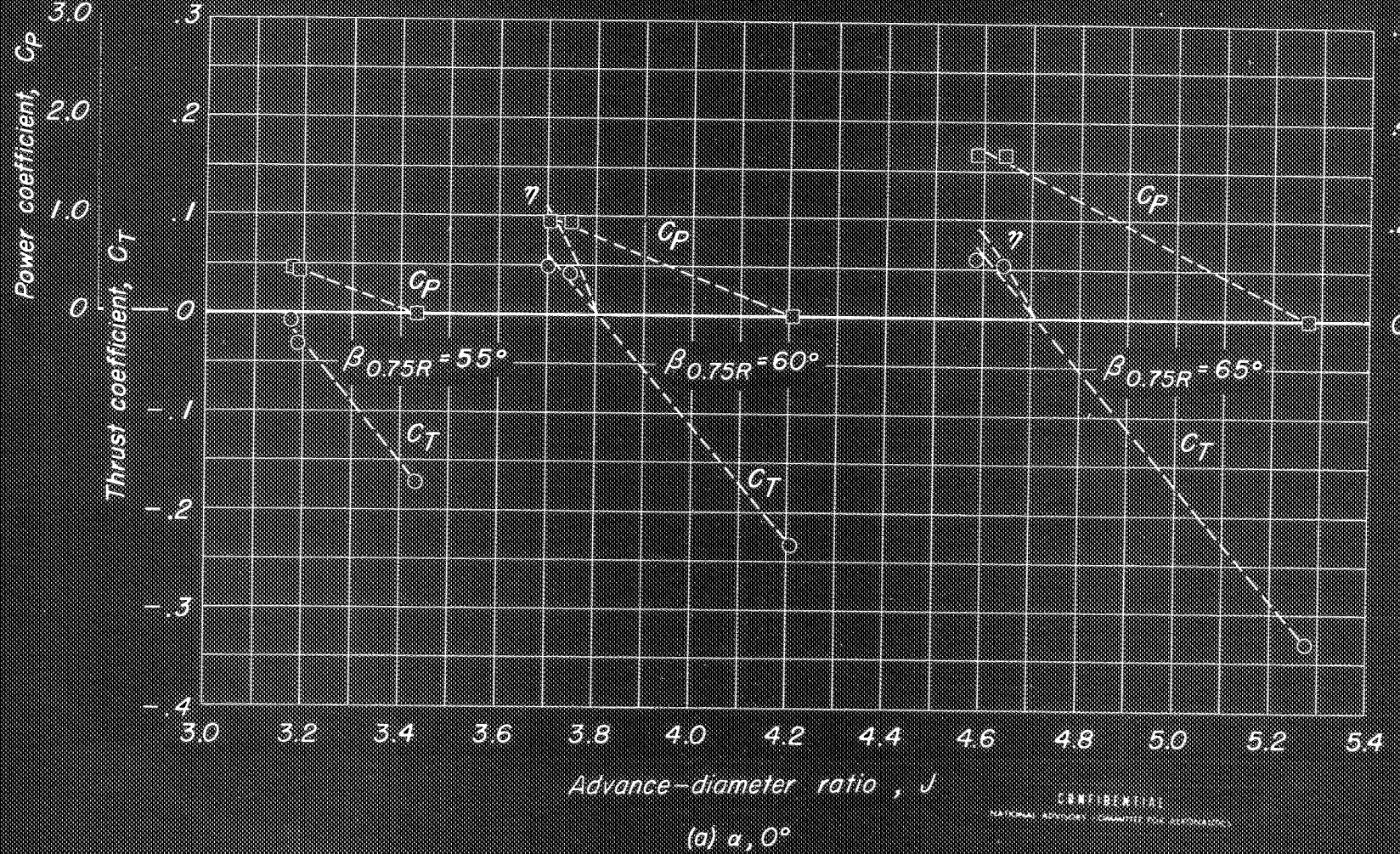

(a) α, 0°

Figure 10.– Characteristics of the Curtiss 1058-1059-XC-4 dual-rotating propeller. M, 0.92.

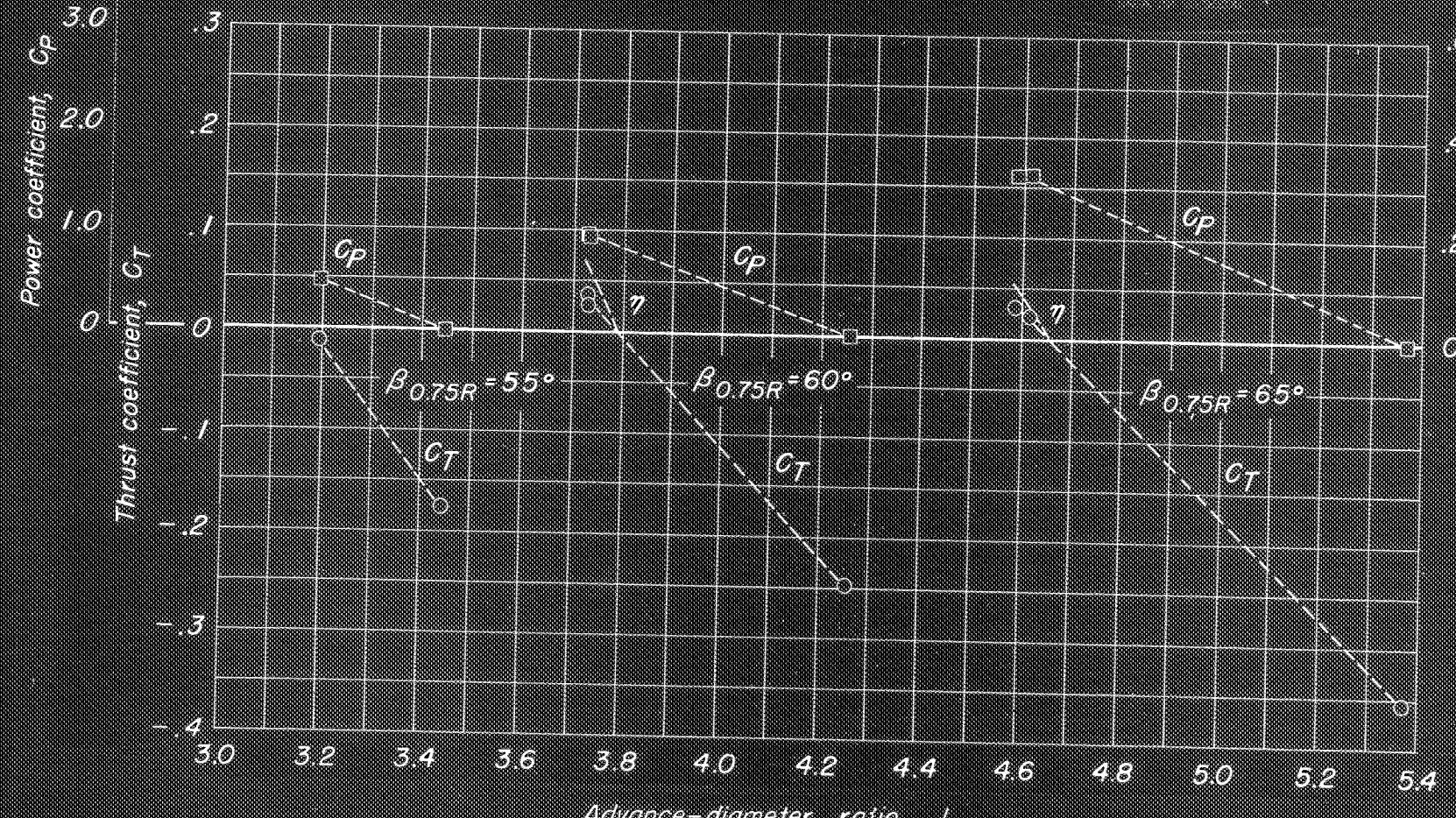

(b) α, 4°

Figure 10.- Continued.

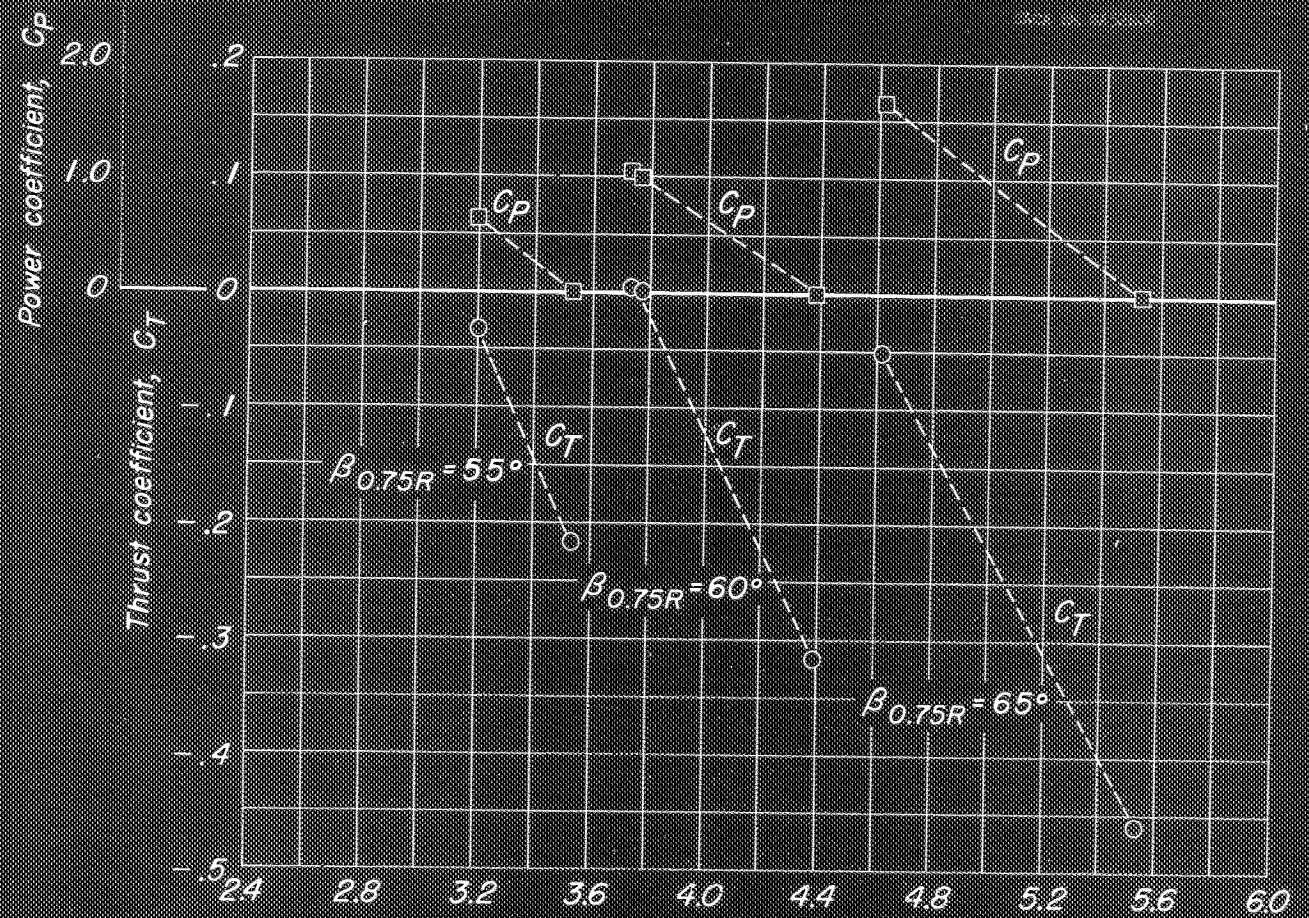

(c) α, 8°

Figure 10.- Concluded.

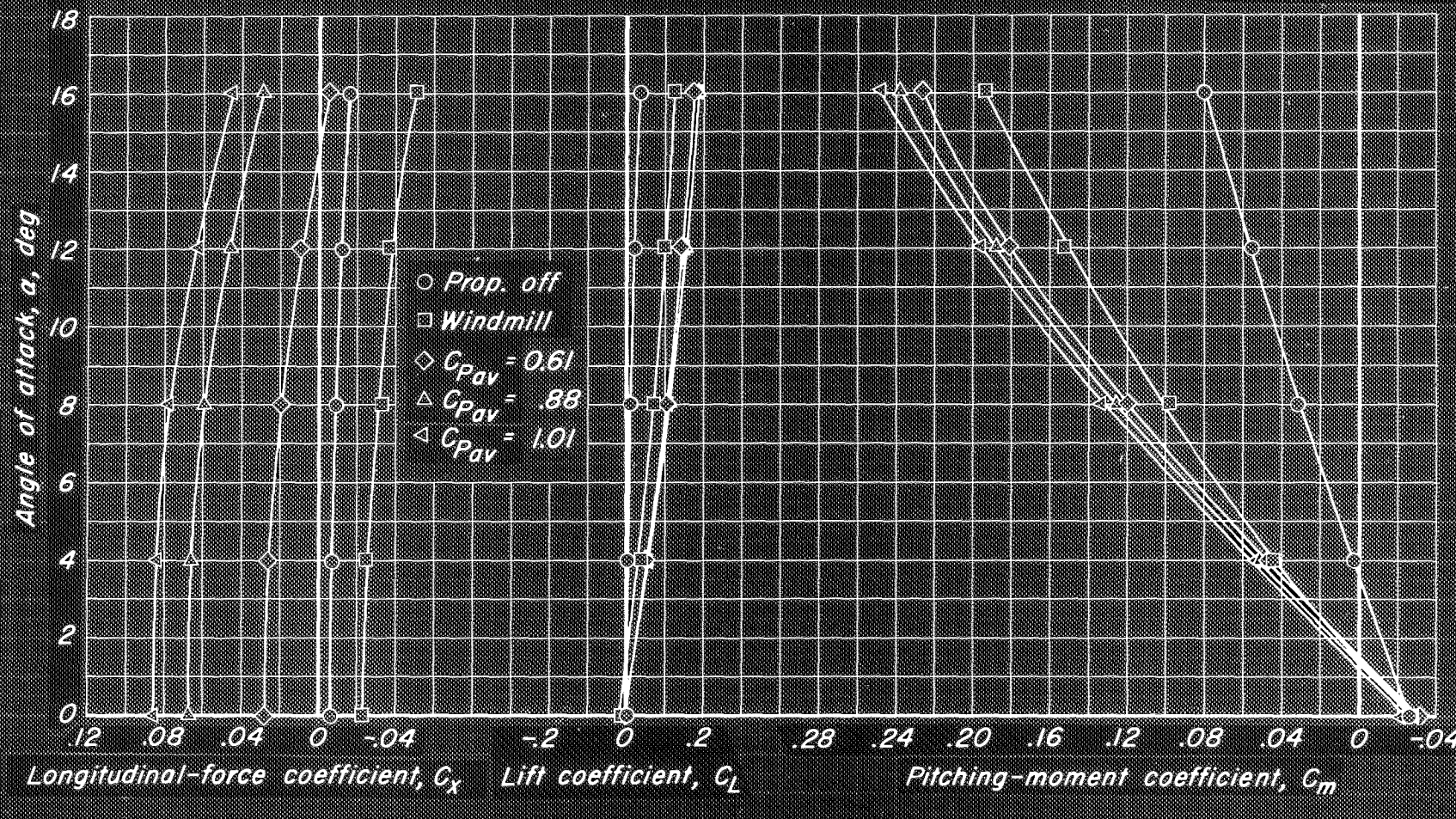

(a) $\beta_{0.75R}$, 50°

Figure 11.- The effect of power on the longitudinal characteristics of the Lockheed XFV-1 model fuselage. M, 0.50.

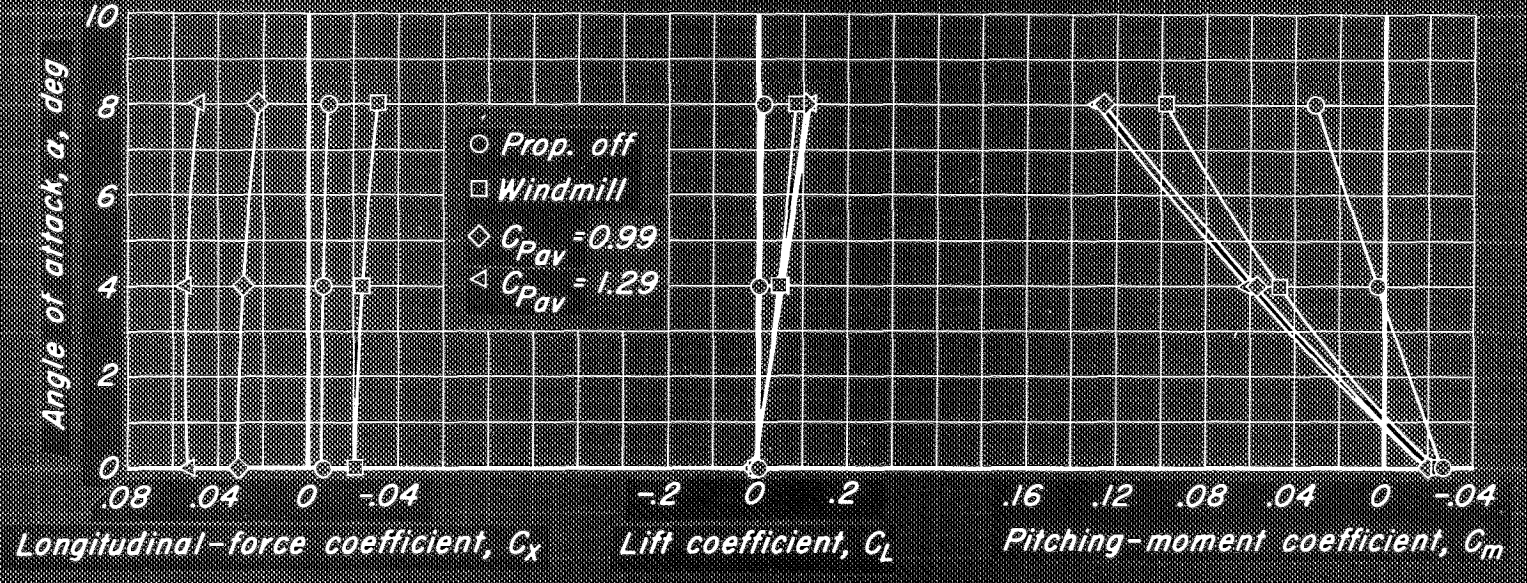

(b) $\beta_{0.75R}$, 55°

Figure 11.- Concluded.

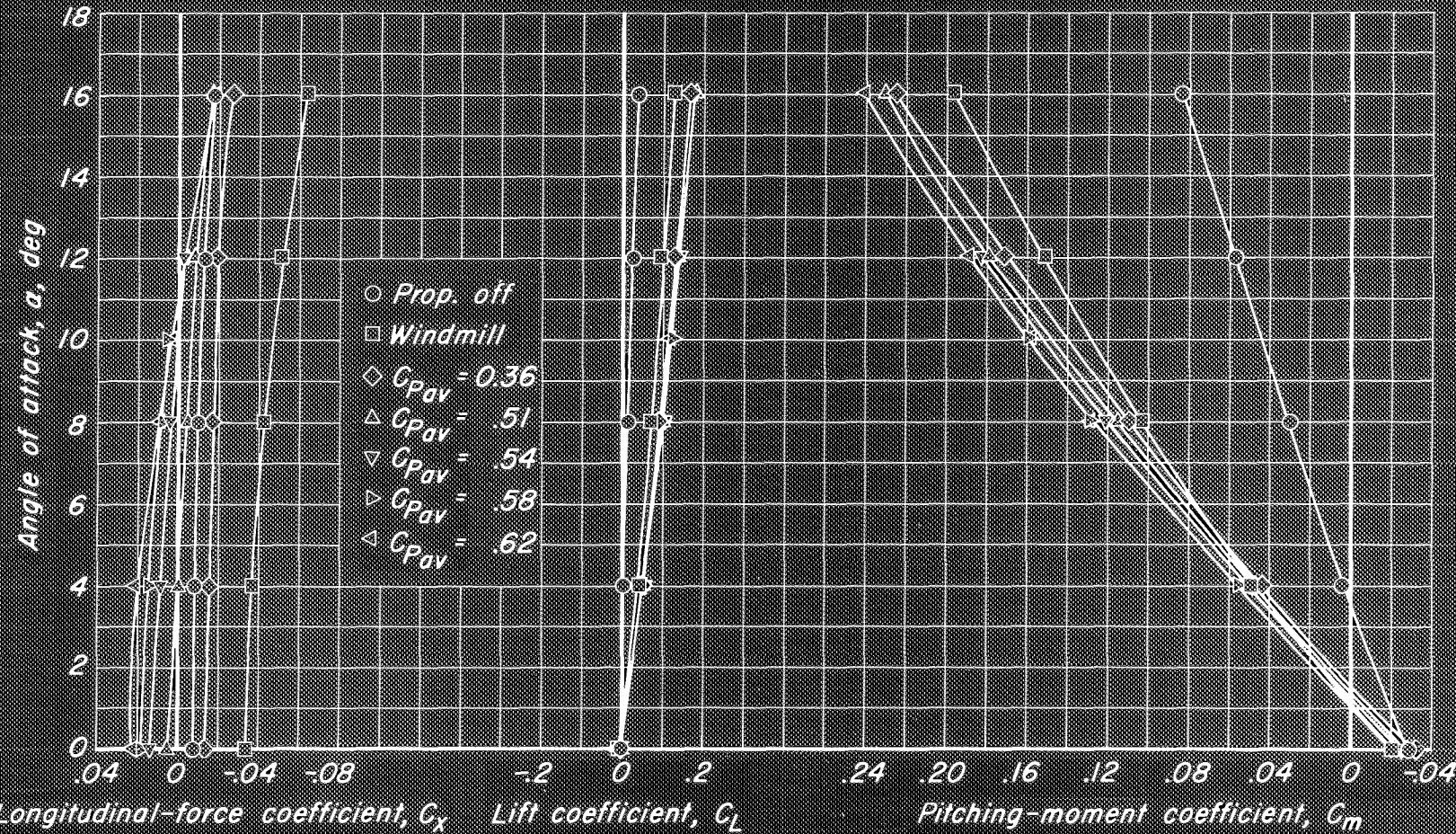

(a) $\beta_{0.75R}$, 50°

CONFIDENTIAL
NATIONAL ADVISORY COMMITTEE FOR AERONAUTICS

Figure 12.- The effect of power on the longitudinal characteristics of the Lockheed XFV-1 model fuselage. M, 0.70.

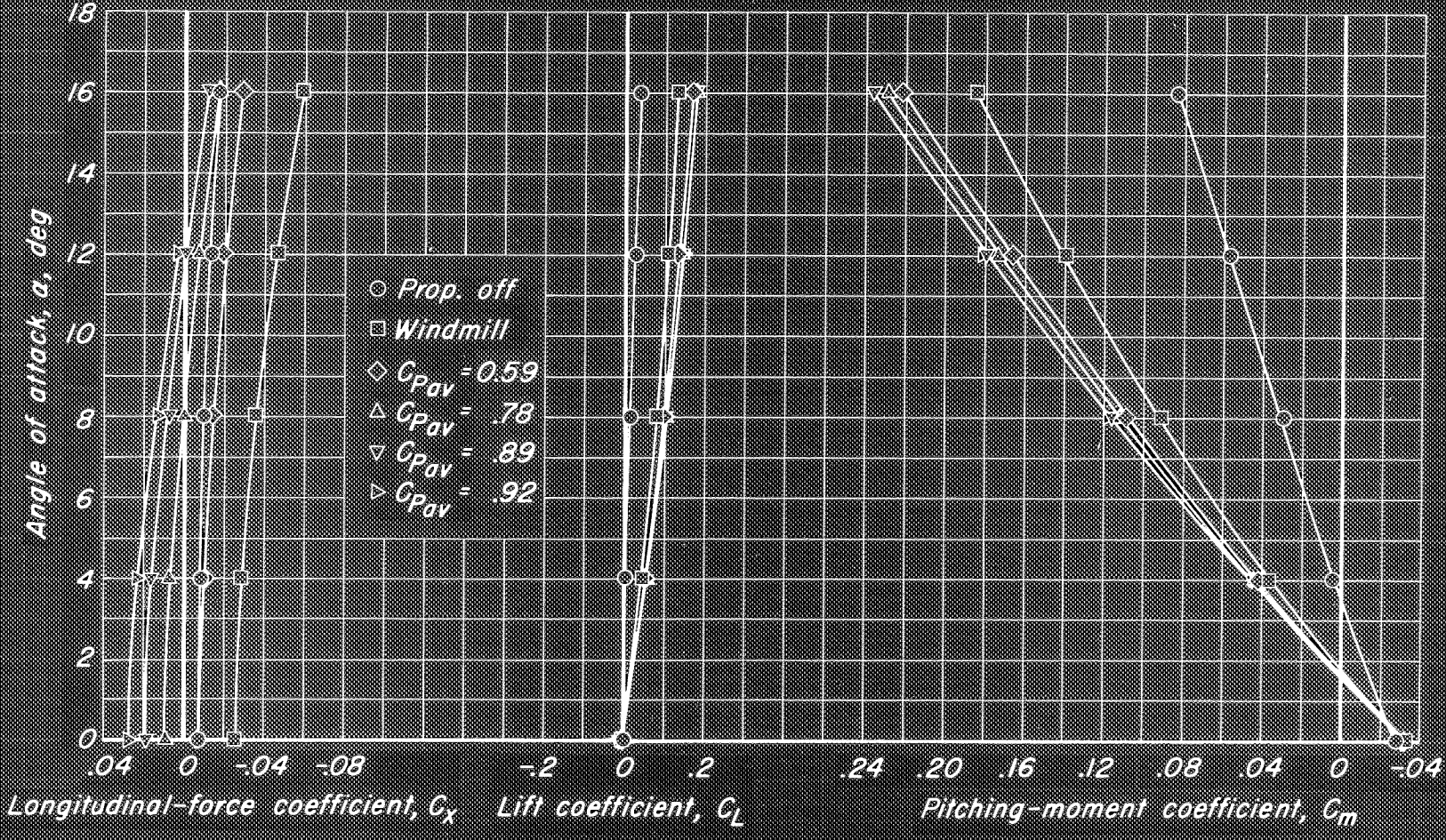

(b) $\beta_{0.75\,R}$, 55°

Figure 12.- Continued.

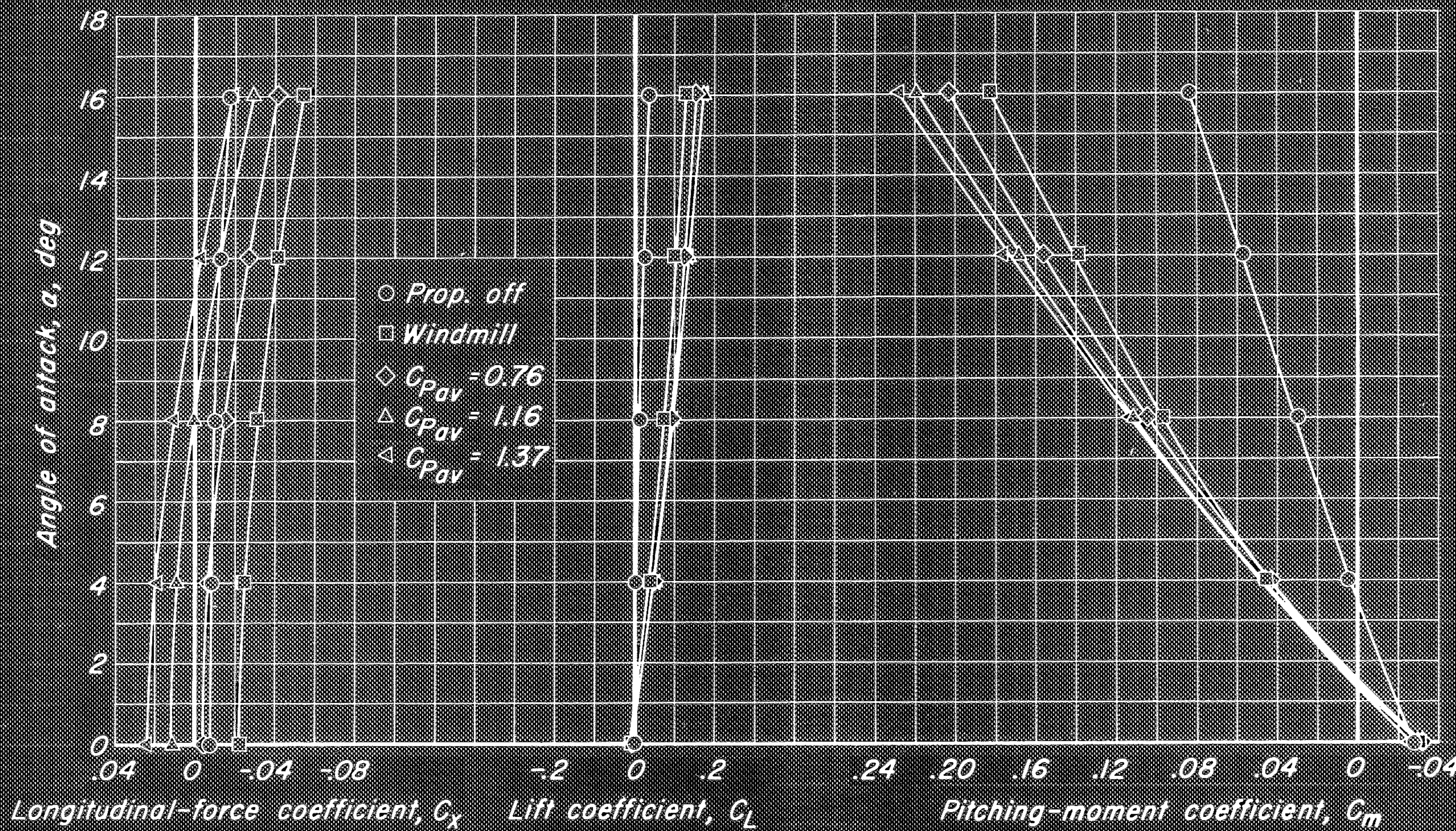

(c) $\beta_{0.75R}$, 60°

Figure 12.- Concluded.

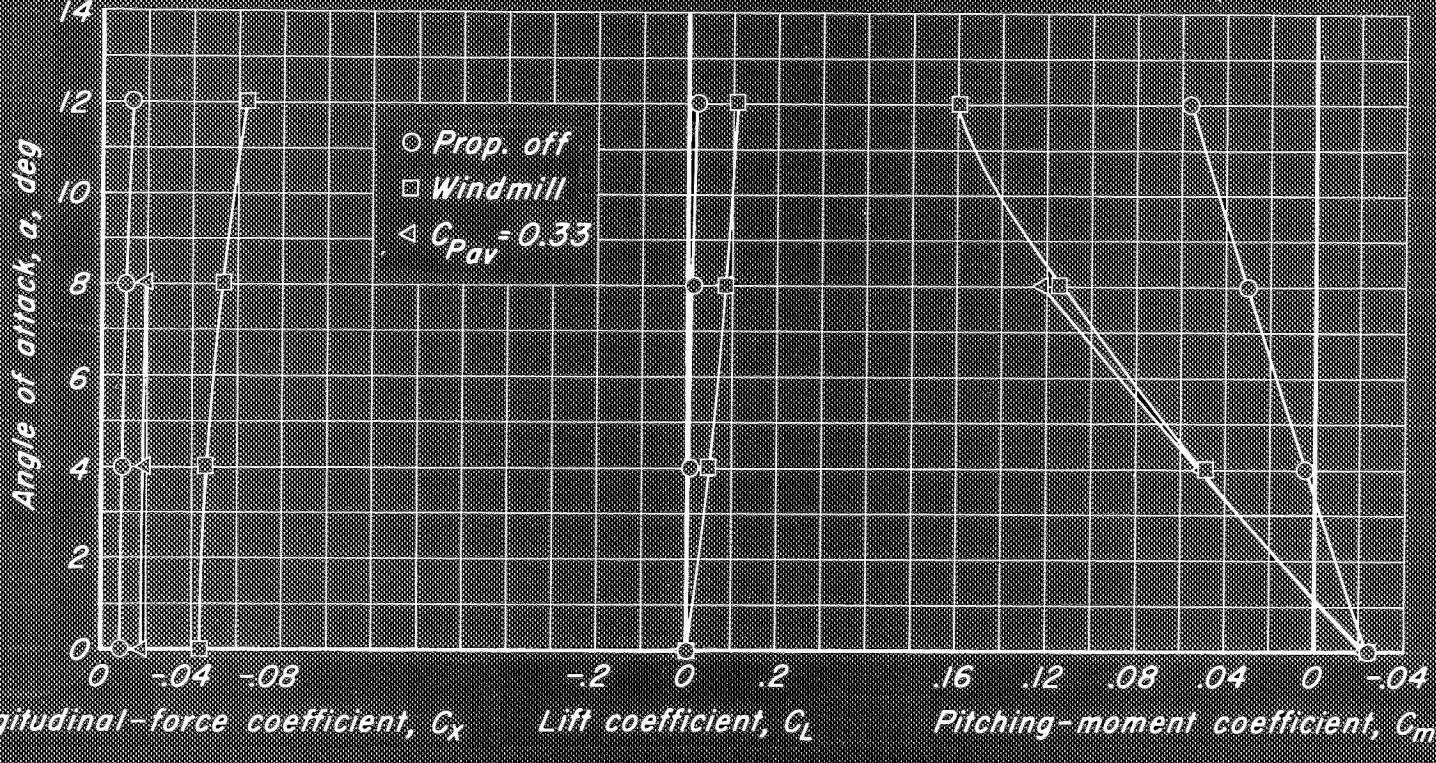

(a) $\beta_{0.75R}$, 50°

Figure 13.- The effect of power on the longitudinal characteristics of the Lockheed XFV-1 model fuselage. M, 0.80.

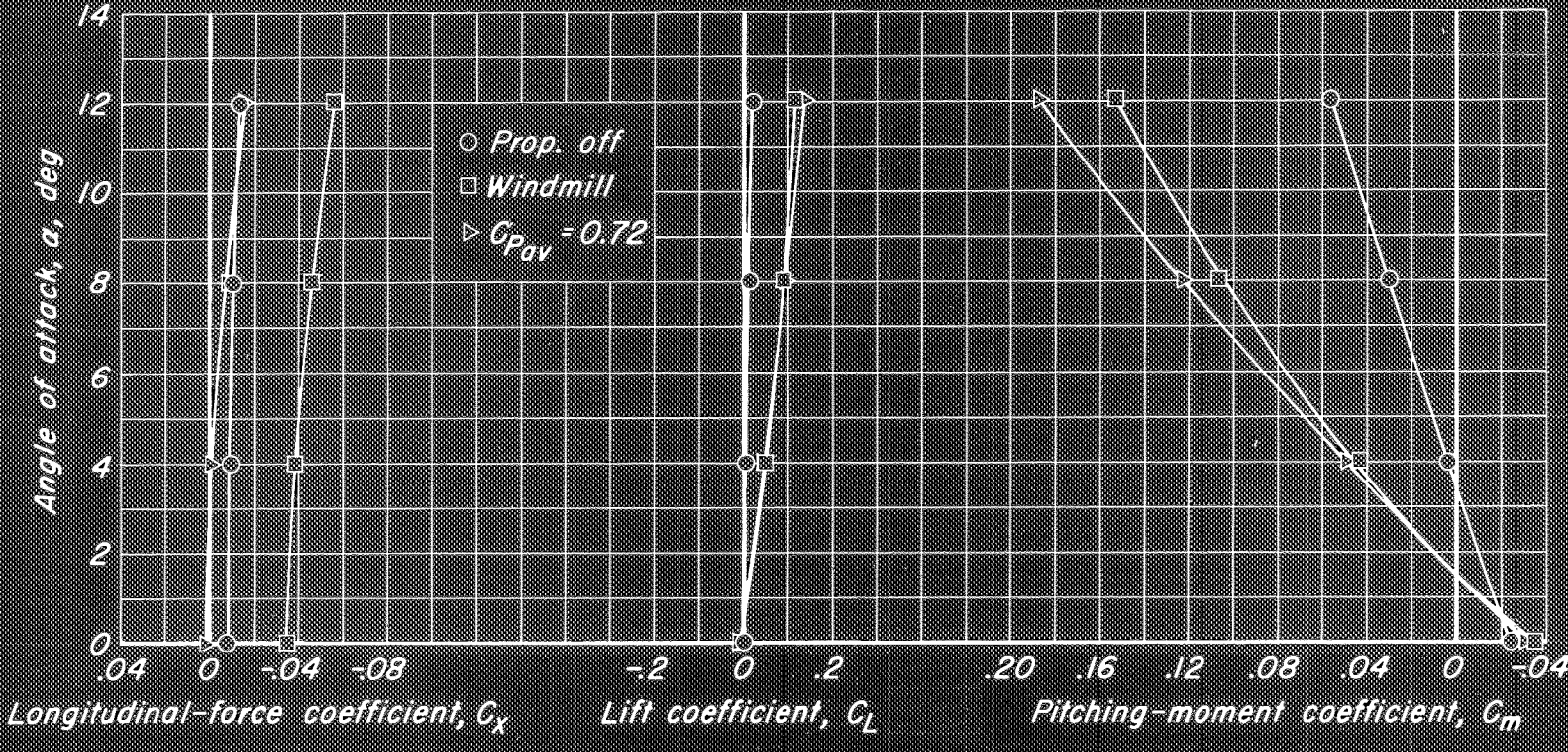

(b) $\beta_{0.75\,R}$, 55°

Figure 13.- Continued.

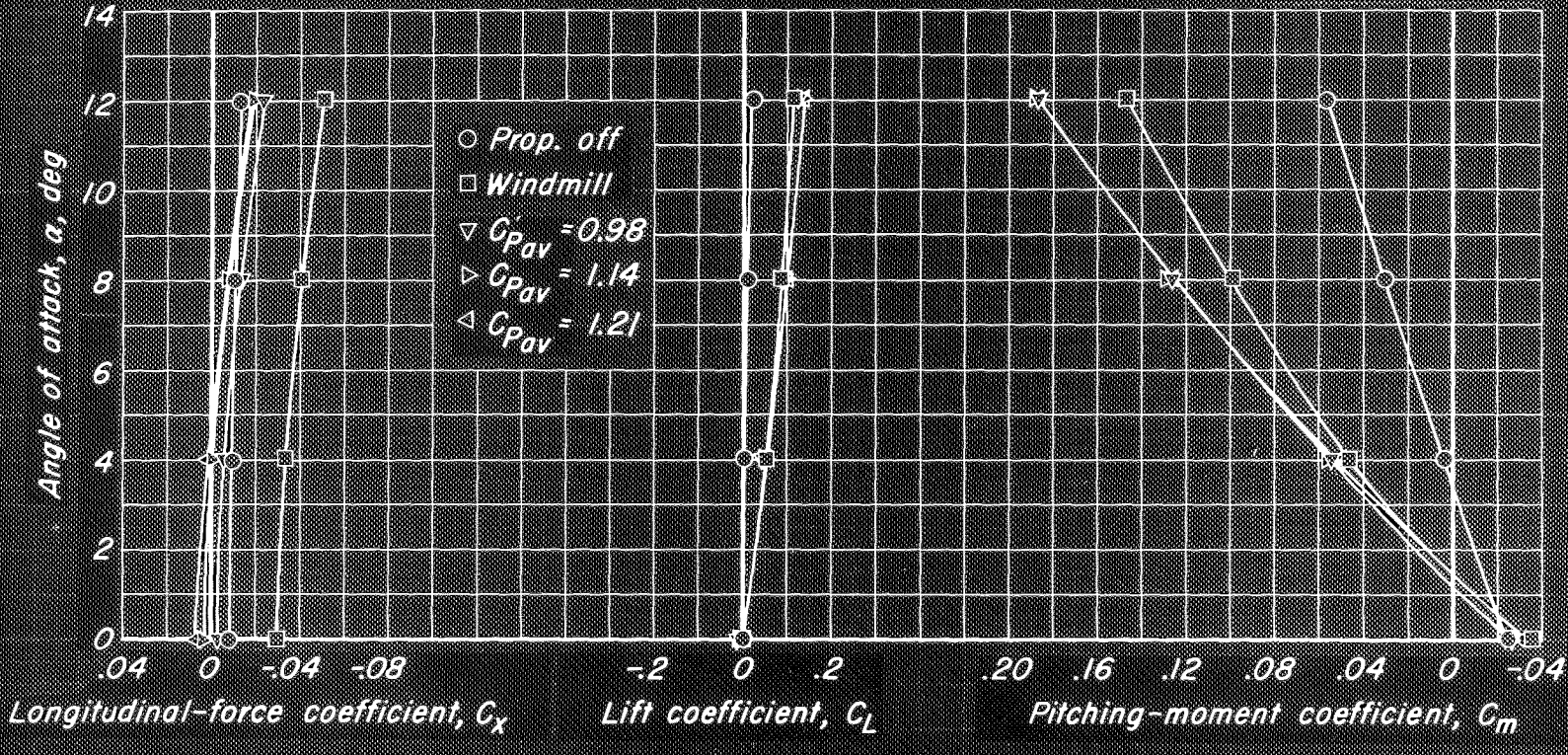

(c) $\beta_{0.75\,R}$, 60°

Figure 13.- Continued.

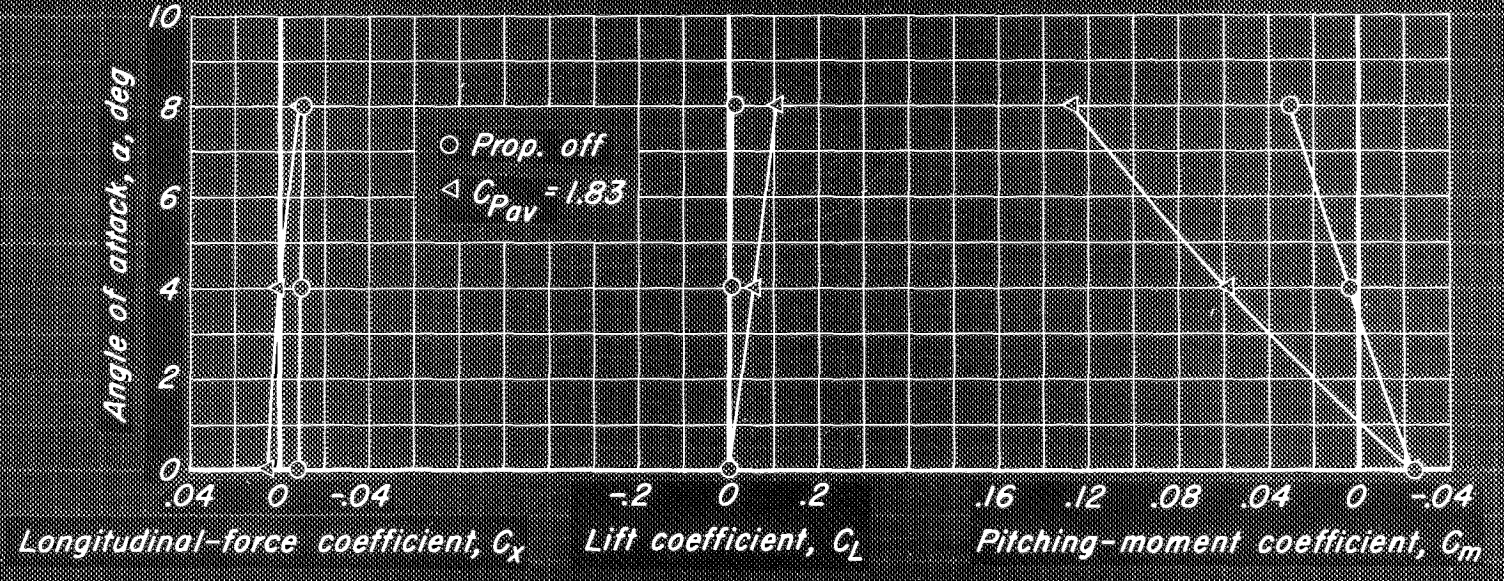

(d) $\beta_{0.75R}$, 65°

Figure 13.- Concluded.

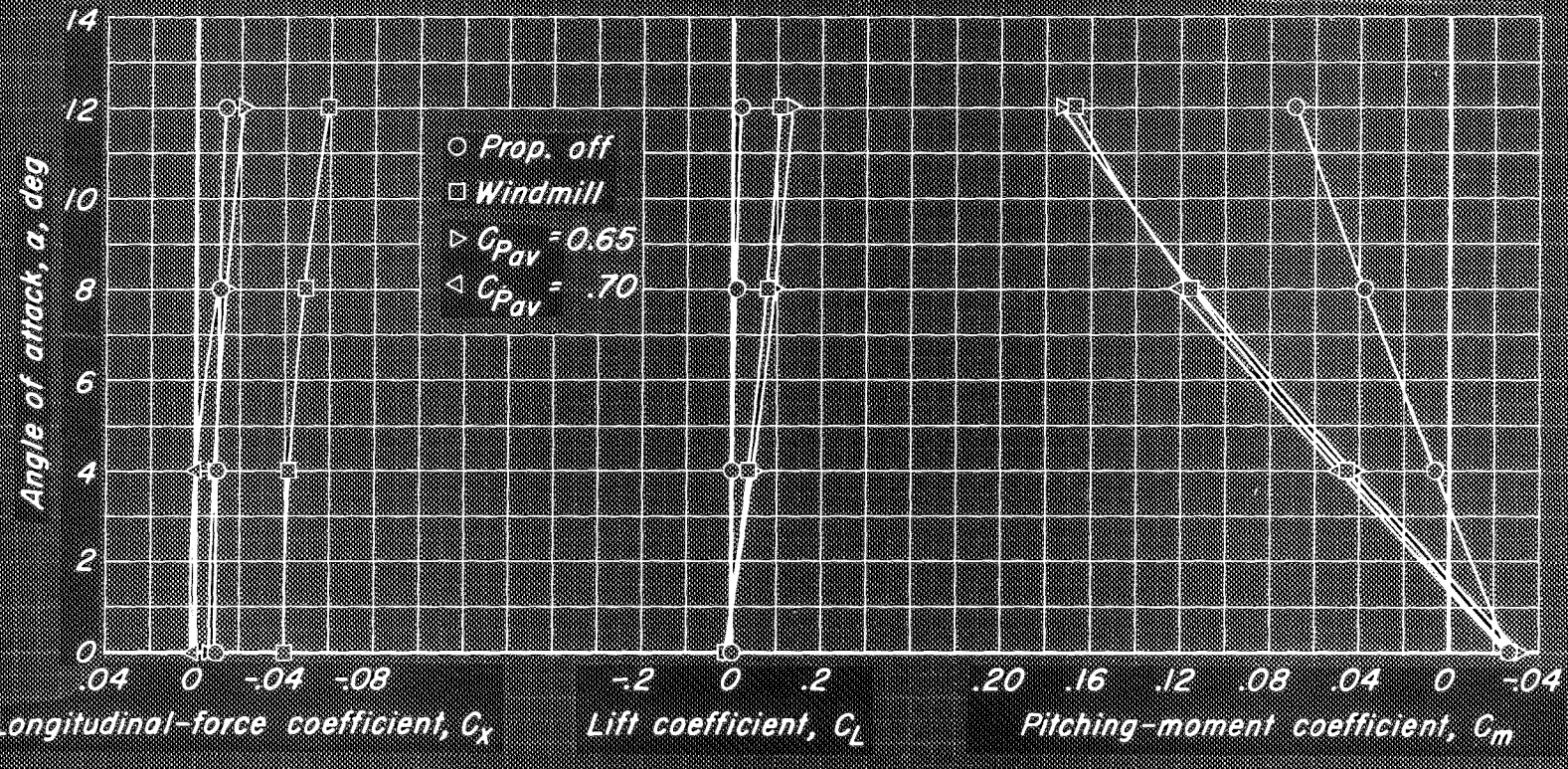

(a) $\beta_{0.75\,R}$, 55°

Figure 14.- The effect of power on the longitudinal characteristics of the Lockheed XFV-1 model fuselage. M, 0.85.

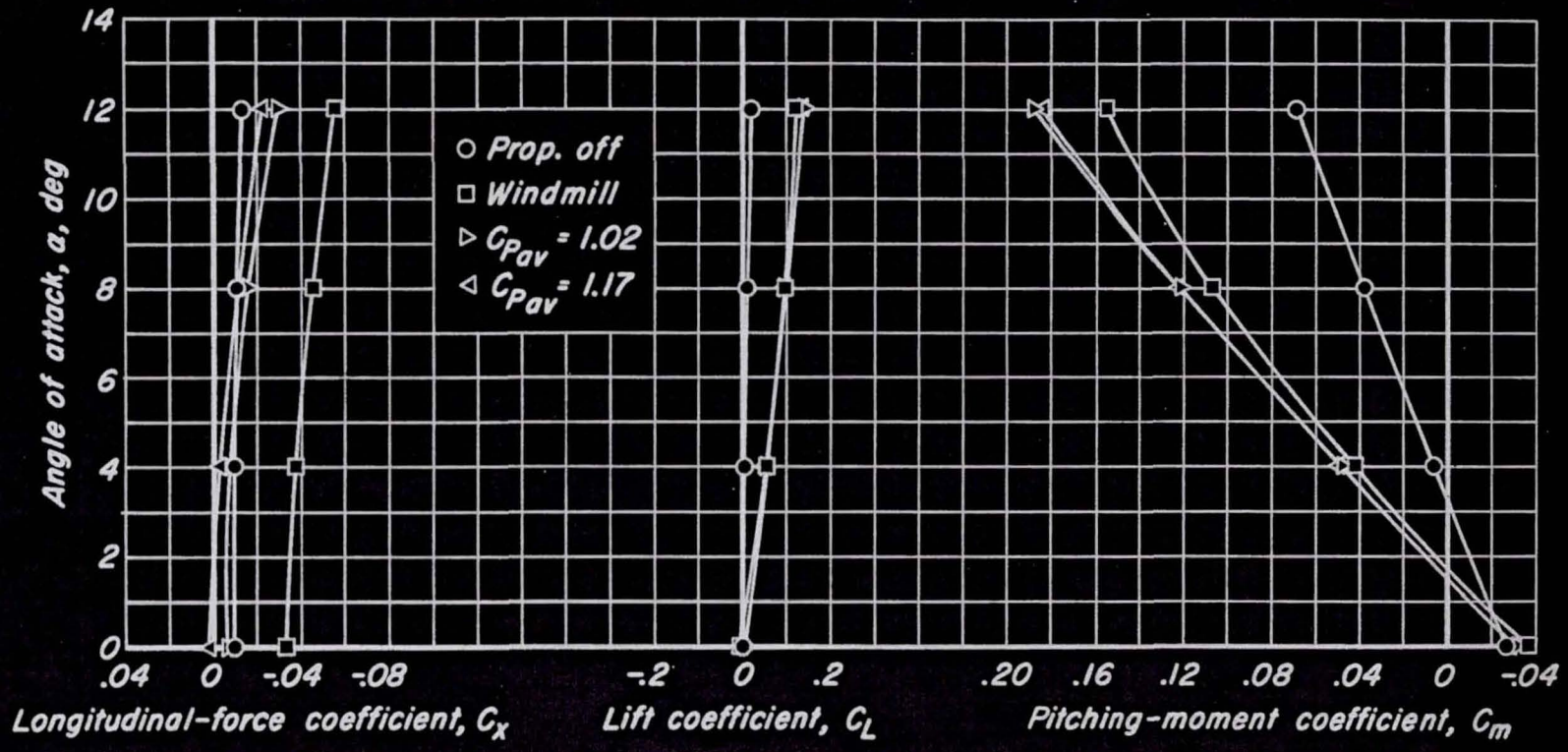

(b) $\beta_{0.75R}$, 60°

Figure 14.- Continued.

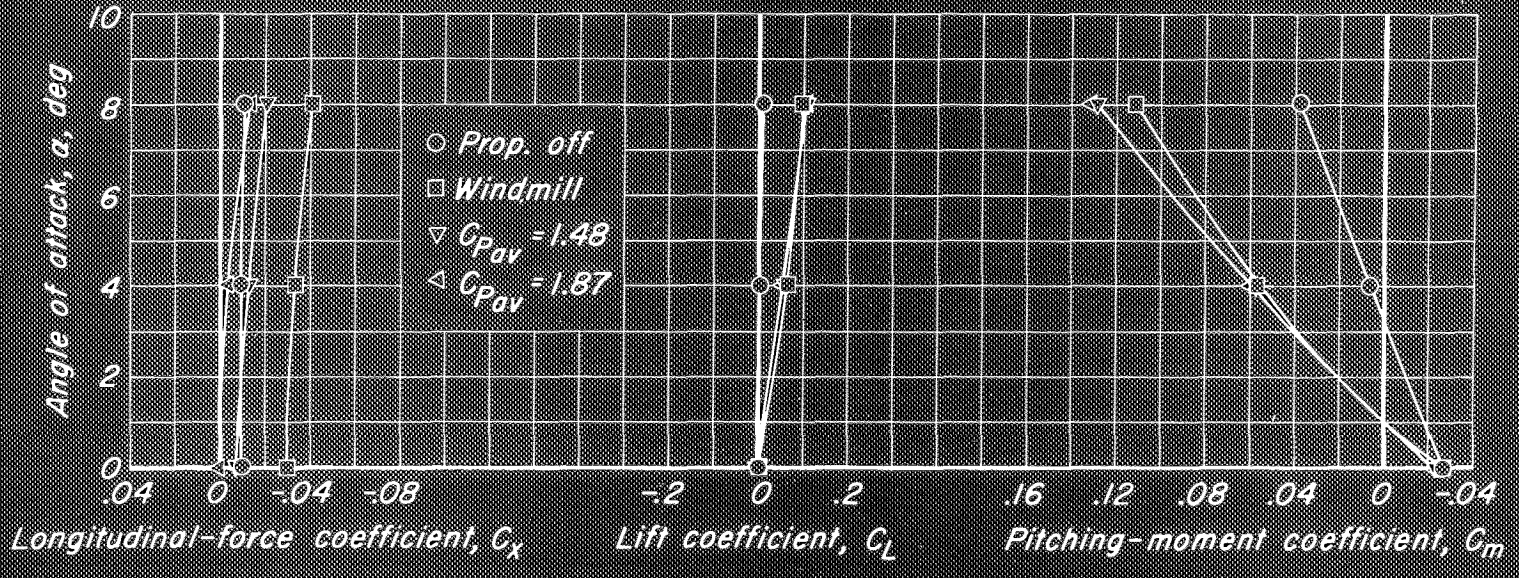

(c) $\beta_{0.75\,R}$, 65°

Figure 14.- Concluded.

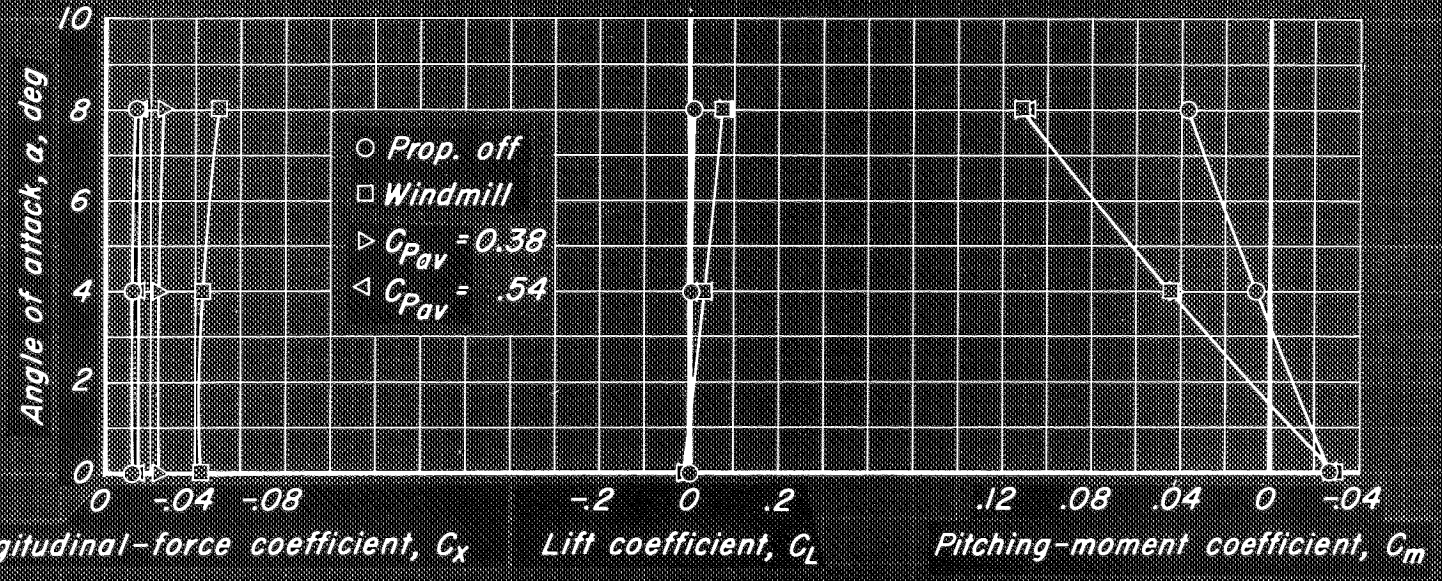

(a) $\beta_{0.75R}$, 55°

Figure 15.- The effect of power on the longitudinal characteristics of the Lockheed XFV-1 model fuselage. M, 0.90.

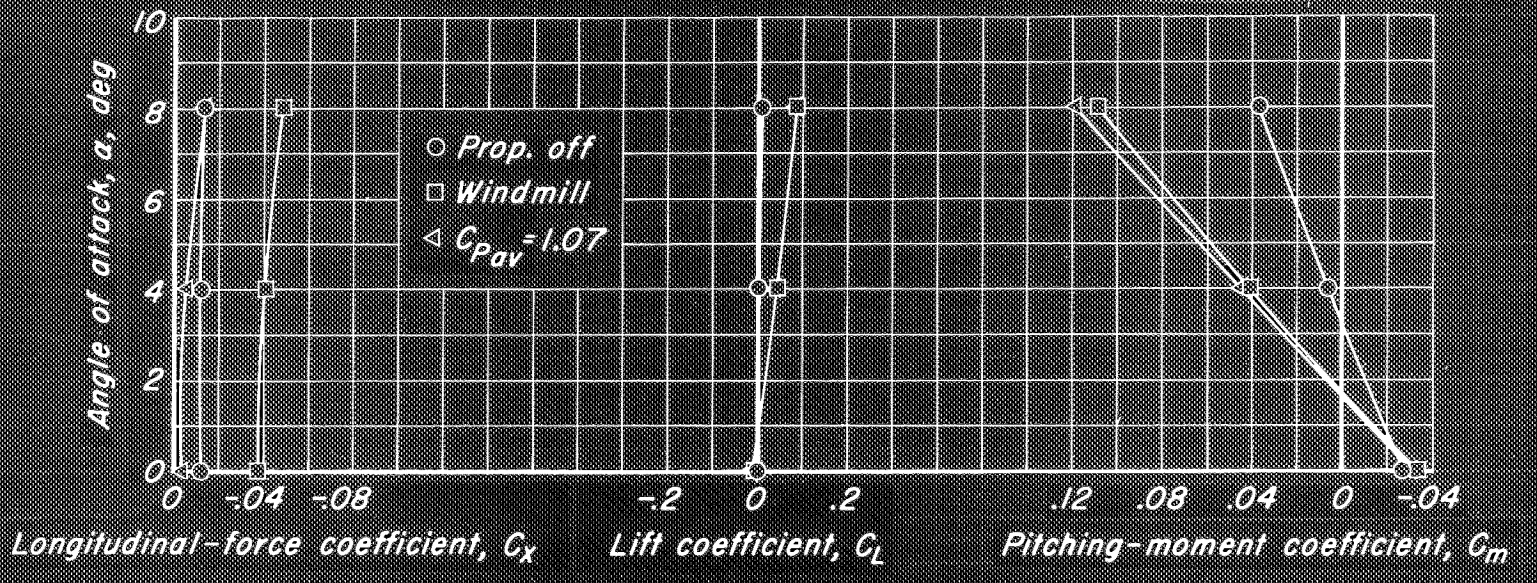

(b) $\beta_{0.75R}$, 60°

Figure 15.- Continued.

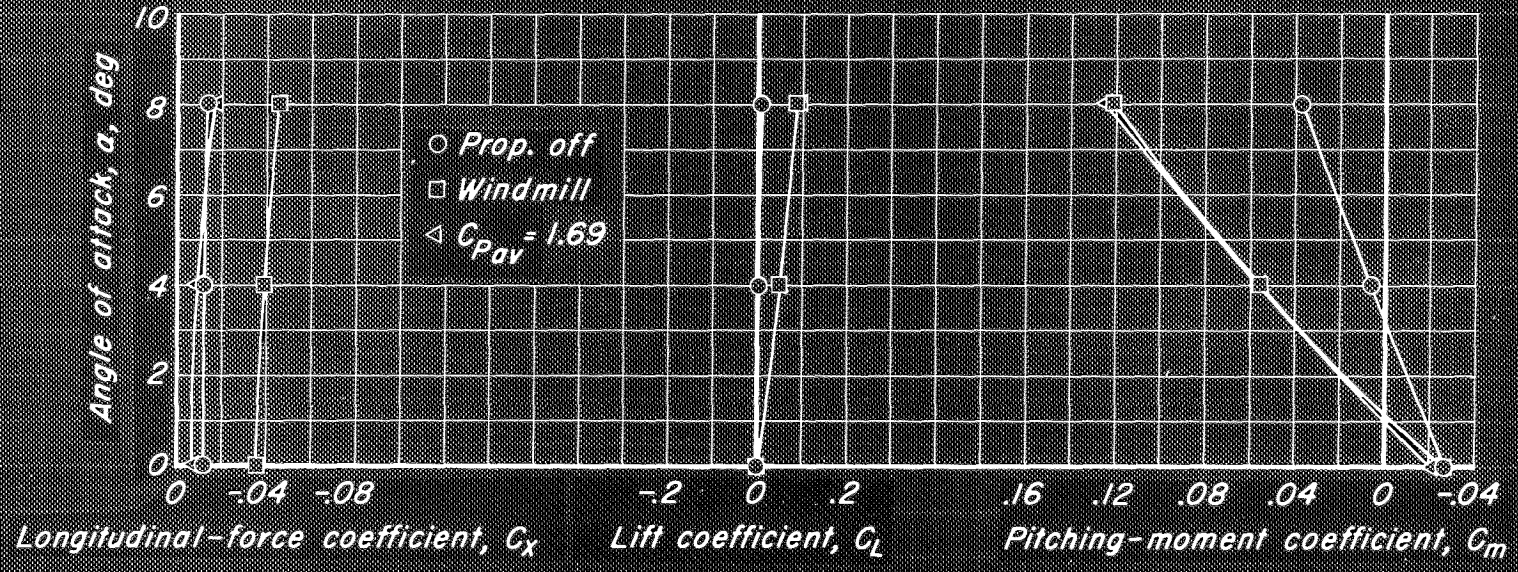

(c) $\beta_{0.75R}$, 65°

Figure 15.- Concluded.

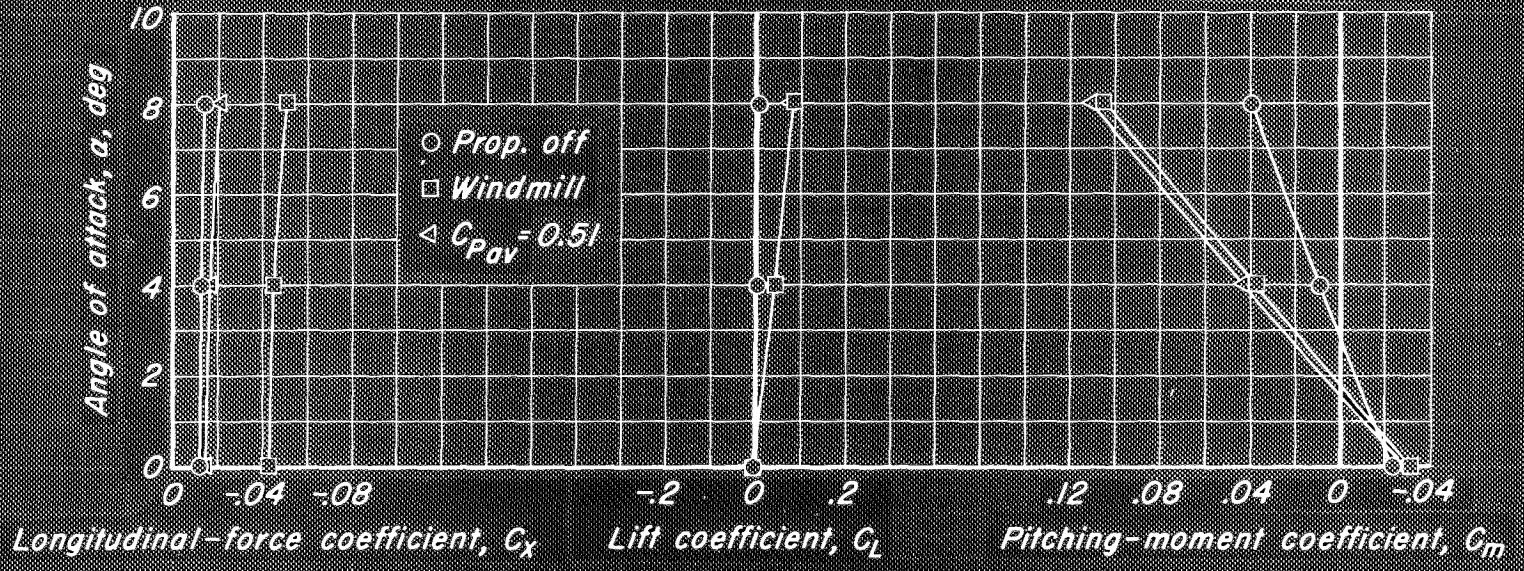

(a) $\beta_{0.75R}$, 55°

Figure 16.- The effect of power on the longitudinal characteristics of the Lockheed XFV-1 model fuselage. M, 0.92.

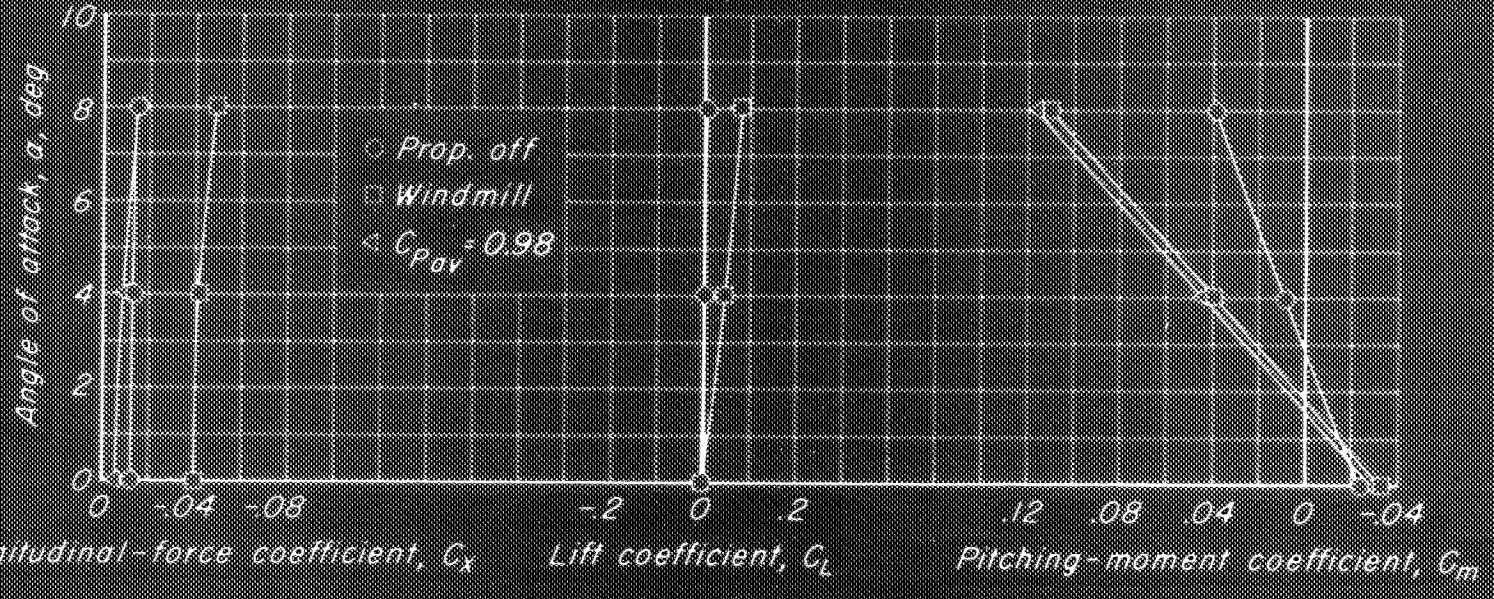

(b) $\beta_{0.75R}$, 60°

Figure 16.- Continued.

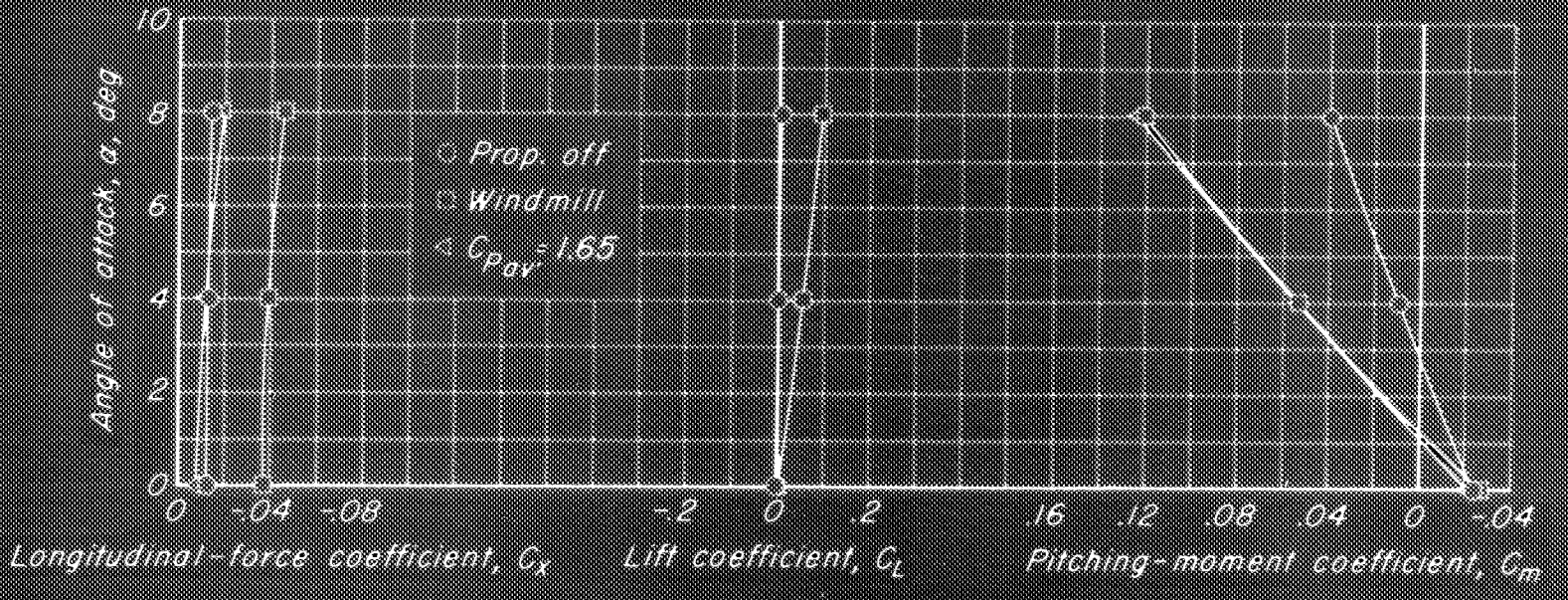

(c) $\beta_{0.75R} = 65°$

Figure 16.- Concluded.

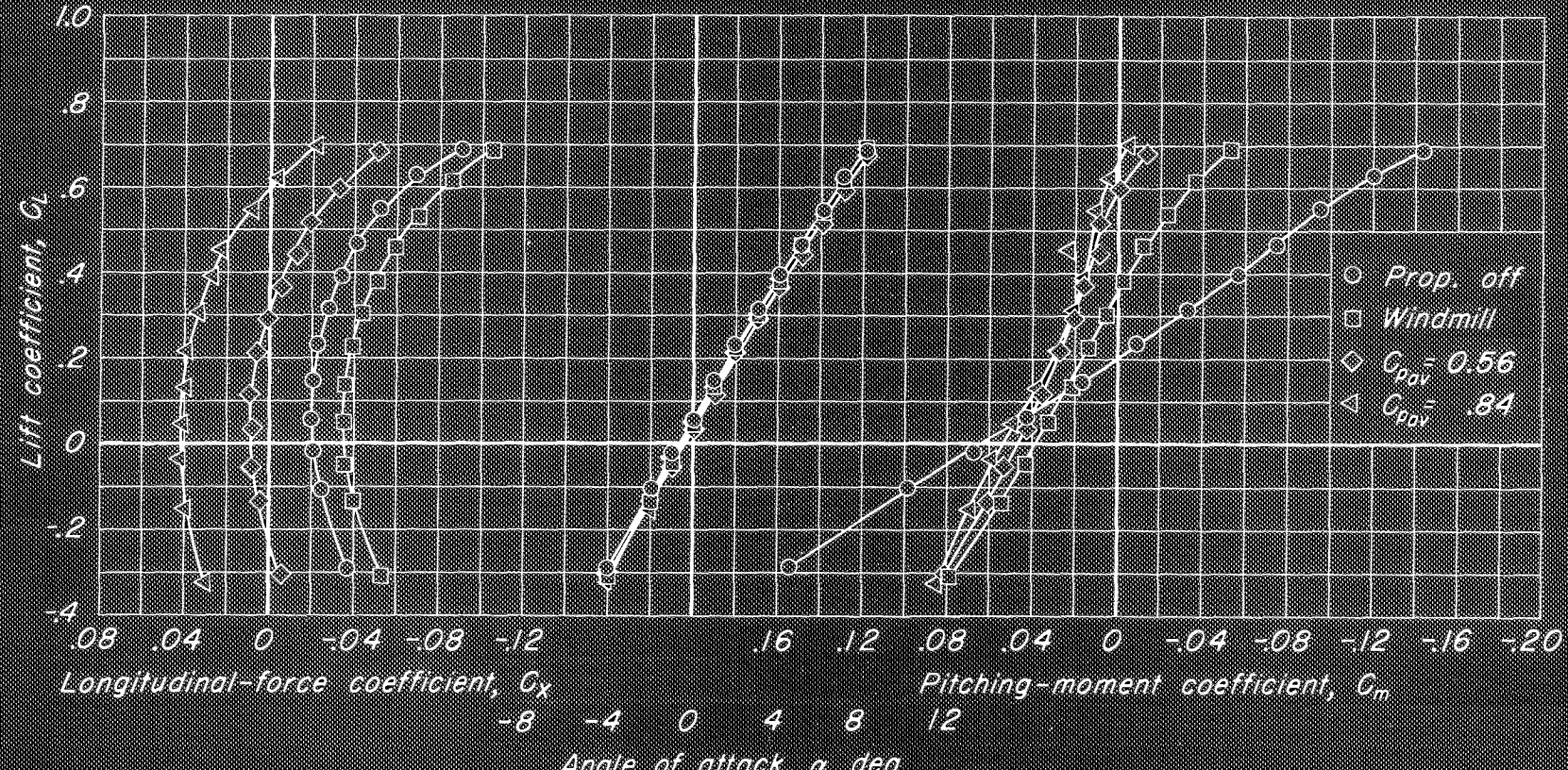

(a) $\beta_{0.75R}$, 50°

Figure 17.- The effect of power on the longitudinal characteristics of the 1/10-scale model of the Lockheed XFV-1 airplane. M_1 0.50.

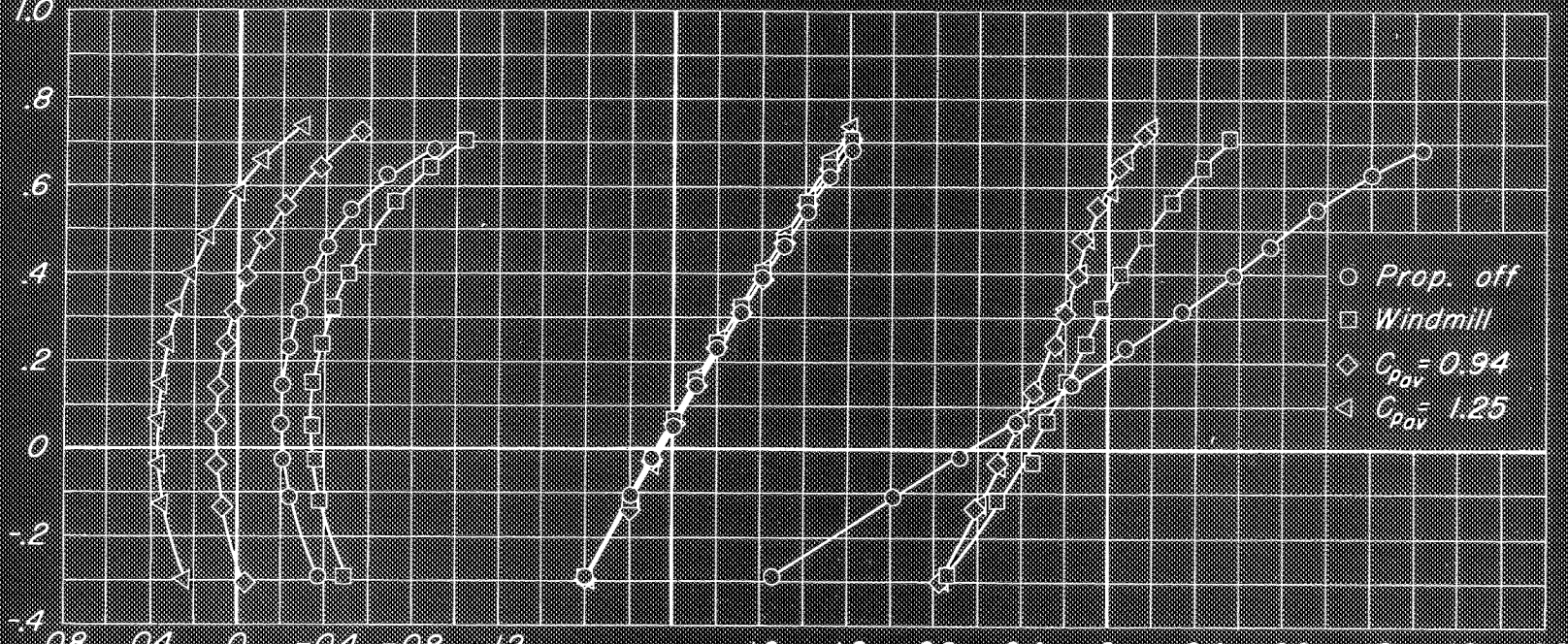

(b) $\beta_{0.75R}$, 55°

Figure 17.- Concluded.

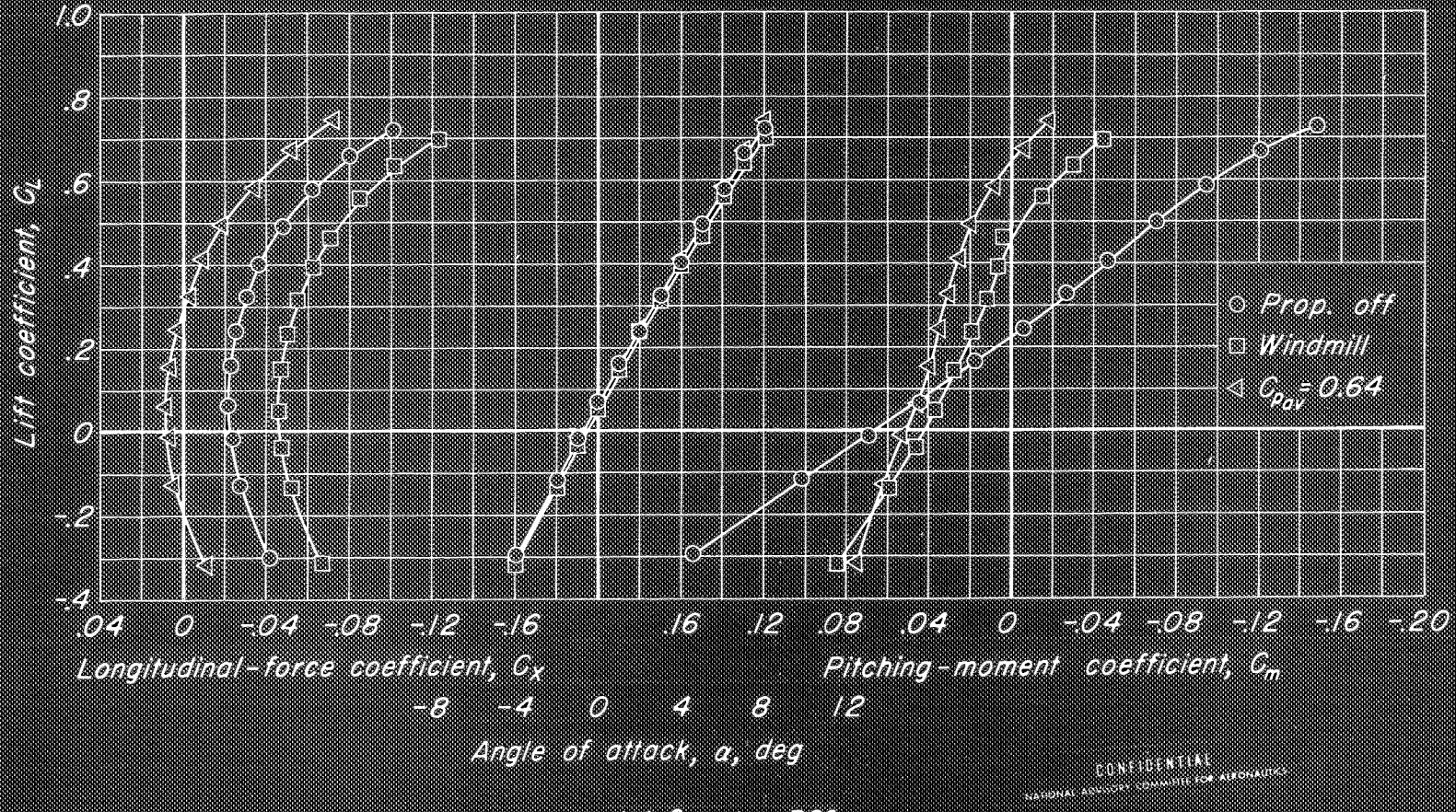

CONFIDENTIAL
NATIONAL ADVISORY COMMITTEE FOR AERONAUTICS

(a) $\beta_{0.75\,R}$, 50°

Figure 18.- The effect of power on the longitudinal characteristics of the 1/10-scale model of the Lockheed XFV-1 airplane. M, 0.70.

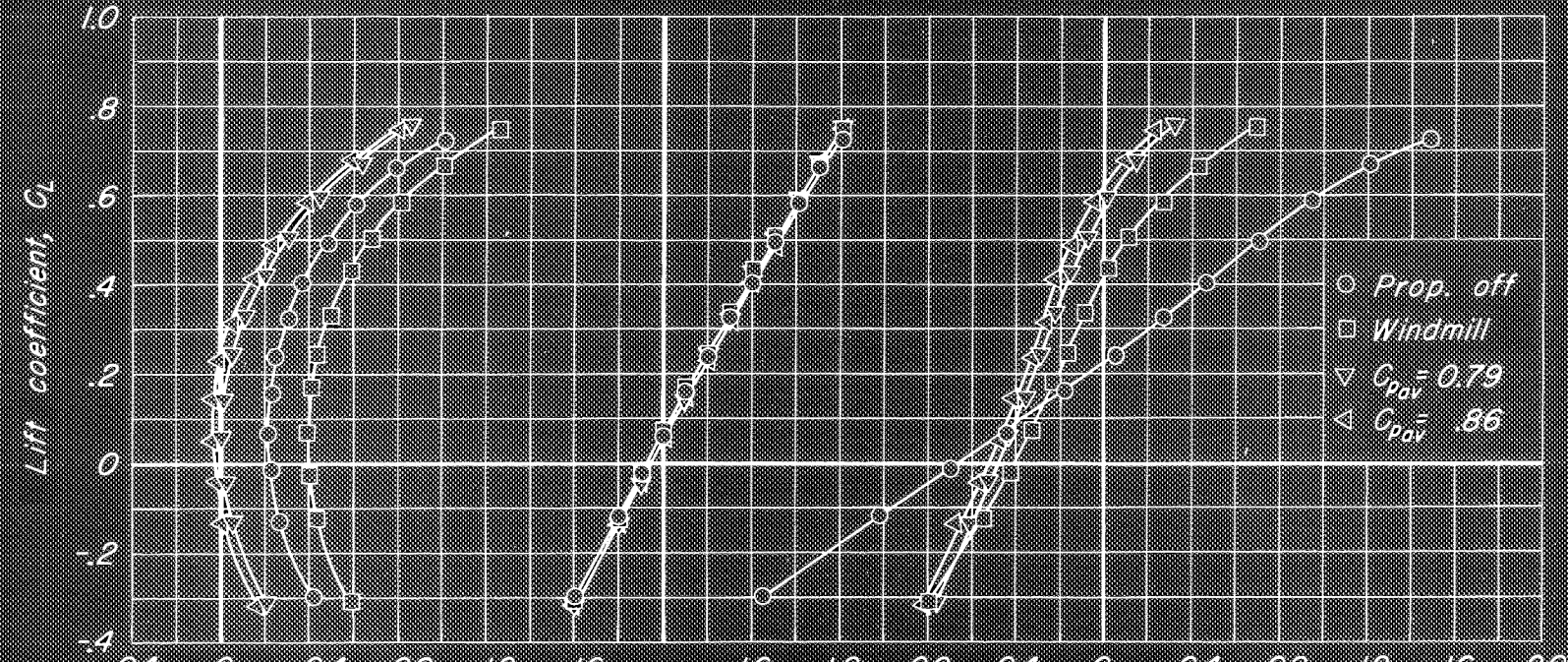

(b) $\beta_{0.75R}$, 55°

Figure 18.- Continued.

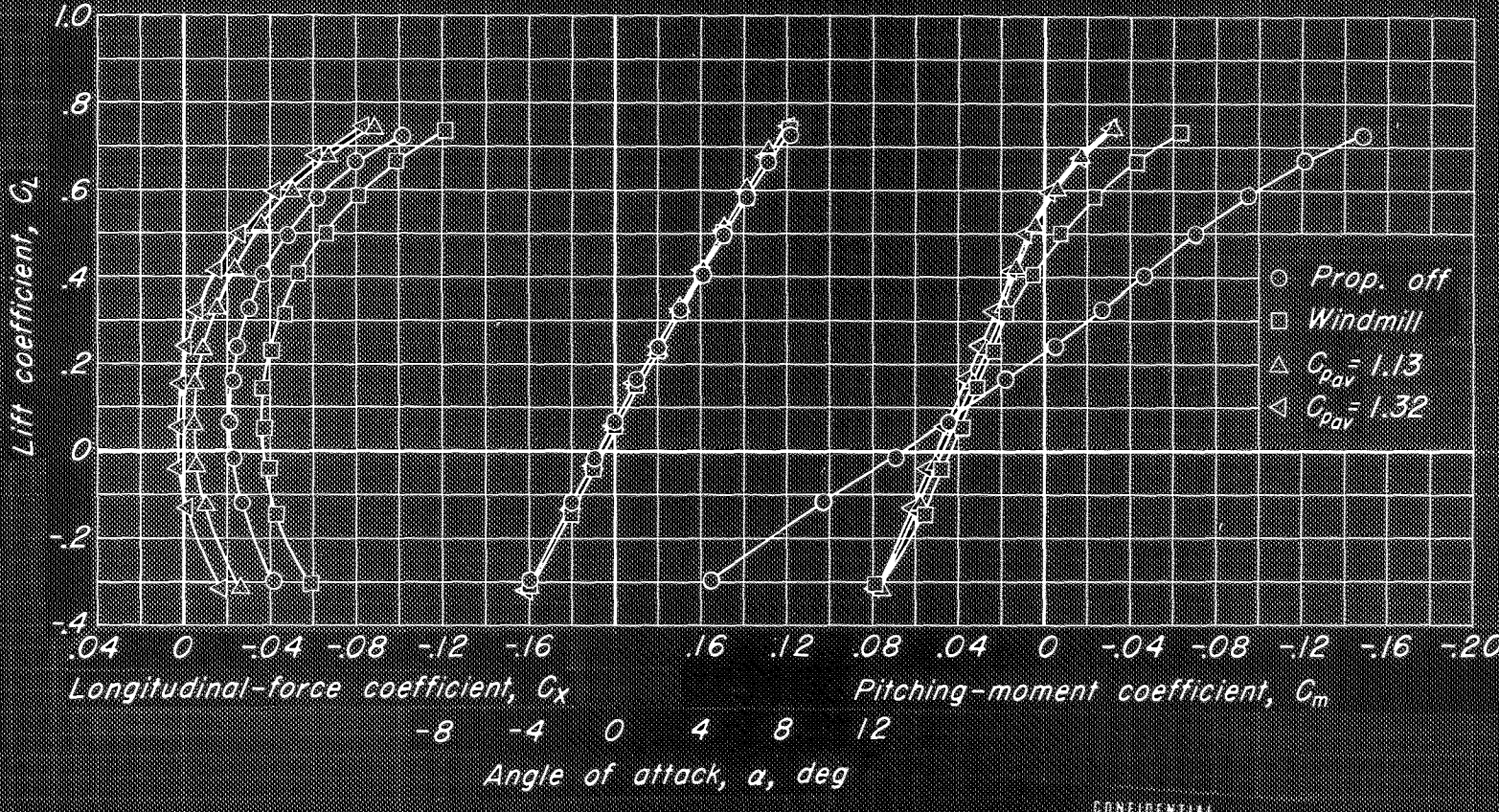

CONFIDENTIAL
NATIONAL ADVISORY COMMITTEE FOR AERONAUTICS

(c) $\beta_{0.75R}$, 60°

Figure 18.- Concluded.

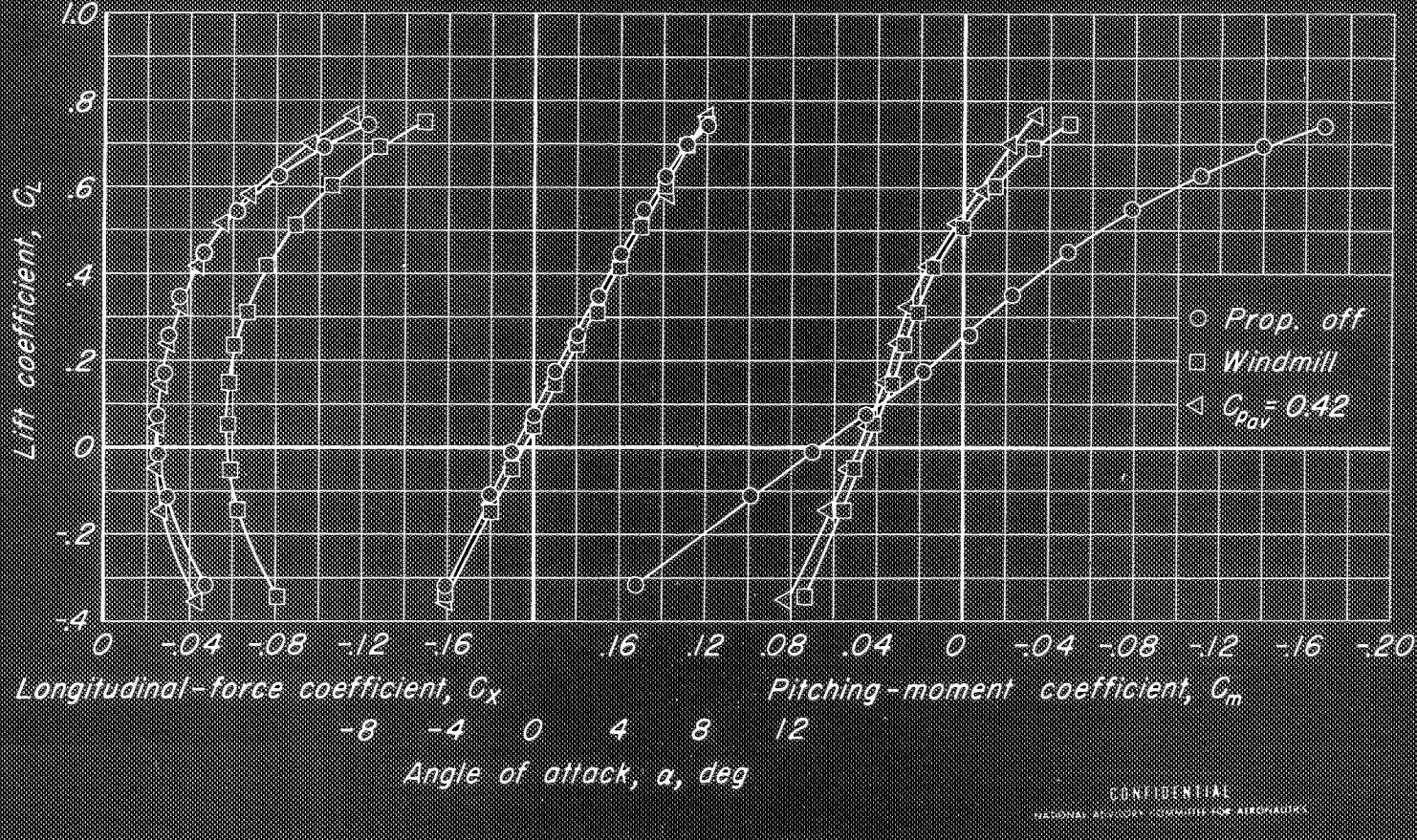

CONFIDENTIAL

(a) $\beta_{0.75R}$, 50°

Figure 19.- The effect of power on the longitudinal characteristics of the 1/10-scale model of the Lockheed XFV-1 airplane. M, 0.80.

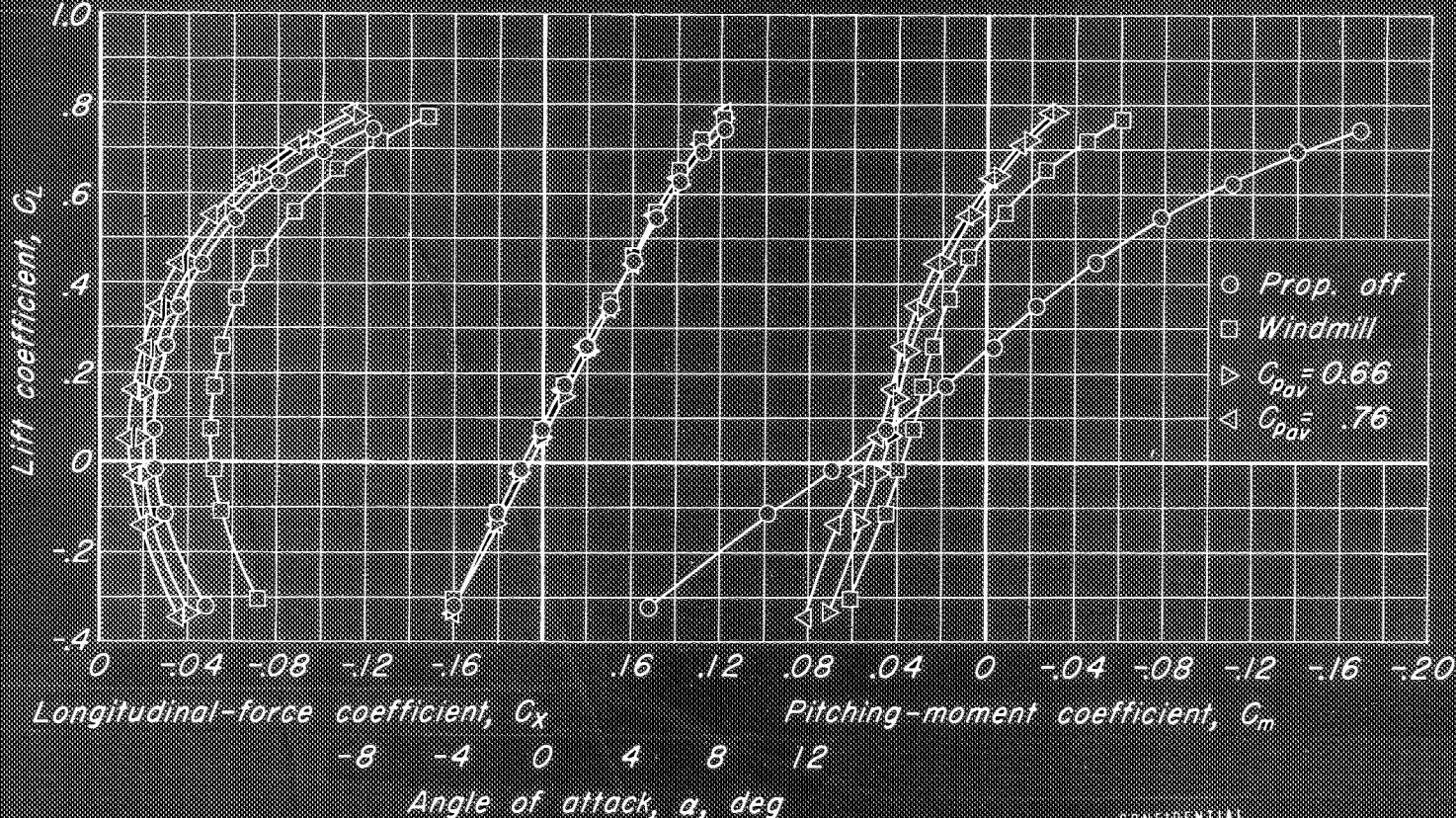

CONFIDENTIAL
NATIONAL ADVISORY COMMITTEE FOR AERONAUTICS

(b) $\beta_{0.75\,R}$, 55°

Figure 19.- Continued.

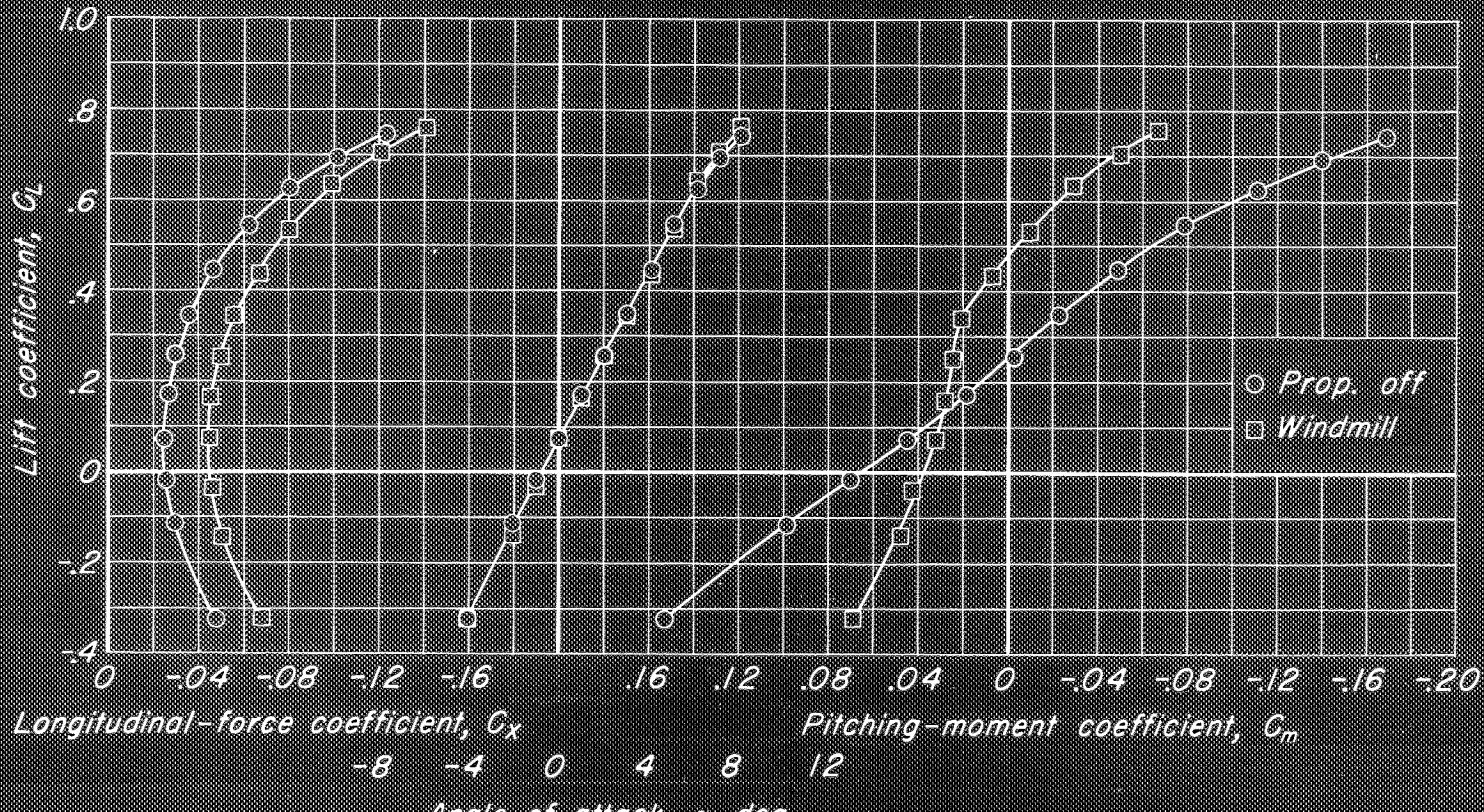

(c) $\beta_{0.75R}$, 60°

Figure 19.- Concluded.

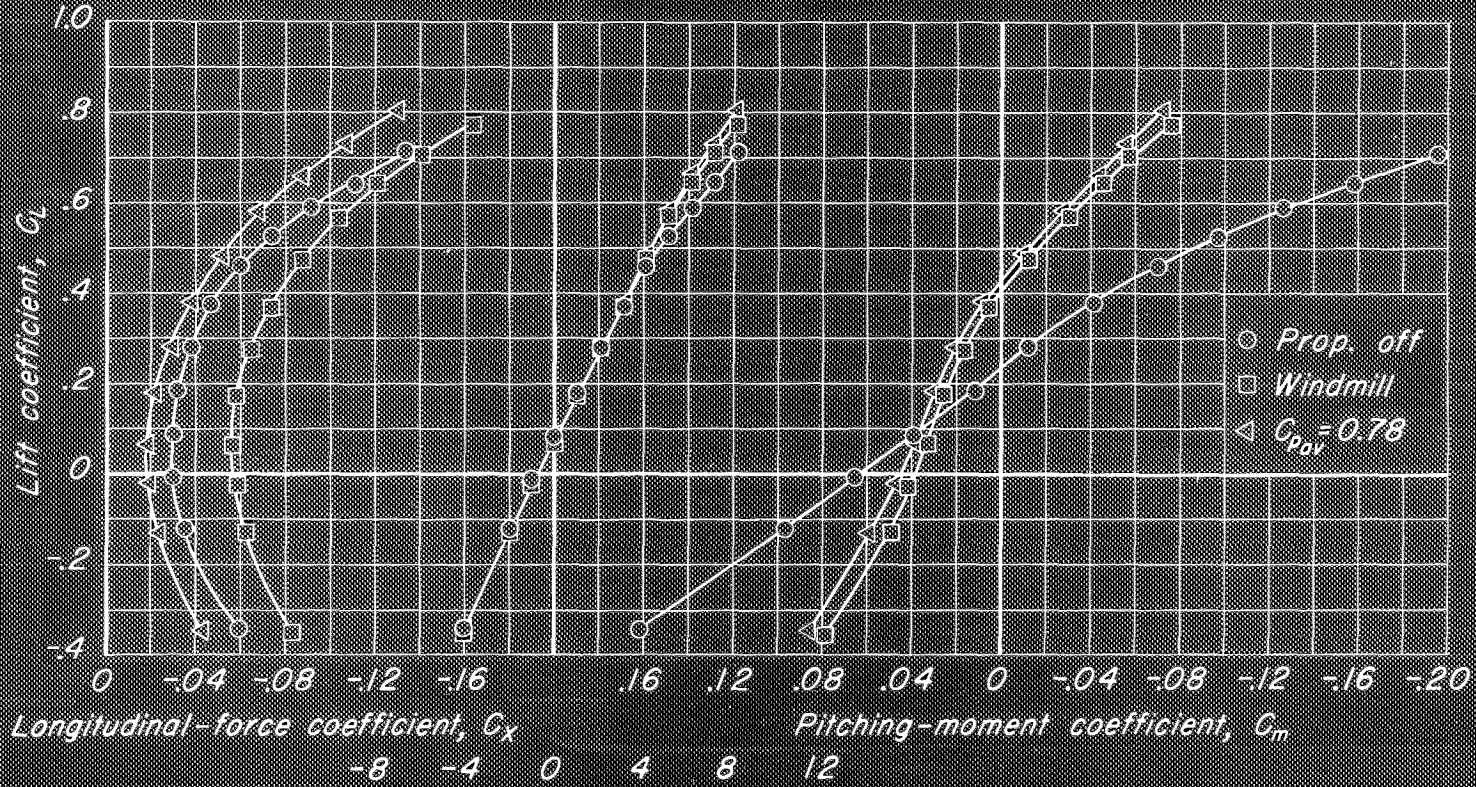

(a) $\beta_{0.75R}$, 55°

Figure 20.- The effect of power on the longitudinal characteristics of the 1/10-scale model of the Lockheed XFV-1 airplane. M_∞ 0.85.

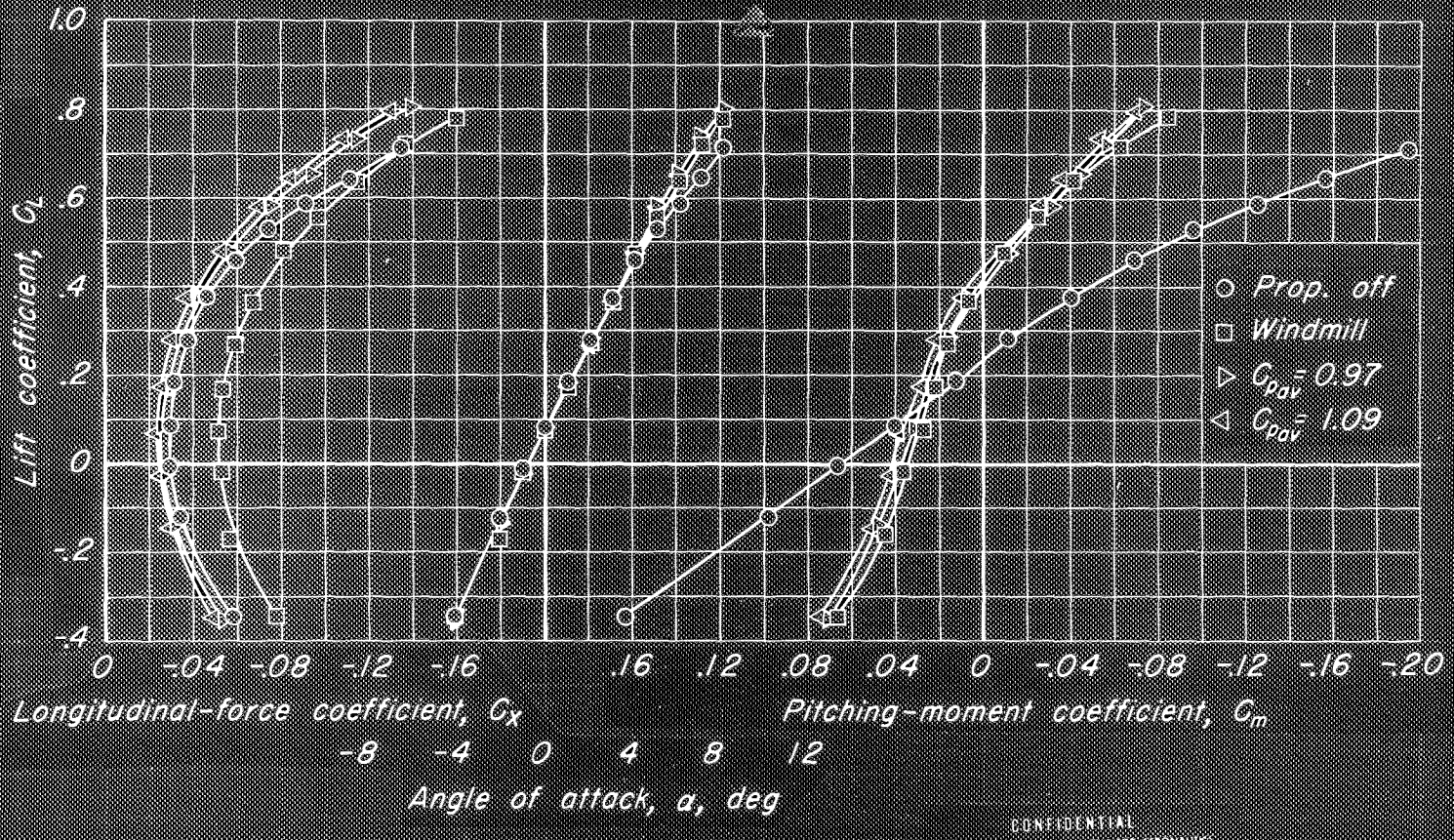

CONFIDENTIAL
NATIONAL ADVISORY COMMITTEE FOR AERONAUTICS

(b) $\beta_{0.75R}$, 60°

Figure 20.- Concluded.

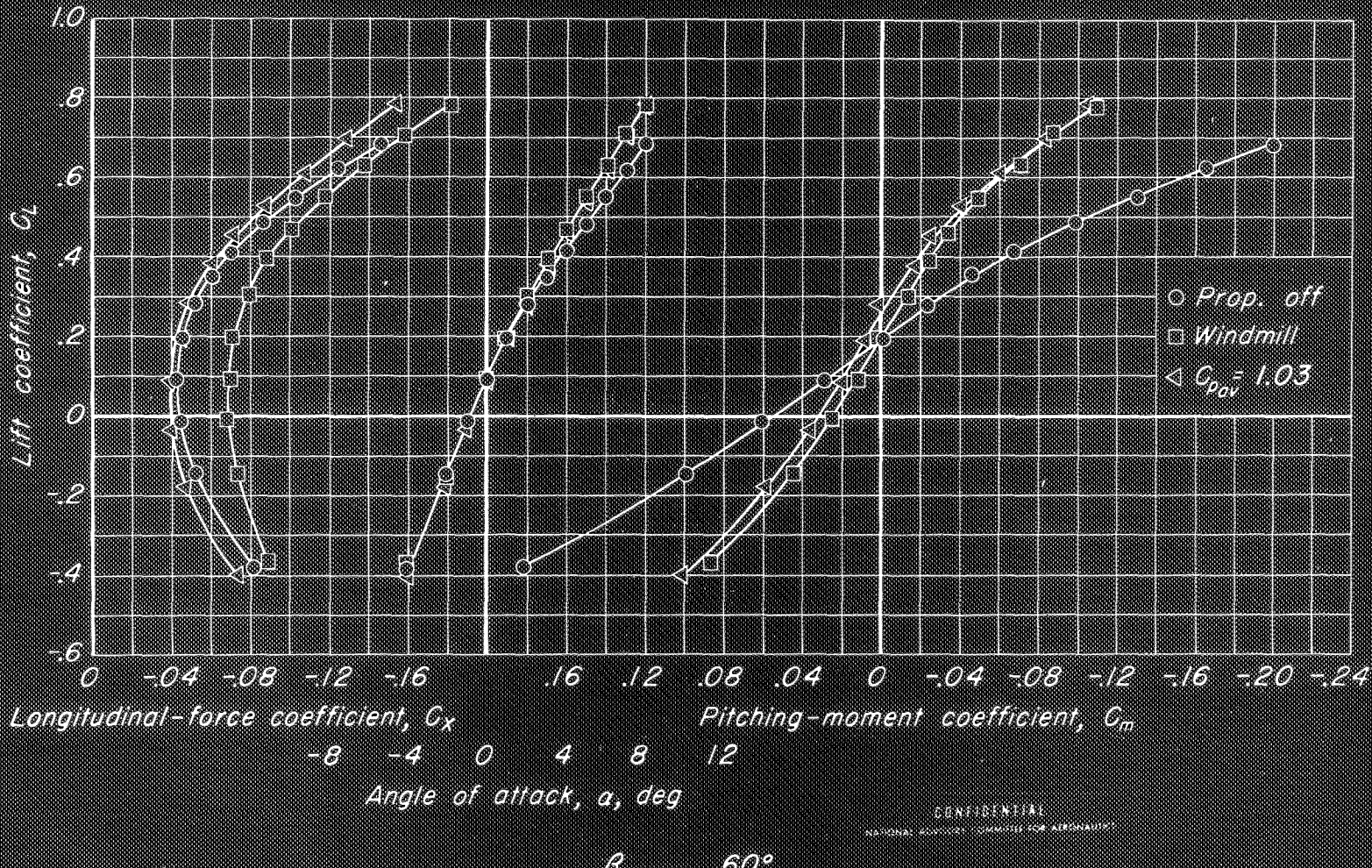

Figure 21.- The effect of power on the longitudinal characteristics of the 1/10-scale model of the Lockheed XFV-1 airplane. M, 0.90.

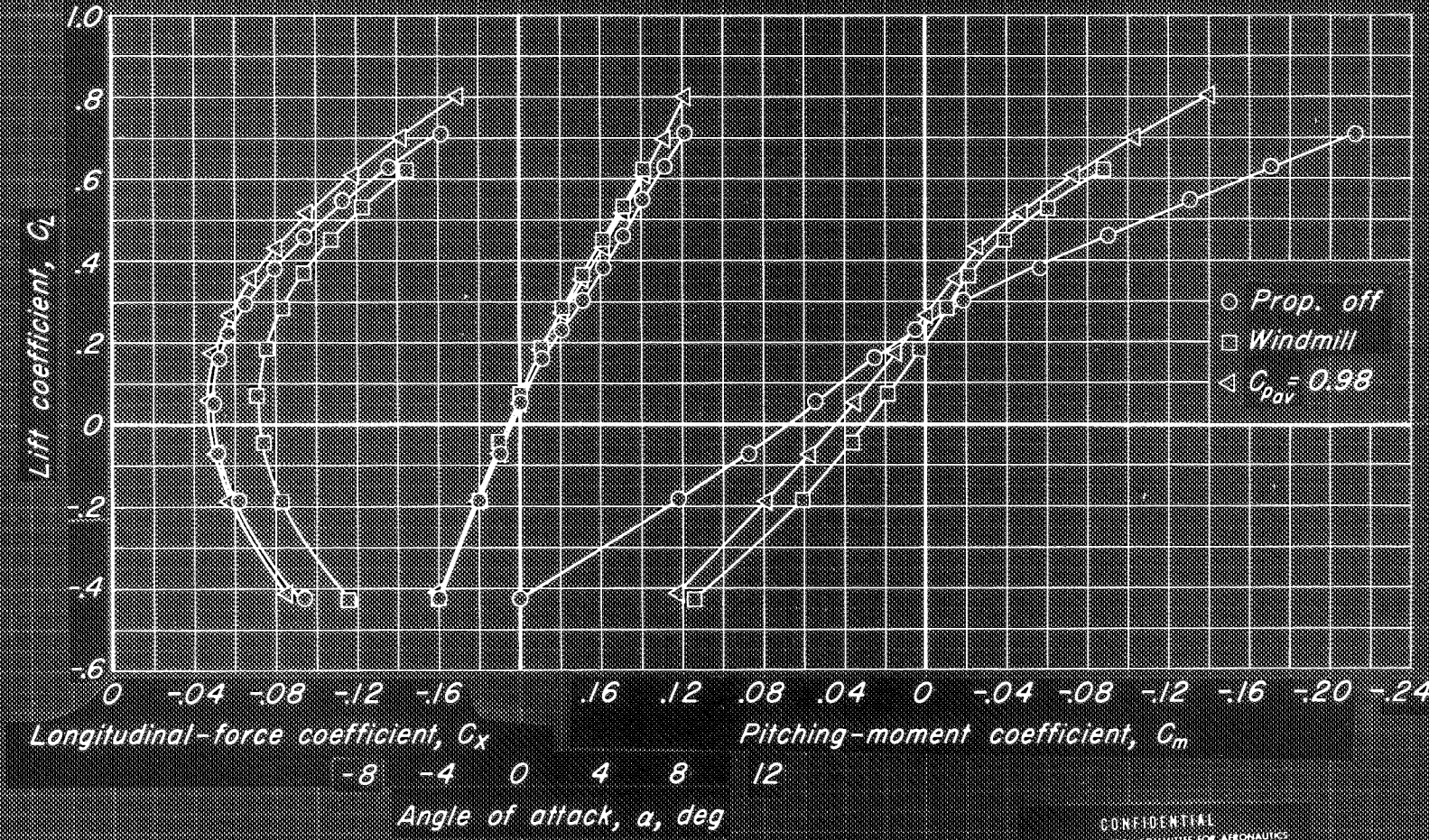

CONFIDENTIAL
NATIONAL ADVISORY COMMITTEE FOR AERONAUTICS

$\beta_{0.75R}$, 60°

Figure 22.-The effect of power on the longitudinal characteristics of the 1/10-scale model of the Lockheed XFV-1 airplane. M, 0.92.

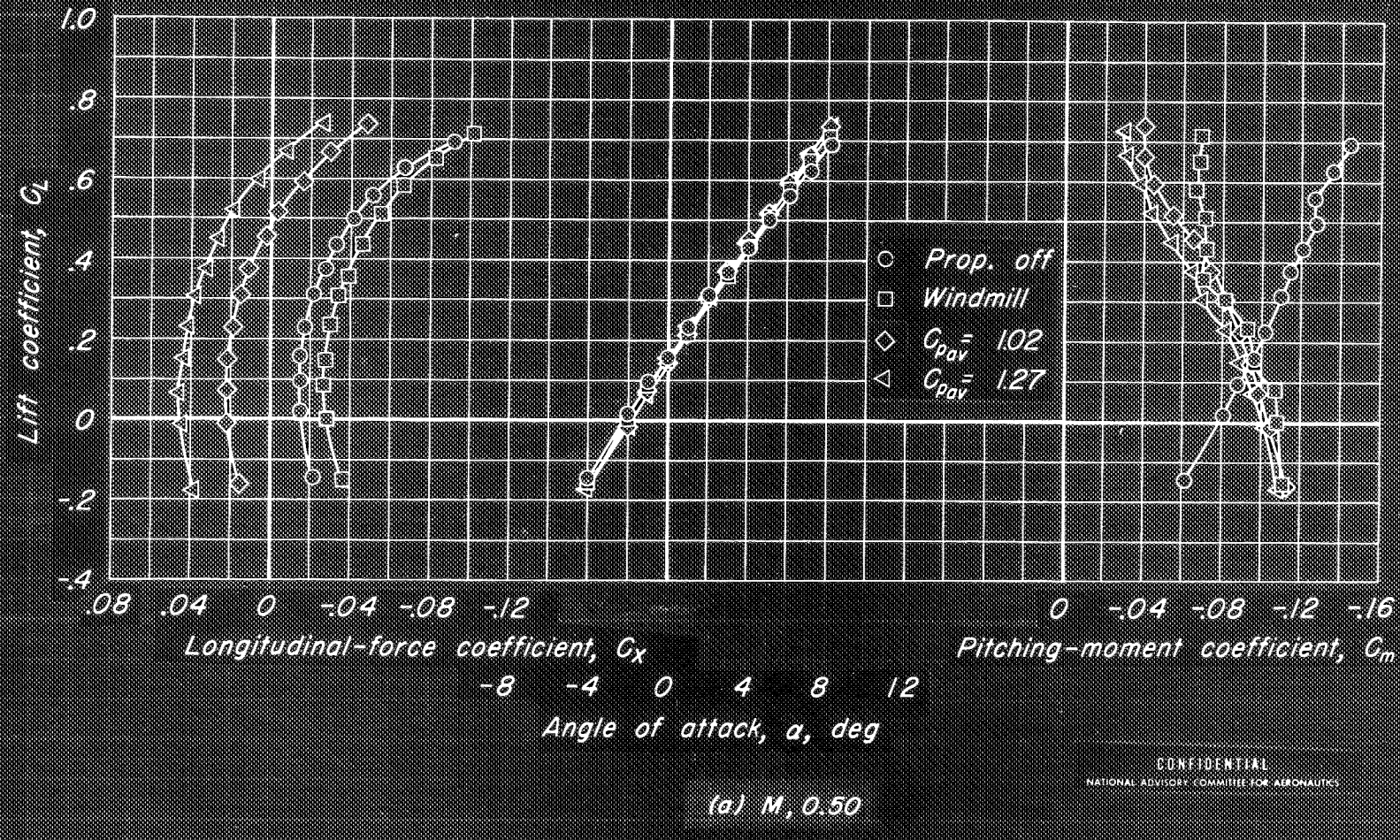

Figure 23.- The effect of power on the longitudinal characteristics of the 1/10-scale model of the Lockheed XFV-1 airplane, tail off. $\beta_{0.75R}$, 55°.

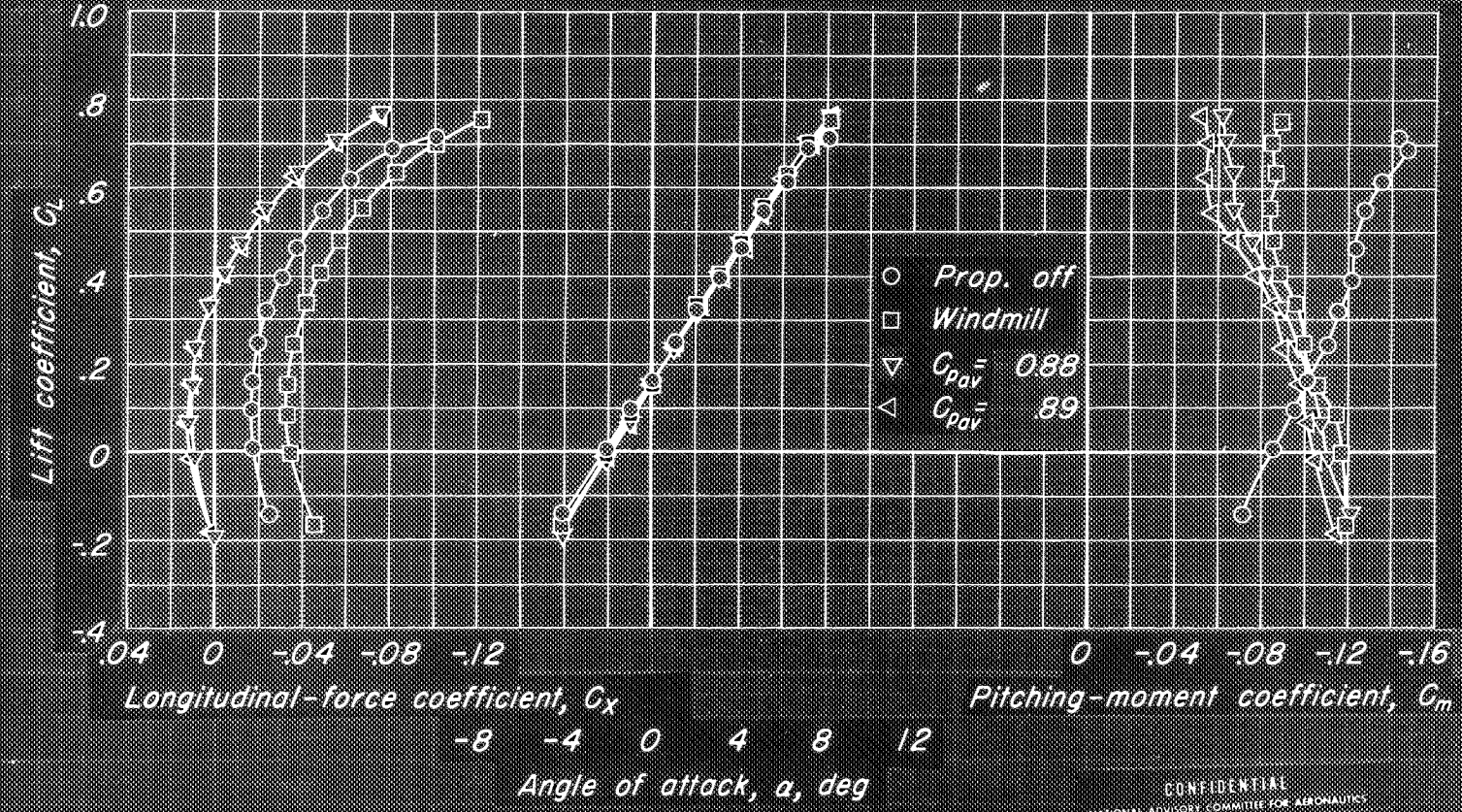

(b) M, 0.70

Figure 23.- Continued.

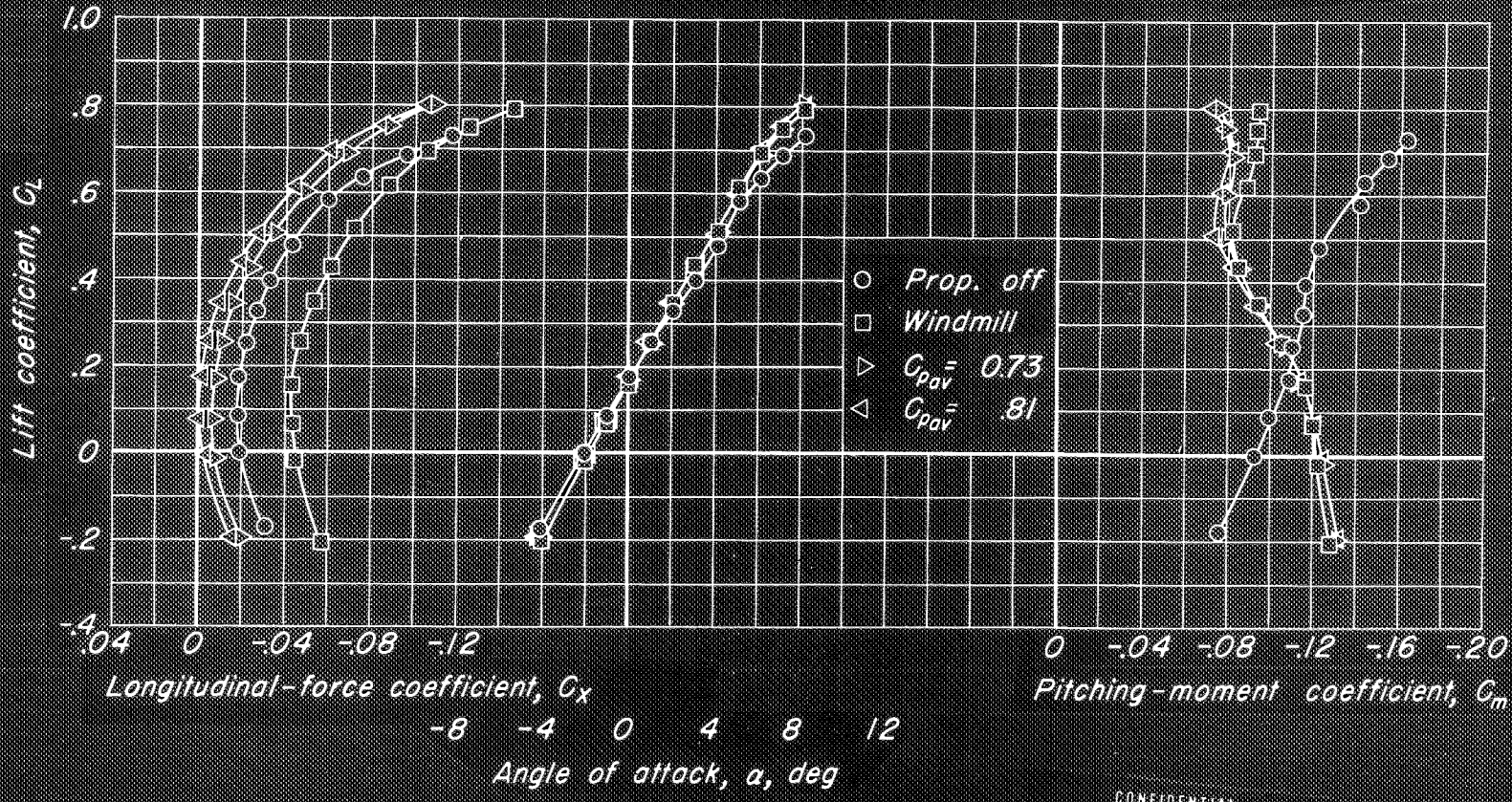

CONFIDENTIAL
NATIONAL ADVISORY COMMITTEE FOR AERONAUTICS

(c) M, 0.80

Figure 23.— Continued.

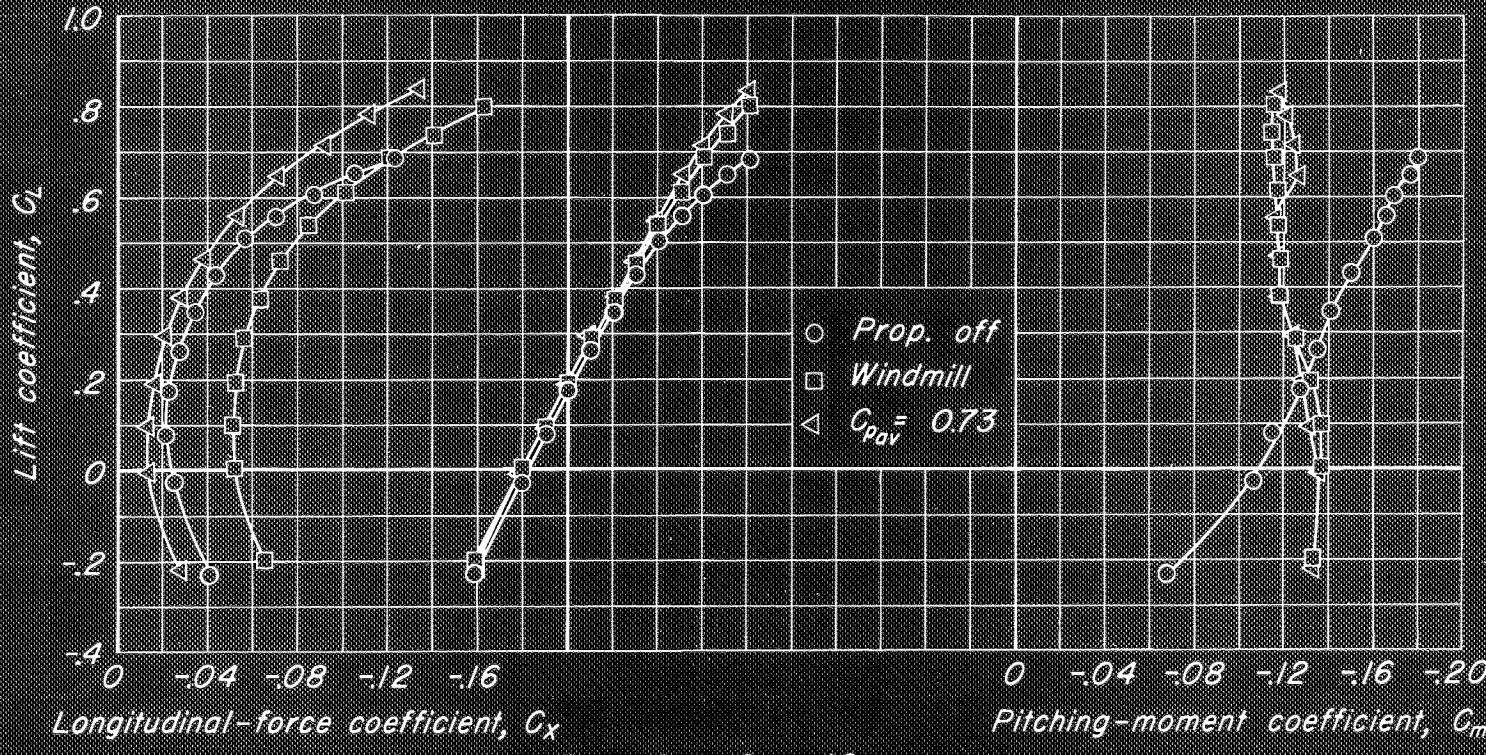

(d) M, 0.85

Figure 23.- Continued.

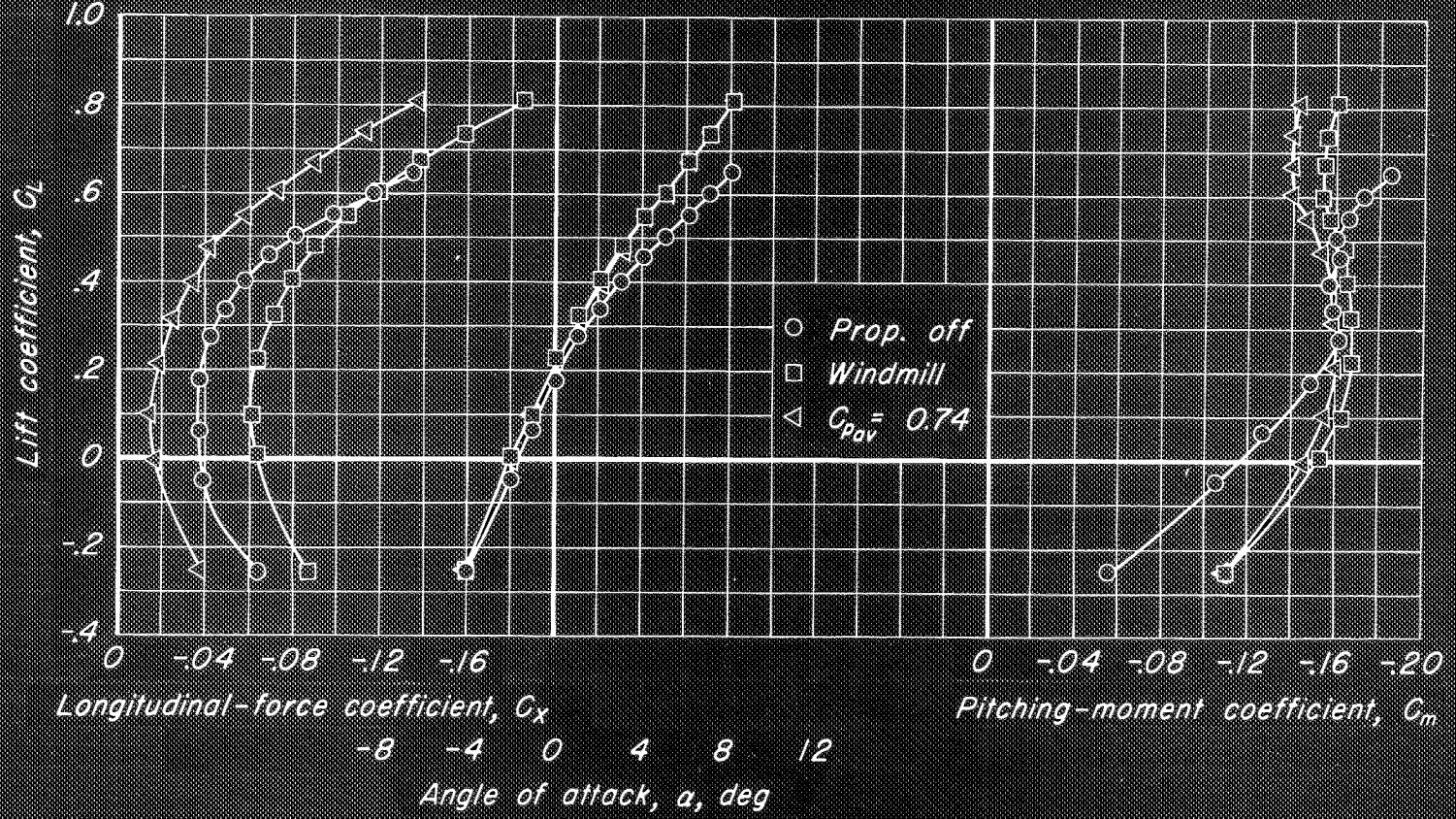

(e) M, 0.90

Figure 23.- Continued.

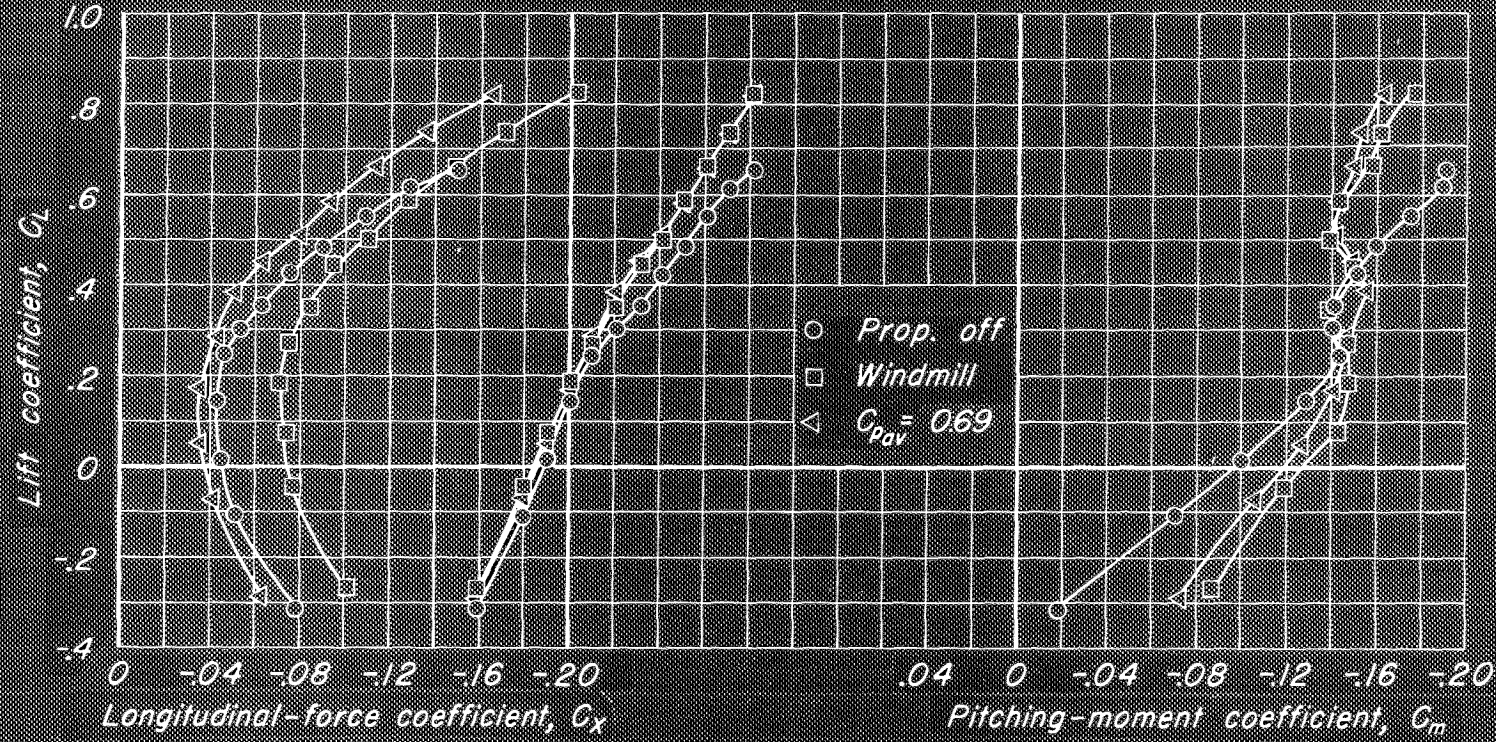

(f) M, 0.92

Figure 23.- Concluded.

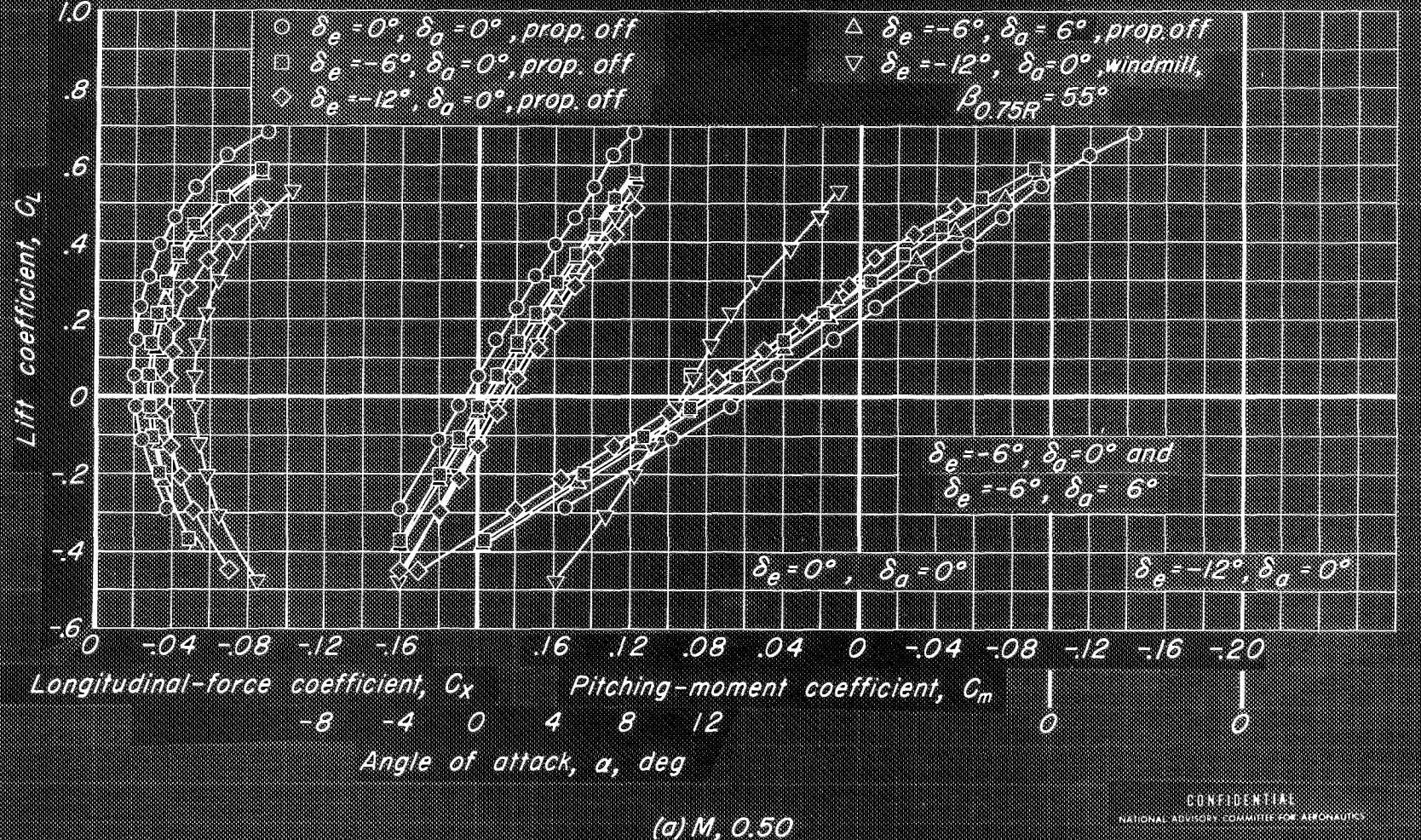

(a) M, 0.50

CONFIDENTIAL
NATIONAL ADVISORY COMMITTEE FOR AERONAUTICS

Figure 24.- Longitudinal-control characteristics of the 1/10-scale model of the Lockheed XFV-1 airplane.

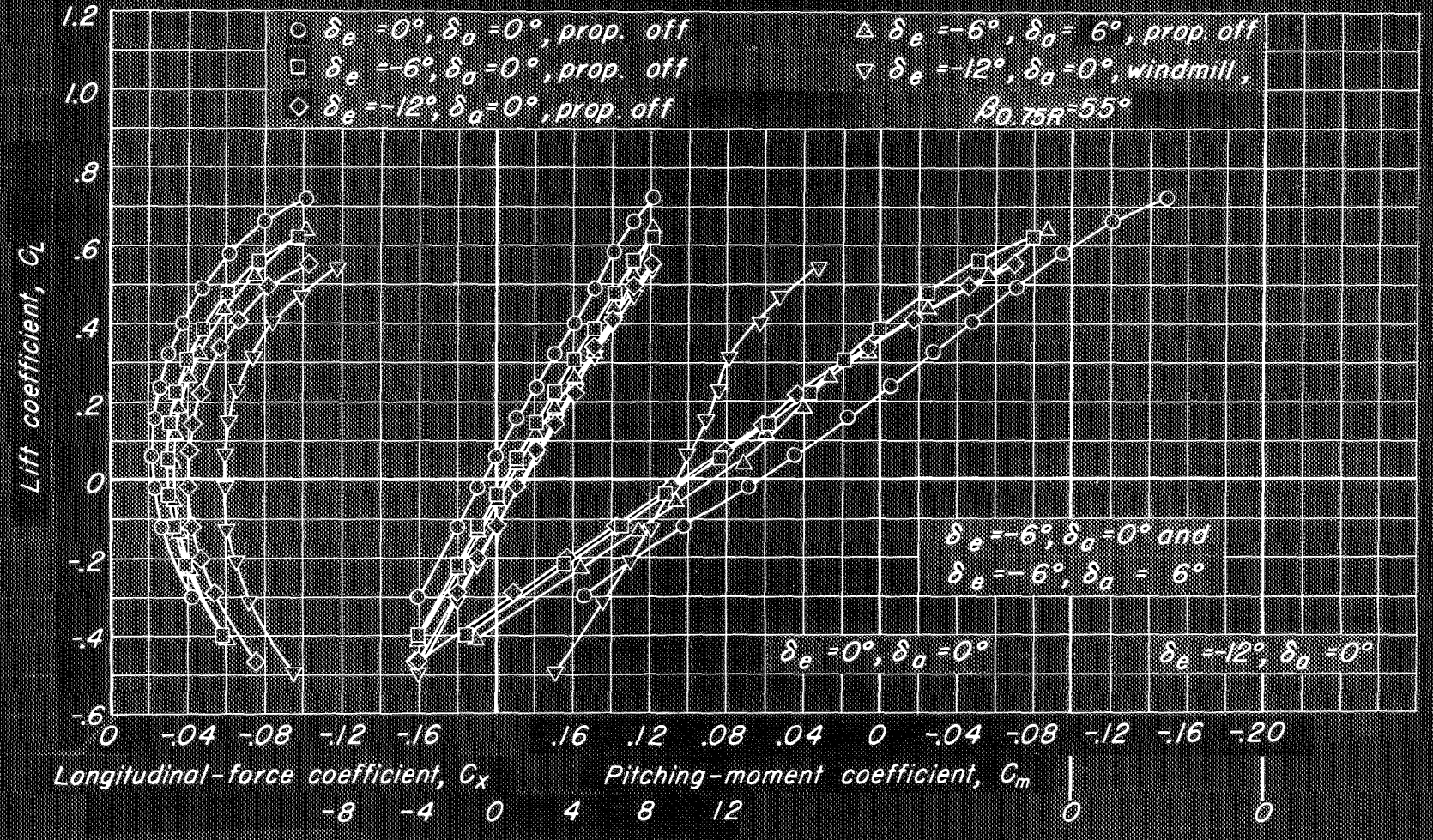

(b) M, 0.70

Figure 24.- Continued.

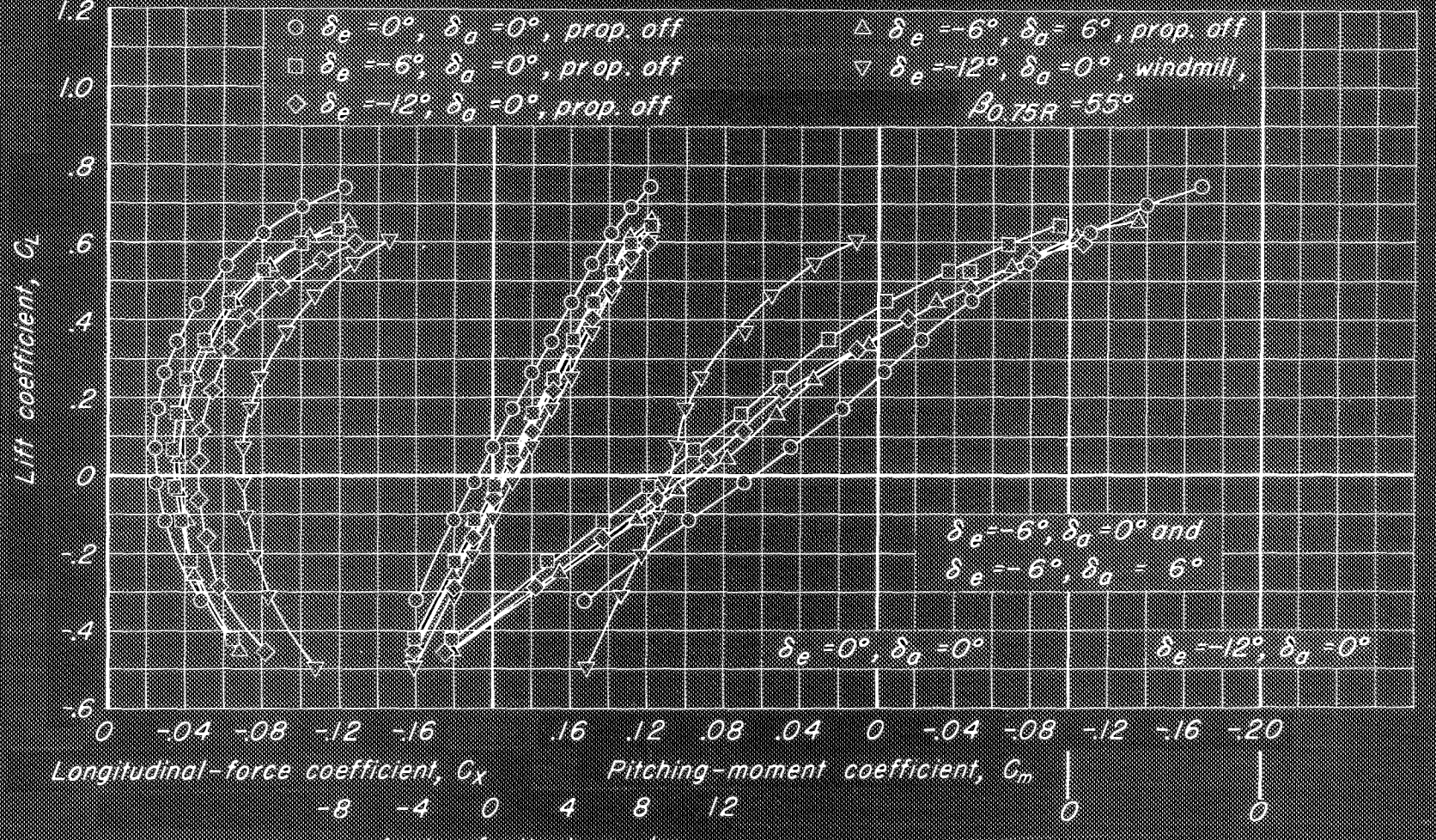

(c) M, 0.80

Figure 24.– Continued.

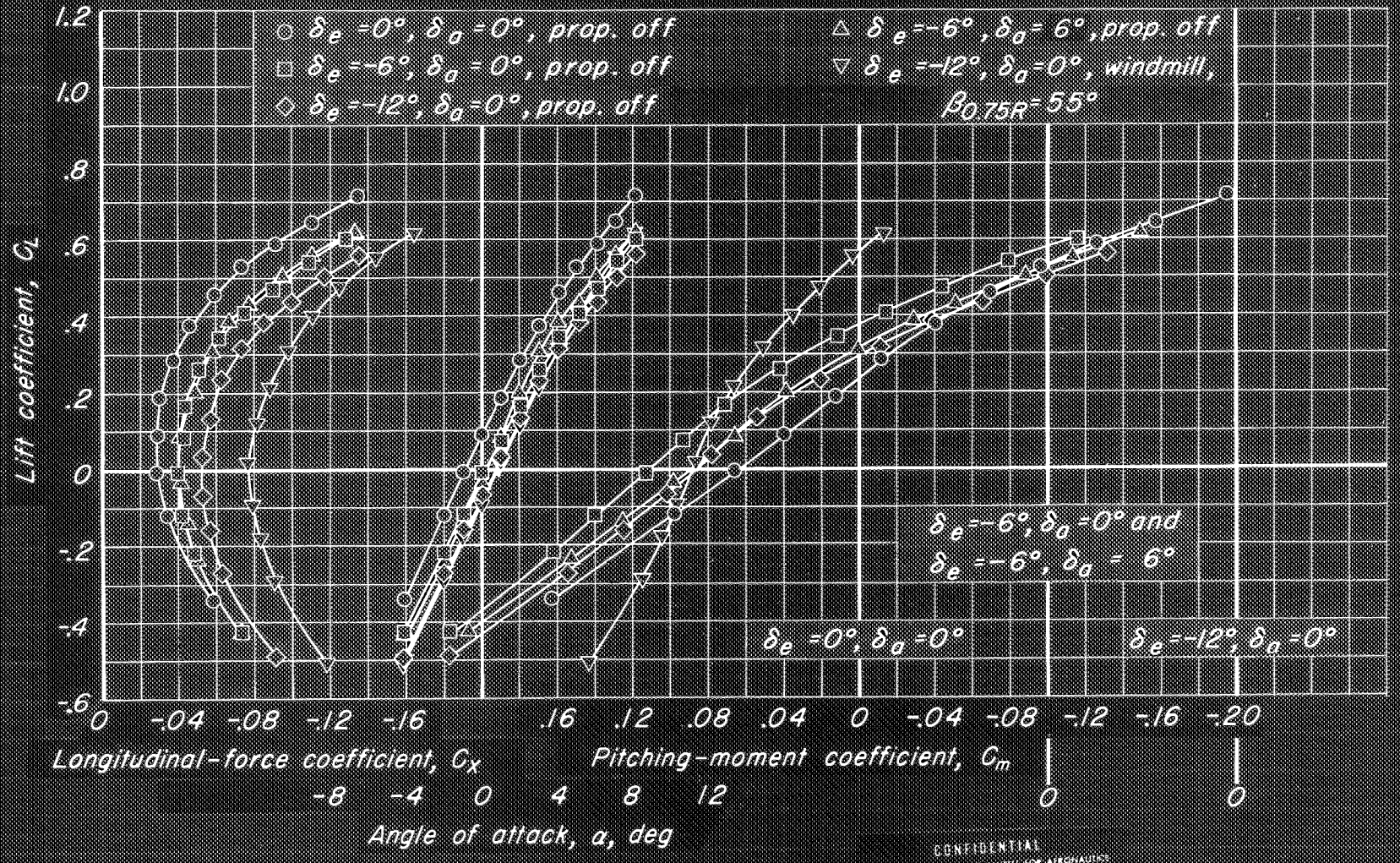

(d) M, 0.85

Figure 24.- Continued.

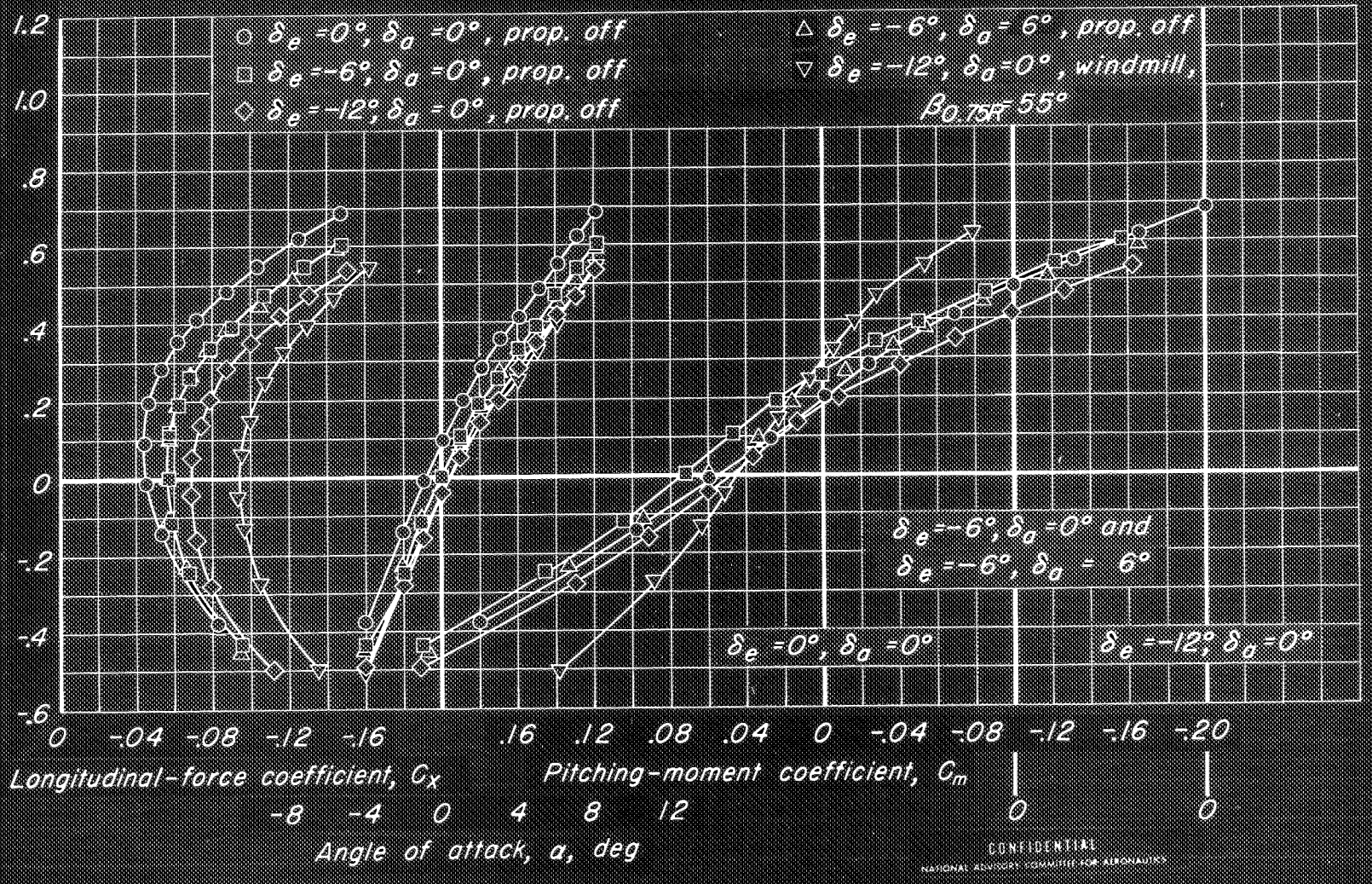

(e) M, 0.90

Figure 24.— Continued.

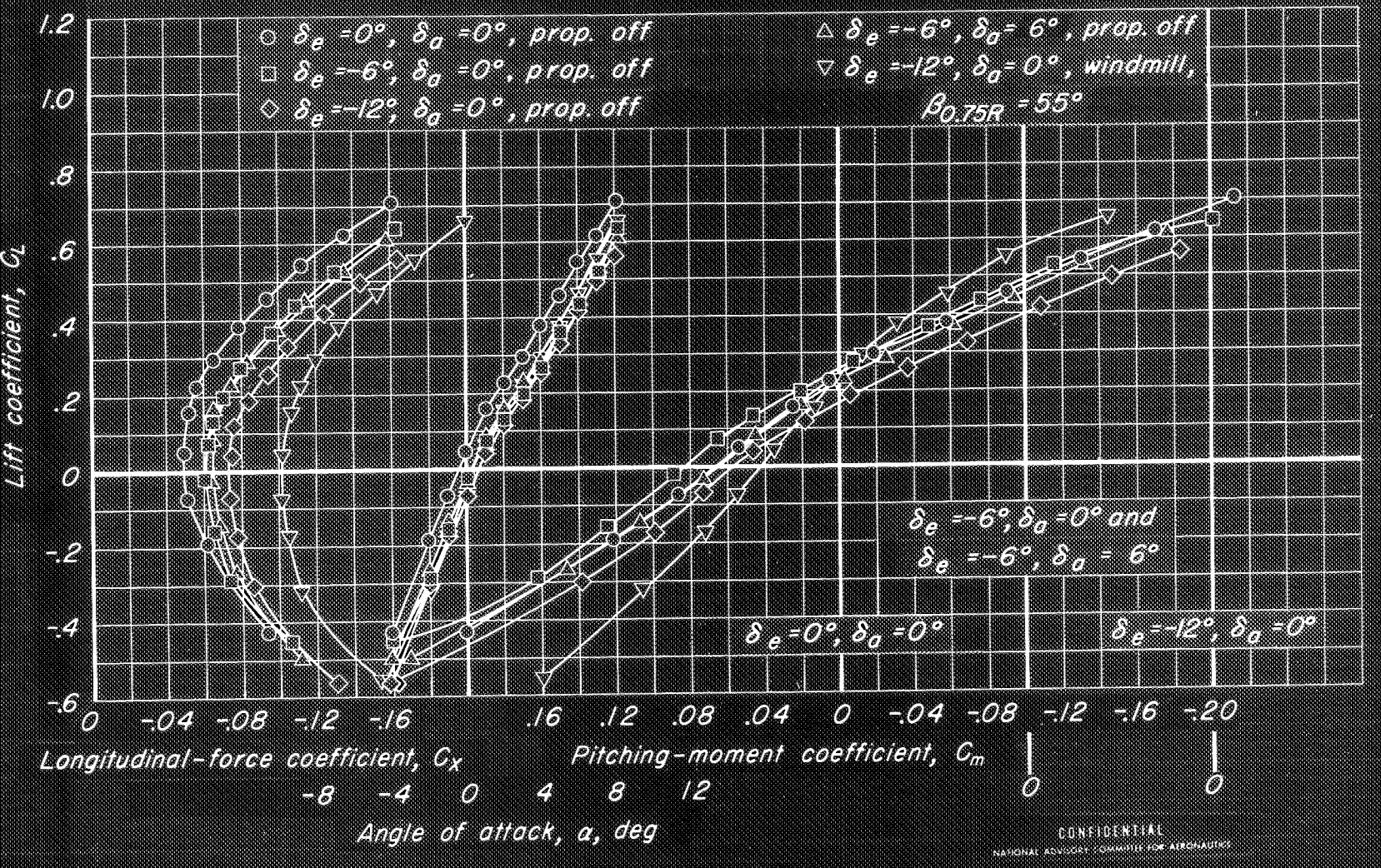

CONFIDENTIAL
NATIONAL ADVISORY COMMITTEE FOR AERONAUTICS

(f) M, 0.92

Figure 24.— Concluded.

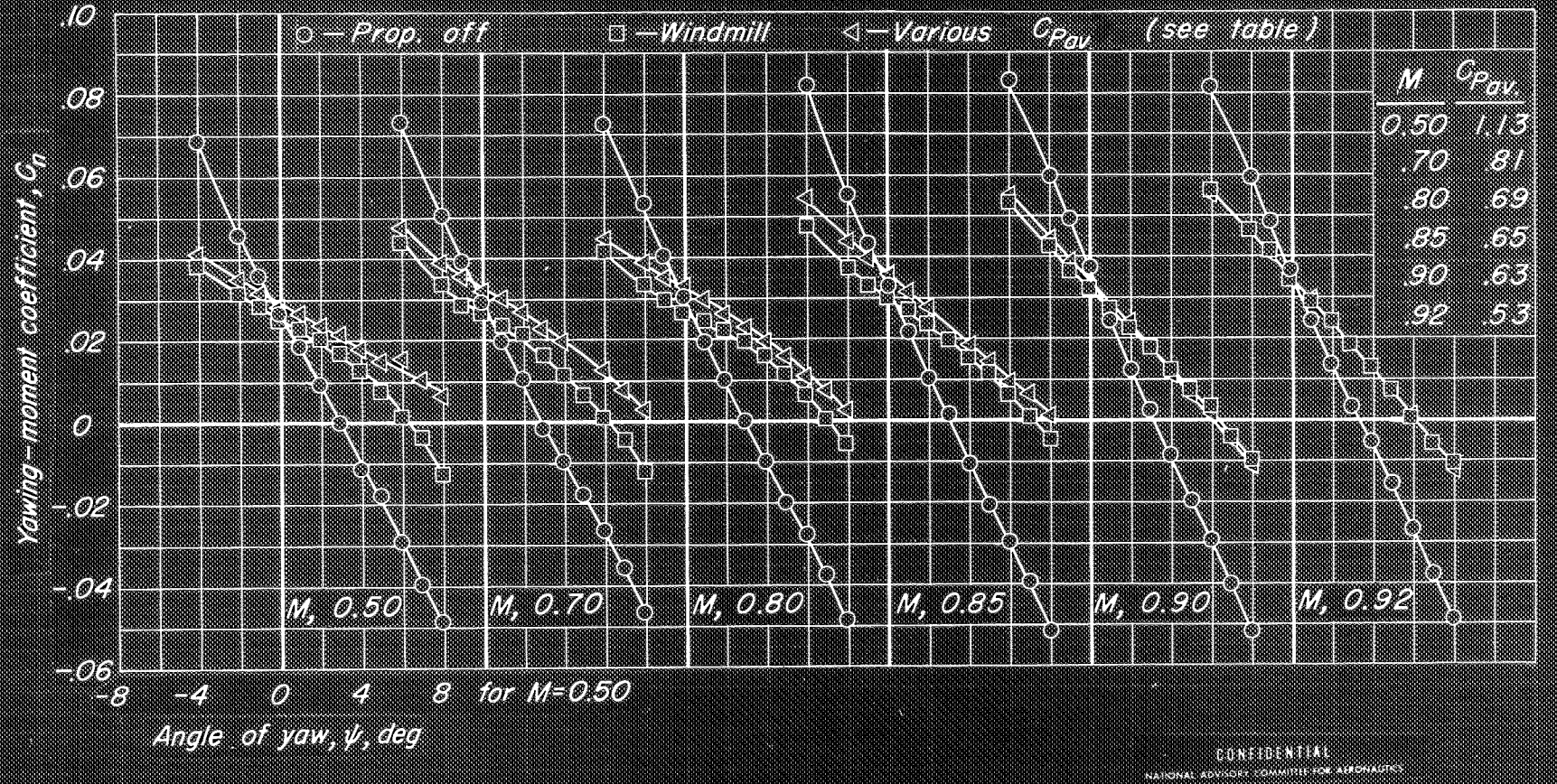

Figure 25.— The effect of power on the simulated yaw characteristics of the 1/10-scale model of the Lockheed XFV-1 airplane. $\beta_{0.75R}$, 55°.

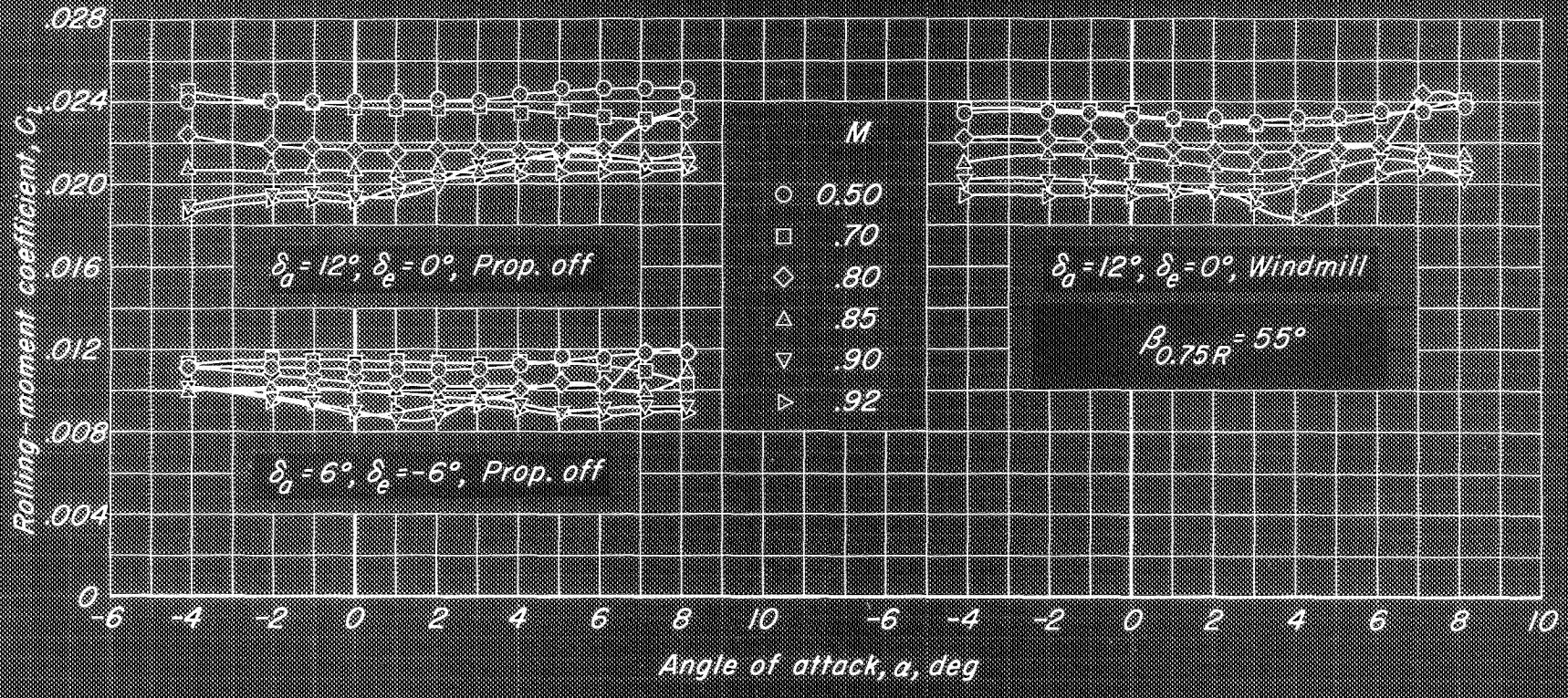

Figure 26.— Roll characteristics of the 1/10-scale model of the Lockheed XFV-1 airplane. ψ_t 0°.

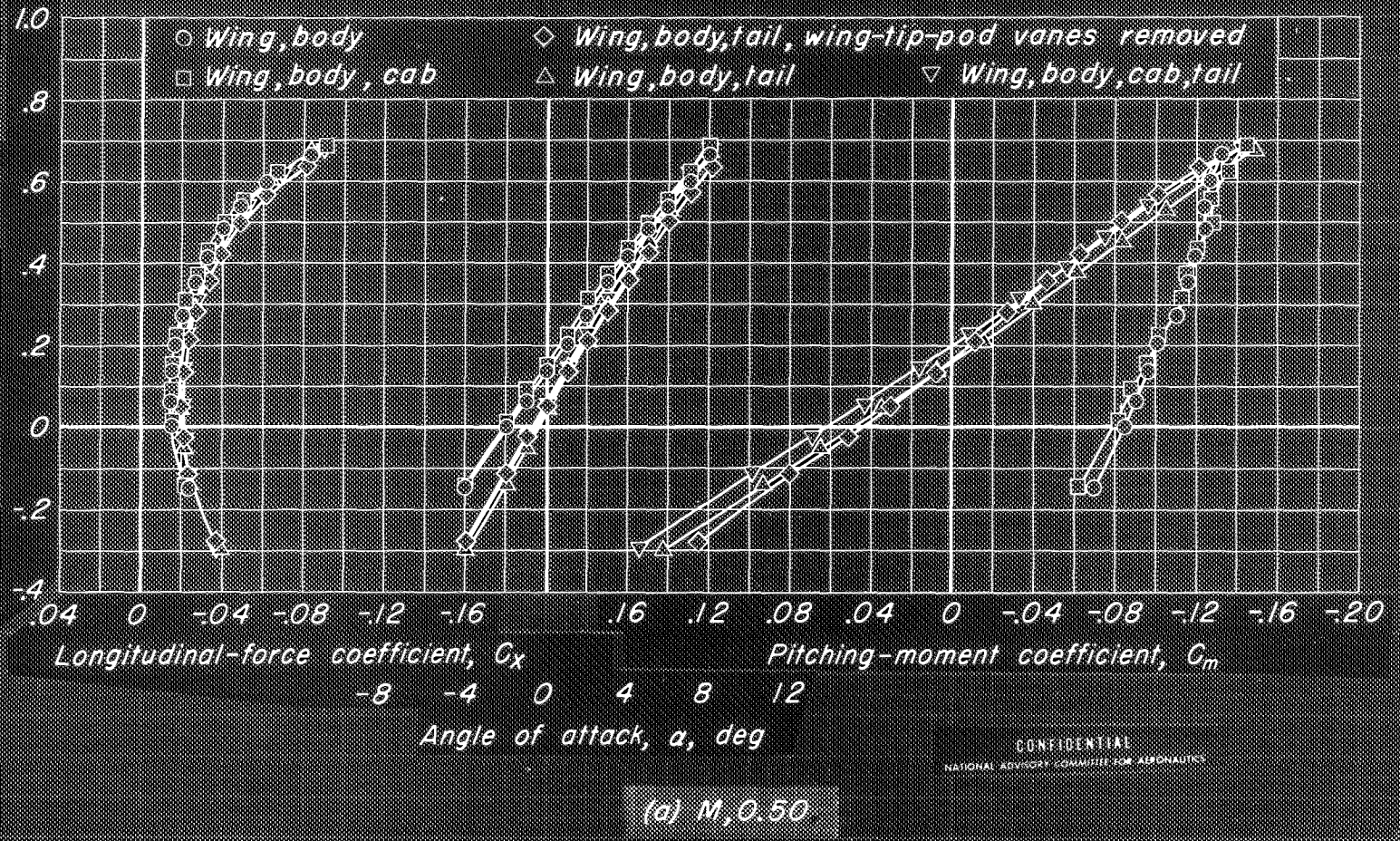

Figure 27.- The longitudinal characteristics of several combinations of model components. Propeller removed.

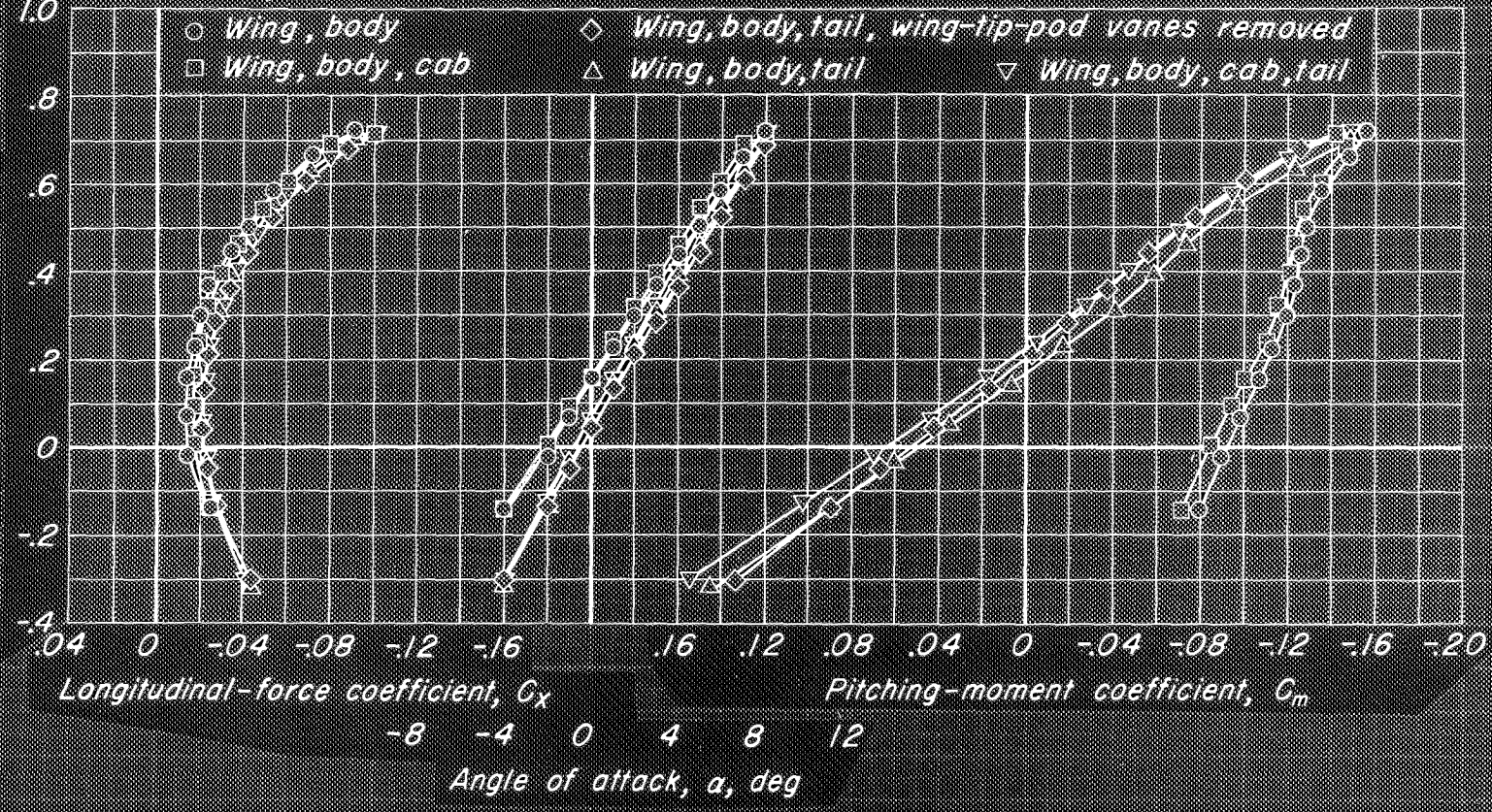

(b) M, 0.70

Figure 27.- Continued.

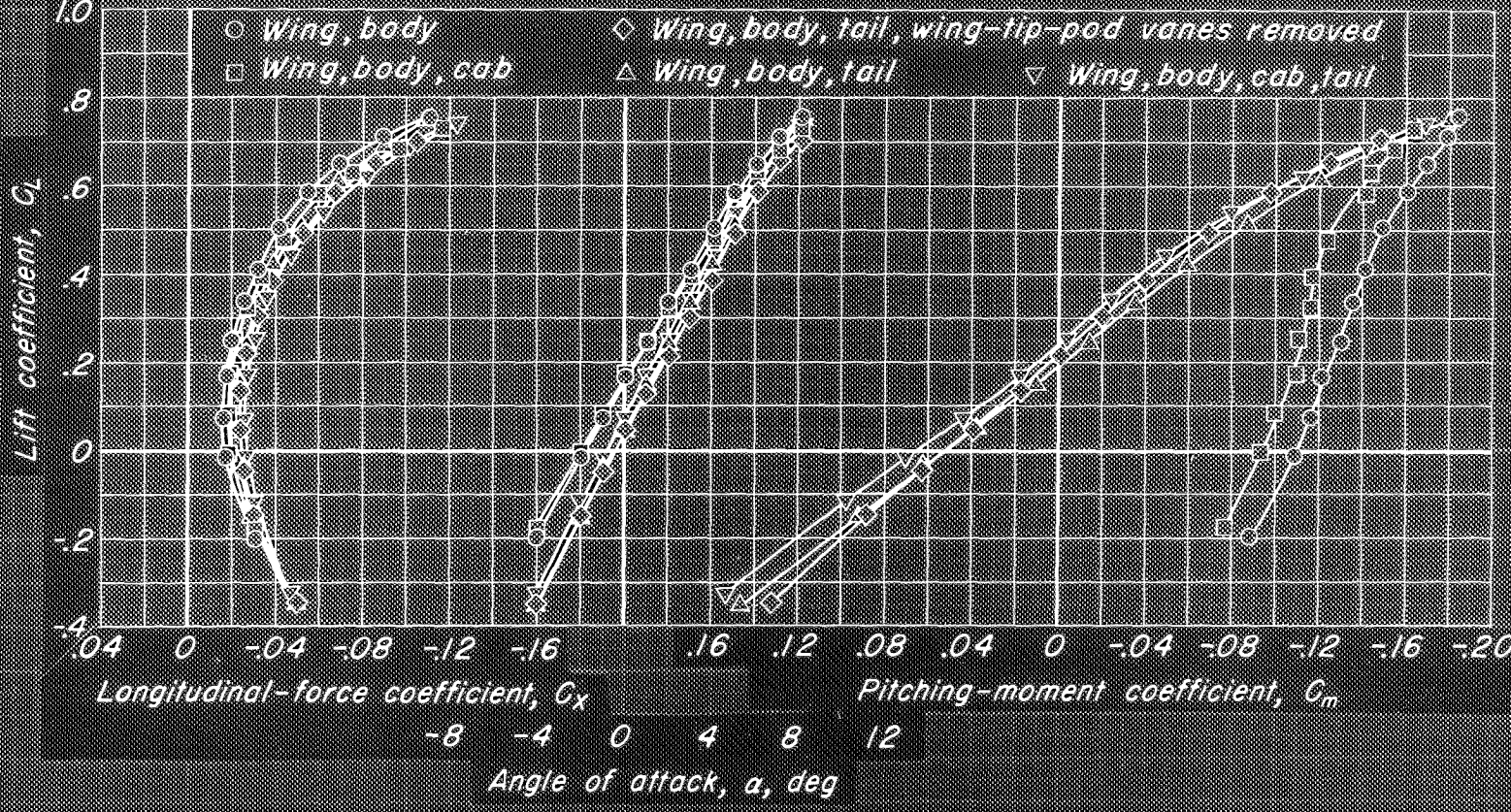

(c) M, 0.80

CONFIDENTIAL

Figure 27.- Continued.

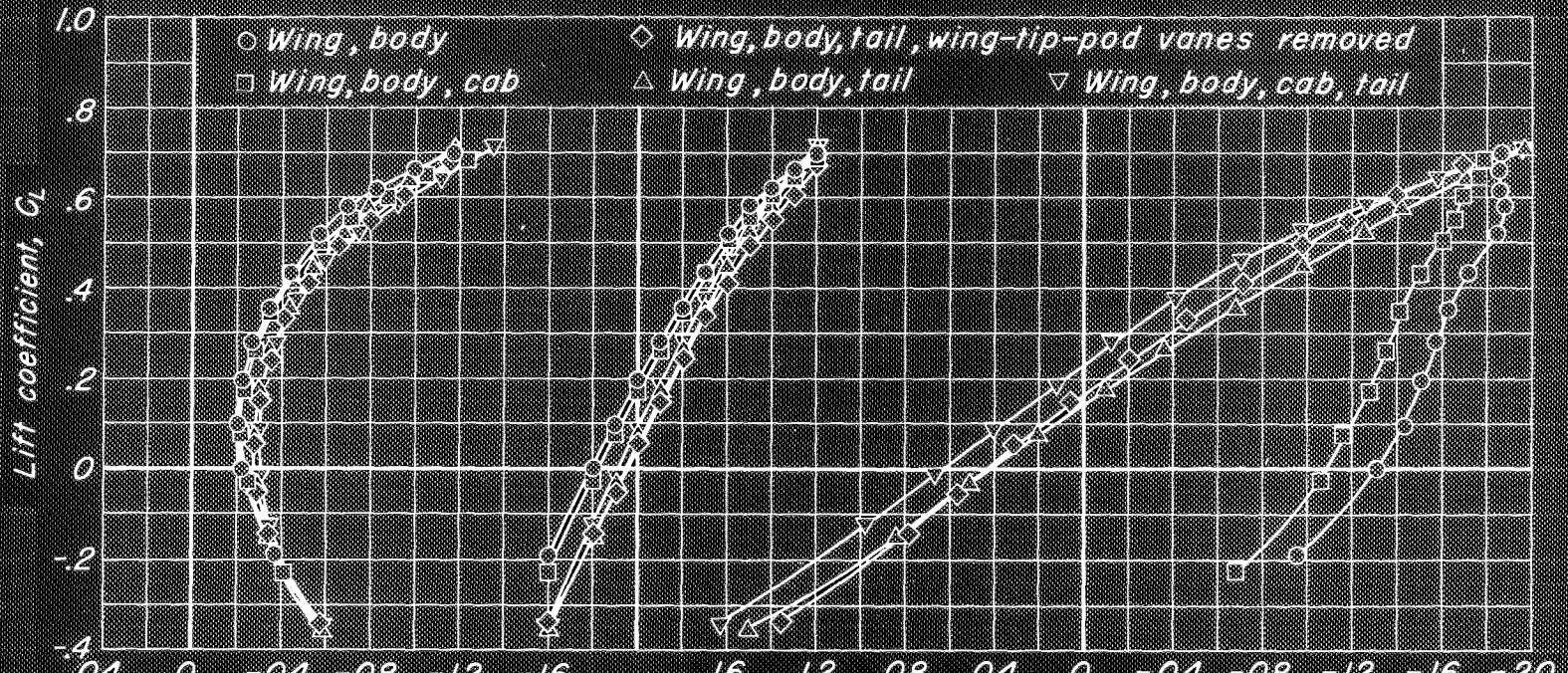

CONFIDENTIAL
NATIONAL ADVISORY COMMITTEE FOR AERONAUTICS

(d) M, 0.85

Figure 27.- Continued.

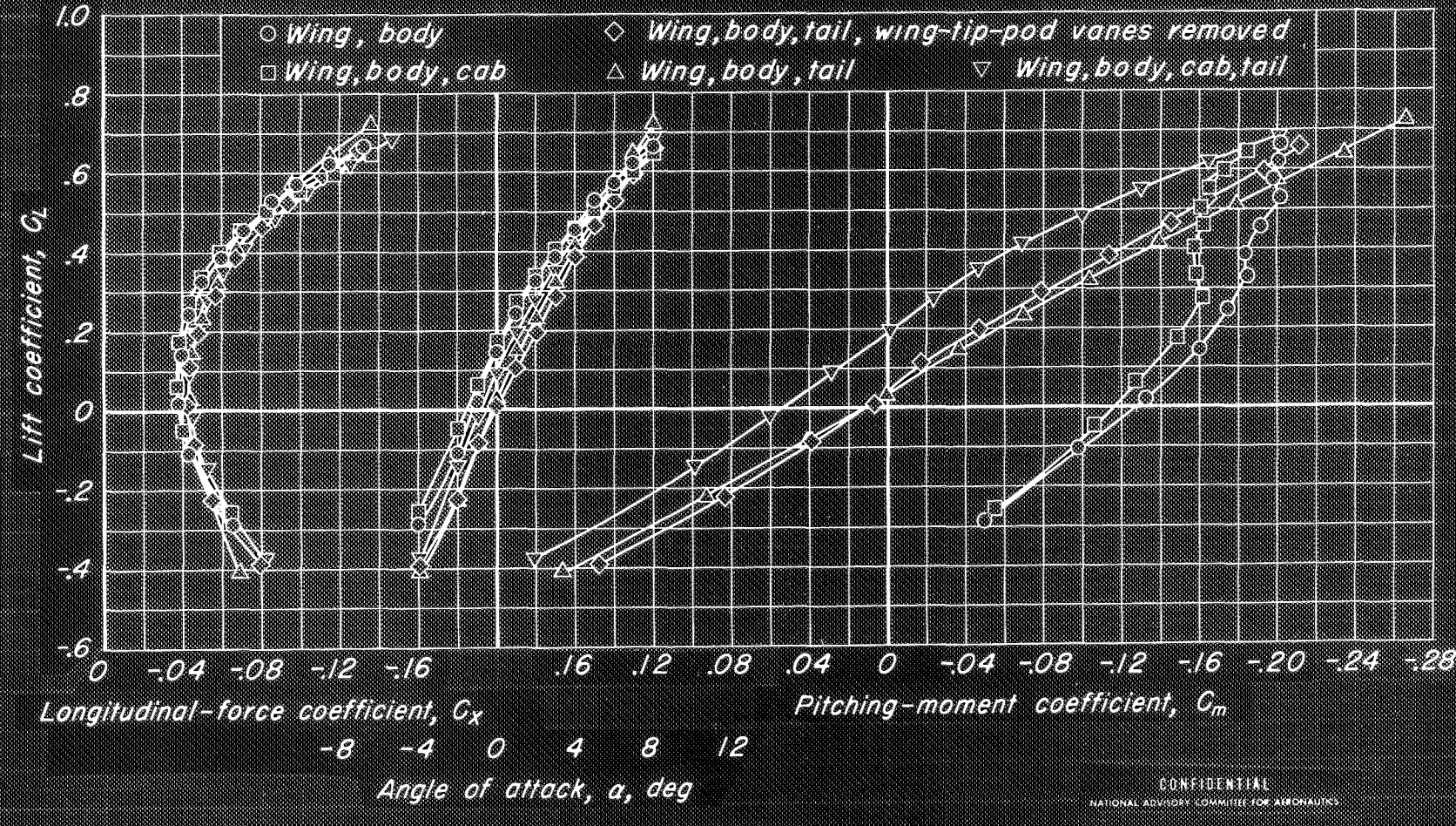

CONFIDENTIAL
NATIONAL ADVISORY COMMITTEE FOR AERONAUTICS

(e) M, 0.90

Figure 27.- Continued.

CONFIDENTIAL
NATIONAL ADVISORY COMMITTEE FOR AERONAUTICS

(f) M, 0.92

Figure 27.- Concluded.

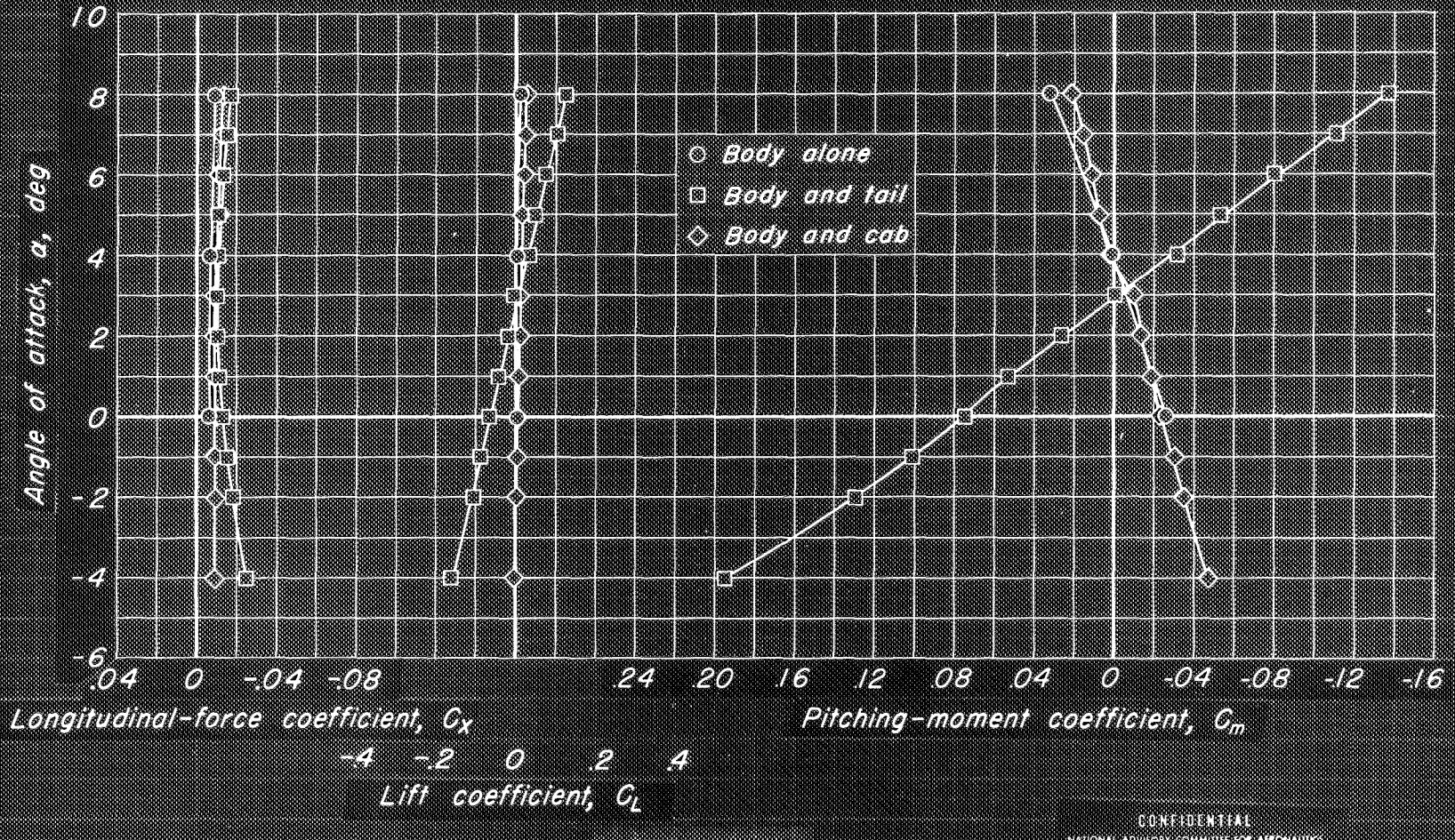

Figure 28.- The longitudinal characteristics of the body alone, the body and tail, and the body and cab. Propeller removed.

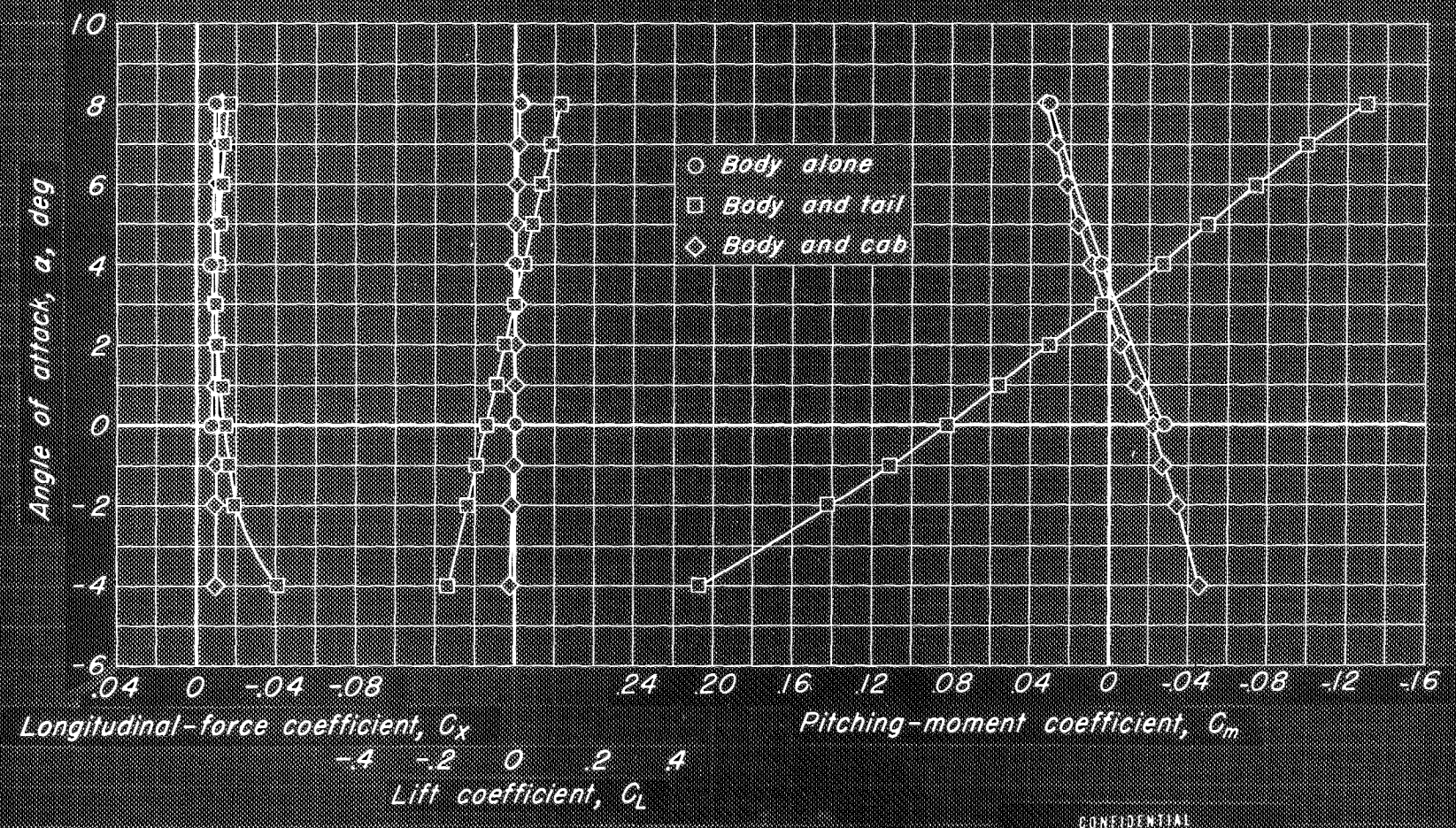

(b) M, 0.70

CONFIDENTIAL
NATIONAL ADVISORY COMMITTEE FOR AERONAUTICS

Figure 28.- Continued.

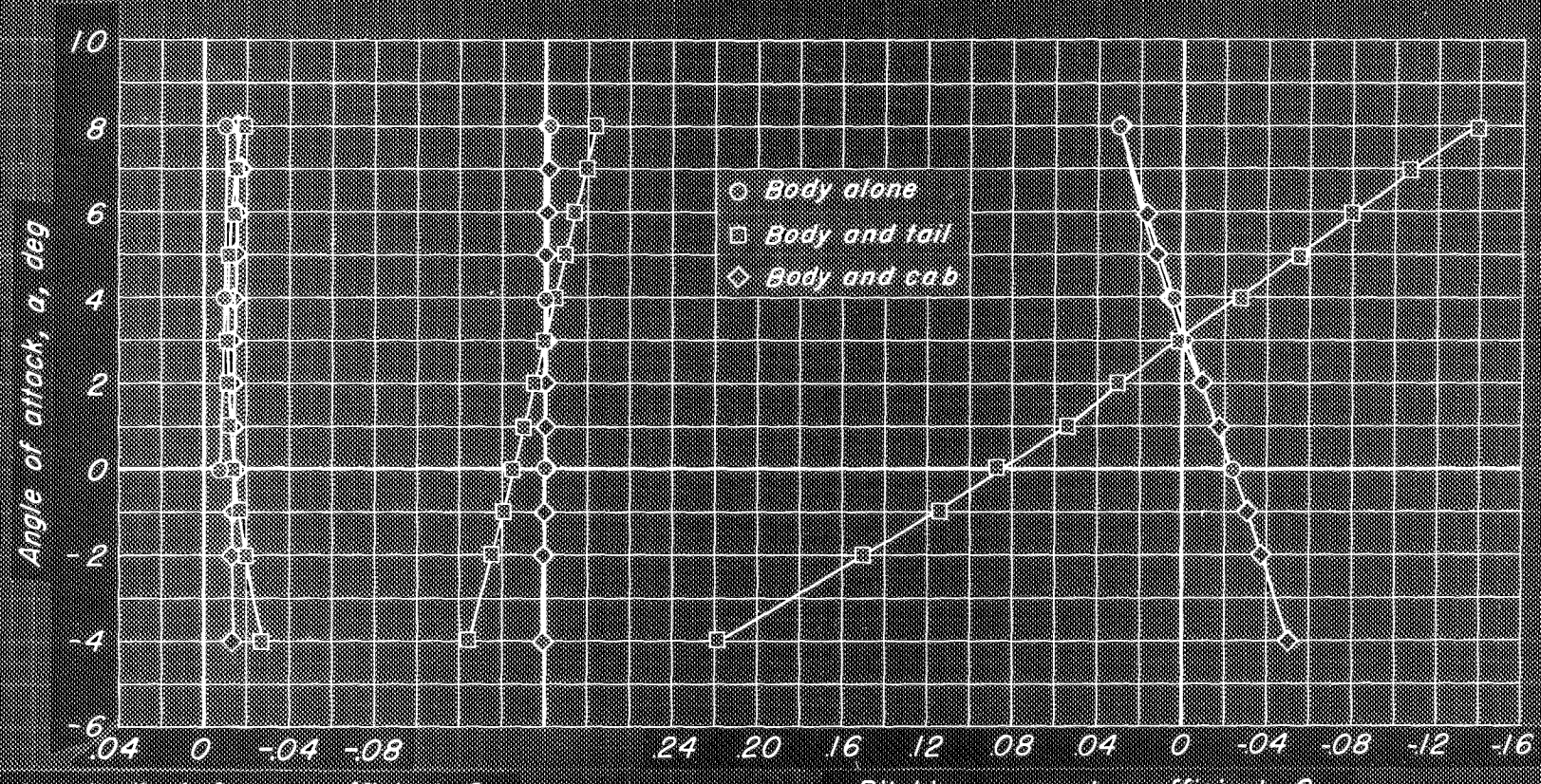

(c) M_1 0.80

Figure 28.- Continued.

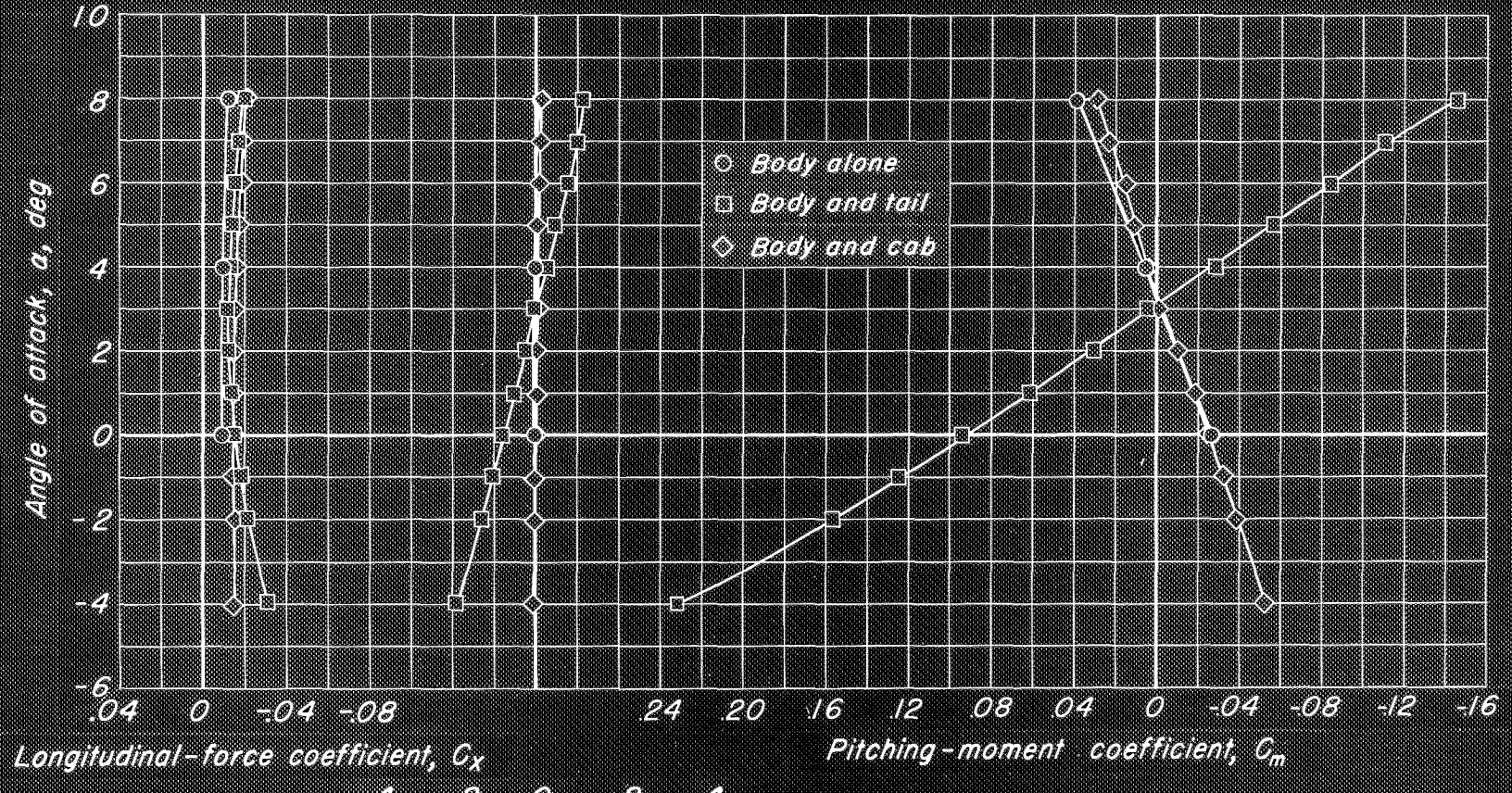

(d) M, 0.85

Figure 28.- Continued.

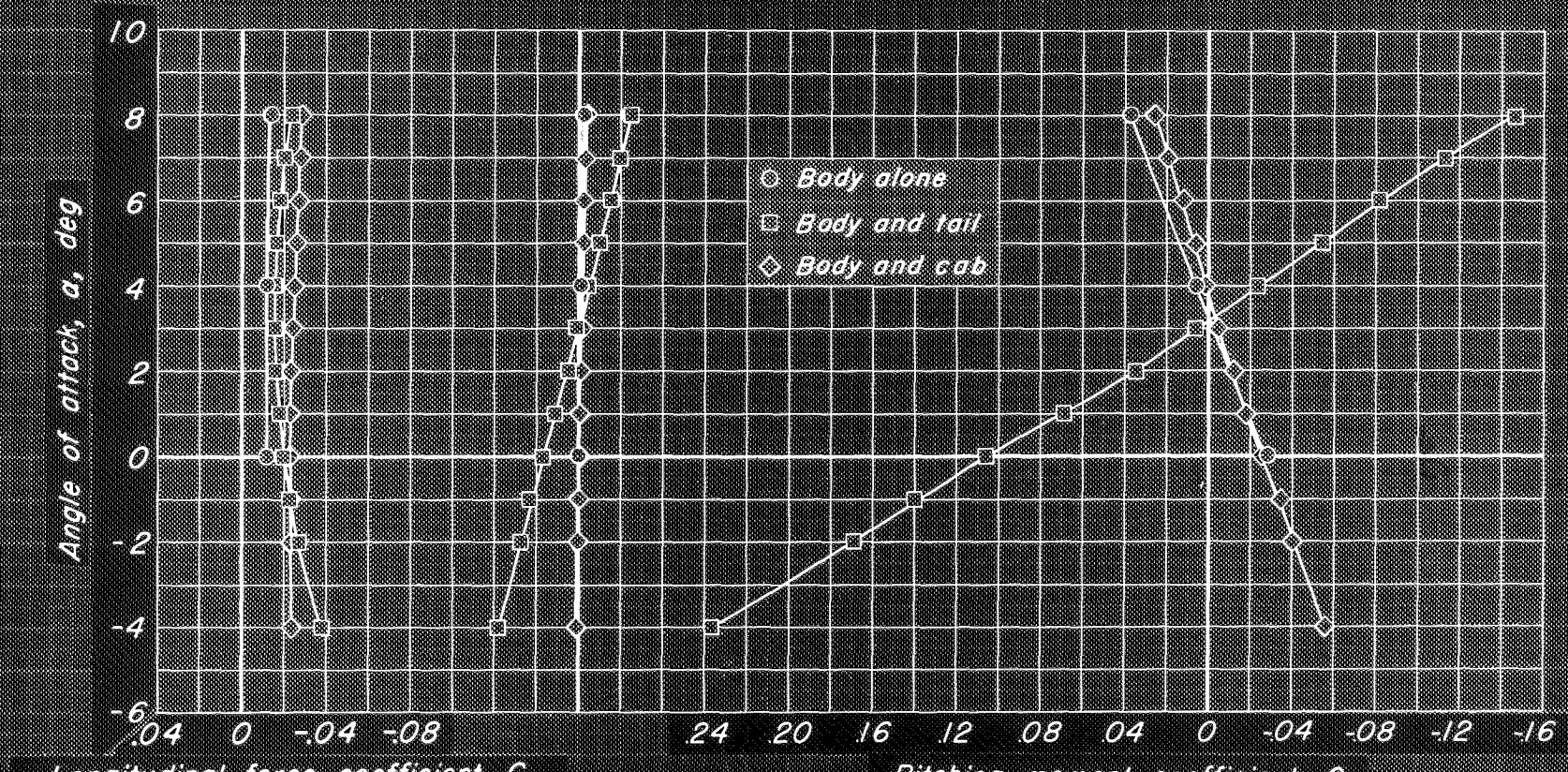

CONFIDENTIAL
NATIONAL ADVISORY COMMITTEE FOR AERONAUTICS

(e) M, 0.90.

Figure 28.- Continued.

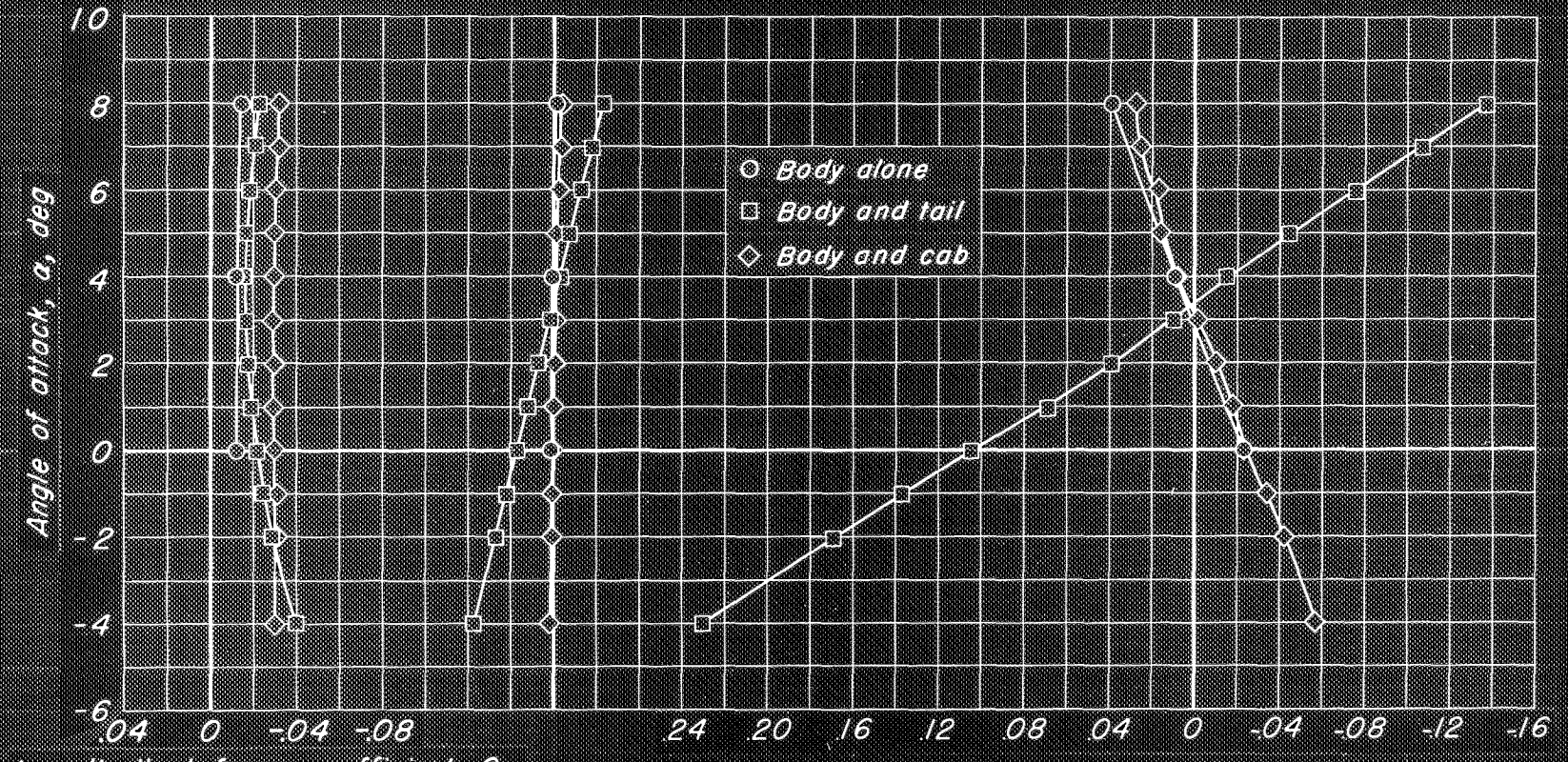

(f) M, 0.92

Figure 28.- Concluded.